University of Southampton

Faculty of Environmental and Life Sciences

School of Ocean and Earth Science

Hop, hop and away: On the take-off leap of *Archaeopteryx*

by

Erik Anthony Meilak

ORCID ID: https://orcid.org/0000-0003-4806-9448

Thesis for the degree of Doctor of Philosophy

December 2021

University of Southampton
Abstract

Faculty of Environmental and Life Sciences
School of Ocean and Earth Science

Doctor of Philosophy

Hop, hop and away: On the take-off leap of *Archaeopteryx*

by
Erik Anthony Meilak

Where take-off is a crucial phase of flight requiring an energy-intensive motion to accelerate into the air, how *Archaeopteryx*, the first bird, took to the air is a subject of great debate. Although it is known that extant land birds take off by leaping, generating the initial take-off velocity primarily from the hindlimbs, the biomechanics of such leaps remain largely unknown. Understanding the detailed musculoskeletal mechanics associated with an extant avian jumping take-off could provide key insight into the evolution of avian flight. As a basis for further analyses, this thesis first developed a computational biomechanical model of a passerine bird (magpie, *Pica pica*), a representative of a class of birds that includes over half of all extant bird species, to quantify the functional hindlimb anatomy in leaping birds. Comprehensive analyses considering key sources of uncertainty provided robust estimates for the moment-generating capacity of its pelvic muscles and demonstrated substantial capability for internal/external rotation as well as flexion/extension, revealing that avian hip muscle function is not limited to the sagittal plane. Informed by these new insights, a computational musculoskeletal model of the zebra finch, *Taeniopygia guttata*, hindlimb was developed and driven with previously published take-off ground reaction forces and 3D kinematics. This first biomechanical model to study the internal biomechanics associated with a take-off leap used an inverse dynamics approach to calculate the external moments at the ankle, knee, and hip joints and contrasted these to the cumulative capacity of the hindlimb muscles to balance these moments across a range of take-off conditions. We report substantial external moments at the hip and ankle joints, reaching magnitudes of about two times values previously reported during the running of a flightless bird. Having confirmed the capability of the computer model to determine the hind limb biomechanics during a successful take-off leap in an extant bird, this thesis proceeded to test the leaping ability of *Archaeopteryx* to become airborne. By carefully adapting a published model of *Archaeopteryx* to reflect the novel understanding of avian hindlimb kinematics and kinetics developed here, we confirm the capability of *Archeopteryx* to leap and determine robust estimates of the maximum take-off velocity powered by their hind limbs. Using a conservative approach to integrate contributions of hindlimbs and wings we then show that *Archaeopteryx*, taking successive leaps like a living bird, could use its hindlimbs to generate sufficient velocity to reach the minimum sustainable flight speed within two to three hops. The state-of-the-art biomechanical analyses developed in this thesis thus provide new quantitative evidence in support of a ground-up leaping mechanism for the evolution of avian flight and offer a methodological framework for rigorous biomechanical hypothesis testing to expand our understanding of the evolution of avian flight.

Table of Contents

Table of Tables

Table of Tables

Table of Figures

Table of Figures

Table of Figures

Research Thesis: Declaration of Authorship

Print name: Erik Anthony Meilak

Title of thesis: Hop, hop and away: using a biomechanical approach to investigate the palaeontological question of the evolution of avian flight

I declare that this thesis and the work presented in it are my own and has been generated by me as the result of my own original research.

I confirm that:

1. This work was done wholly or mainly while in candidature for a research degree at this University;
2. Where any part of this thesis has previously been submitted for a degree or any other qualification at this University or any other institution, this has been clearly stated;
3. Where I have consulted the published work of others, this is always clearly attributed;
4. Where I have quoted from the work of others, the source is always given. With the exception of such quotations, this thesis is entirely my own work;
5. I have acknowledged all main sources of help;
6. Where the thesis is based on work done by myself jointly with others, I have made clear exactly what was done by others and what I have contributed myself;
7. Parts of this work have been published as:

Journal Article:

On the 3D Nature of the Magpie (Aves: Pica pica) Functional Hindlimb Anatomy During the take-Off Jump

E. A. Meilak, N. J. Gostling, C. Palmer, M. O. Heller. Frontiers in Bioengineering and Biotechnology, 9, (2021)

Included in chapter 4.

Conferences:

1. **Detailed analysis of the functional anatomy of the magpie (Pica pica) reveals 3D nature of hindlimb design**
   E. A. Meilak, C. Palmer, N.J. Gostling, M.O. Heller. 11th Conference of the German Society for Biomechanics (DGfB); 03-05.04.2019; Berlin, Germany. 2019, abstract number: 153
   Included in chapter 4

2. **Is relative hindlimb muscle mass a determinant of avian take-off kinetics?**
   E. A. Meilak, C. Palmer, N. J. Gostling, M. Warner, M. O. Heller. 25th Congress of the European Society of Biomechanics (ESB), 07-10.07.2019, Vienna, Austria. 2019, abstract number: 807
   Included in chapter 5

3. **Detailed analysis of the functional anatomy of the magpie (Pica pica) reveals 3D nature of the hindlimb design**
   E. A. Meilak, C. Palmer, N.J. Gostling, M.O. Heller. 25th Congress of the European Society of Biomechanics (ESB), 07-10.07.2019, Vienna, Austria. 2019, abstract number: 847
   Included in chapter 4

4. **The 3D nature of the magpie (Aves: Pica pica) functional hindlimb anatomy revealed**
   E. A. Meilak, C. Palmer, N.J. Gostling, M.O. Heller. International Congress of Vertebrate Morphology, 21-24.07.2019, Prague, Czechia.
   Included in chapter 4

Future publications from the material in this thesis:

1. The material in chapter 5 has been submitted as a preprint research article and is under review in Royal Society Interface.
   On the hindlimb biomechanics of the avian take-off leap
   E. A. Meilak, P. Provini, C. Palmer, N.J. Gostling, M. O. Heller, (2021). On the hindlimb biomechanics of the avian take-off leap. bioRxiv, DOI: 10.1101/2021.11.19.469279

2. The material in chapter 6 has been prepared as a research journal article investigating the biomechanics of the take-off leap of the extinct *Archaeopteryx* to be submitted to Nature Communications.

Signature: ..... Date: .....

Statement of contribution

This thesis contains contributions from co-authors and collaborators as detailed below for each chapter.

Chapter 1: Erik A. Meilak, Colin Palmer, Neil J Gostling, Markus O. Heller
Writing –original draft: EAM, Writing – review and editing: E.A.M., C.P., N.J.G., M.O.H.

Chapter 2: Erik A. Meilak, Colin Palmer, Neil J Gostling, Markus O. Heller
Writing –original draft: EAM, Writing – review and editing: E.A.M., C.P., N.J.G., M.O.H., Visualization: E.A.M., M.O.H.

Chapter 3: Erik A. Meilak, Colin Palmer, Neil J Gostling, Markus O. Heller
Writing –original draft: EAM, Writing – review and editing: E.A.M., C.P., N.J.G., M.O.H..

Chapter 4: Erik A. Meilak, Colin Palmer, Neil J Gostling, Markus O. Heller
Conceptualization: E.A.M., C.P., N.J.G., M.O.H., Methodology: E.A.M., M.O.H., Formal analysis: E.A.M. M.O.H, Investigation: E.A.M., M.O.H., Data curation: E.A.M., N.J.G., M.O.H., Writing – original draft: E.A.M., M.O.H., Writing – review and editing: E.A.M., C.P., N.J.G., M.O.H., Visualization: E.A.M., M.O.H., Funding acquisition: C.P., N.J.G., M.O.H.

Chapter 5: Erik A. Meilak, Pauline Provini, Colin Palmer, Neil J Gostling, Markus O. Heller
Conceptualization: E.A.M., P.P., C.P., N.J.G., M.O.H., Methodology: E.A.M., P.P., M.O.H., Formal analysis: E.A.M., P.P., M.O.H, Investigation: E.A.M., P.P., M.O.H., Data curation: E.A.M., P.P., M.O.H., Writing – original draft: E.A.M., P.P., M.O.H., Writing – review and editing: E.A.M., P.P., C.P., N.J.G., M.O.H., Visualization: E.A.M., M.O.H., Funding acquisition: P.P., C.P., N.J.G., M.O.H.

Chapter 6: Erik A. Meilak, Neil J Gostling, Colin Palmer, Pauline Provini, Markus O. Heller
Conceptualization: E.A.M., P.P., C.P., N.J.G., M.O.H., Methodology: E.A.M., P.P., M.O.H., C.P., Formal analysis: E.A.M., M.O.H, Investigation: E.A.M., M.O.H., Data curation: E.A.M., P.P., M.O.H.,

Statement of contribution

Writing – original draft: E.A.M., N.J.G., M.O.H., Writing – review and editing: E.A.M., P.P., C.P., N.J.G., M.O.H., Visualization: E.A.M., M.O.H., Funding acquisition: C.P., N.J.G., M.O.H.

Chapter 7: Erik A. Meilak, Colin Palmer, Neil J Gostling, Markus O. Heller
Writing –original draft: EAM, Writing – review and editing: E.A.M., C.P., N.J.G., M.O.H.

Acknowledgements

I would like to express my gratitude to my supervisor, mentor and friend Markus Heller, who always made time to discuss the project and offer guidance. He took me under his wing and taught me what it means to be a scientist, for this, I am grateful.

My thanks to my co-supervisors Neil Gostling and Colin Palmer for their constant support and contribution without which this project would not have taken off.

I am grateful to Pauline Provini for a truly seamless and fruitful collaboration and for swiftly replying to my many queries and questions throughout this project.

My thanks go to all my friends who joined me on this journey in the Bioengineering Research student office. I could not have asked for a friendlier environment in which to work and will always relish the memories of lavishly decorating the office at Christmas in truly remarkable styles. To my dear friends Sara Ferri and Gareth LuTheryn, I cannot express how much I valued our conversations, laughs and practical jokes; I could not have done this without you. My thanks to Tom Mabey for always offering help whenever I needed it and for the genius puns that got me through the day. I will miss the weekly catch-ups at the pub with David Price, thank you for your support and friendship.

I would like to thank the kayaking community for giving me the opportunity to indulge in my passion for kayaking, without which I would have gone mad.

Finally, I would like to thank family, especially my parents, Manuela and Andrew Meilak for teaching me to be curious and instilling me with a hard work ethic, I could not have done this without you.

Definitions and Abbreviations

ABAD ..... abduction/adduction

ACS ..... anatomical coordinate system

AoR ..... axis of rotation

BW ..... bodyweight

CE ..... contractile velocity

CoM ..... centre of mass

CoP ..... centre of pressure

CoR ..... centre of rotation

CV ..... coefficient of variation

DoF ..... degree of freedom

EPB ..... extant phylogenetic bracketing

FE ..... flexion/extension

GRF ..... ground reaction force

ID ..... inverse dynamics

IER ..... internal/external rotation

IK ..... inverse kinematics

IR ..... infrared

JCS ..... joint coordinate system

OPA ..... ordinary Procrustes analyses

PEC ..... parallel elastic component

RoM ..... range of motion

SD ..... standard deviation

SEC ..... series elastic components

XRoMM ..... X-ray reconstruction of moving morphology

Chapter 1 Thesis overview

Chapter 1 An overview of the background and significance of the research and an outline of the organisation of the thesis.

1.1 Background and significance

Birds (Aves) are one of the most successful extant tetrapod vertebrates clades, containing over 10,000 species (Prum et al., 2015). The evolutionary path of birds from their carnivorous dinosaurian ancestors to small feathered specialist fliers is now one of the most studied and best understood evolutionary transitions. However, the evolution of birds has been a subject of great debate since Darwin published "On the Origin of Species" in 1859 (Darwin, 1859). It is generally accepted that birds evolved from theropod dinosaurs and that the formation of the avian body plan occurred over millions of years whereby the key avian characteristics essential for flight were gradually assembled (Burgers and Chiappe, 1999; Brusatte et al., 2014; Brusatte et al., 2015).

Archaeopteryx, the first bird, recognised as such since the 1860s, by Thomas Henry Huxley (Huxley, 1868), and more recently confirmed in 2013 by Godefroit, *et al.*, (2013) (Godefroit et al., 2013), encompassed many of the key traits that define a bird (Ostrom, 1976; Sereno and Chenggang, 1992; Padian and Chiappe, 1998; Mayr et al., 2005; Brusatte et al., 2014; Foth et al., 2014). The avian characteristics, defining *Archaeopteryx* as the first bird, the bipedal posture, asymmetric vaned flight feathers, the furcula (wishbone), and wings evolved in its dinosaurian ancestors. The take-off, a crucial phase of flight requiring energy-intensive motion to accelerate in to the air, of basal birds such as *Archaeopteryx,* is a subject of great debate, intrinsically linked to the evolution of birds (Burgers and Chiappe, 1999; Dyke et al., 2013; Heers, 2013; Voeten et al., 2018).

Over ten distinct hypotheses have been published on the evolution of avian flight but few proposed that the take-off behaviour of basal avians is still seen in extant birds today (Heers, 2013). The jumping model, first proposed by Garner (1999) and expanded upon by Earls (2000), suggests that the first birds were jumping with enough velocity that they could use their feathered forelimbs to extend their jump trajectory (Garner et al., 1999; Earls, 2000). Earls reported on the ground take-off jumps of small extant birds, starling *Sturnis vulgaris* and quail *Coturnix coturnix*, discovering that both taxa produce 80-90% of take-off velocity with the hindlimbs. Jumping to take to the air is a behaviour still commonly used by modern birds today, whilst explaining the evolutionary pressure for a more developed wing to evolve. The jumping model offers the most tangible, testable and simplest hypothesis putting the least restrictions on the predicted behaviour of *Archaeopteryx*.

Computational biomechanical analysis is an effective method to determine internal mechanical parameters in a musculoskeletal system which are otherwise very difficult to measure (Frankel and Nordin, 2001; Hall, 2007) and thus is the ideal approach to investigate the avian take-off jump. Musculoskeletal models are often developed using dedicated CT and MRI scans and a combination of techniques to quantify skeletal and muscle geometry (Heller et al., 2001b; Heller et al., 2005; Taylor et al., 2006; Delp et al., 2007; Seth et al., 2011; Trepczynski et al., 2012; Seth et al., 2018).

The computationally efficient inverse approach (Anderson and Pandy, 2001; Heller et al., 2001b) relies on measured external forces (kinetics) and motion data (kinematics) to drive an inverse dynamics analysis to calculate the external joint moments that the muscles need to balance in order to generate the measured forces and motion.

Kinematics and kinetics of the avian hindlimb jump and terrestrial locomotion have been recorded over a wide phylogenetic range of birds. However, despite the availability of techniques and data necessary to simulate the avian take-off leap, to date, there has been no study into the internal hindlimb joint mechanics of a flying bird as it leaps into the air. Furthermore, using the extant phylogenetic bracketing (EPB) technique, musculoskeletal models of extant avians, including *Archaeopteryx*, have been characterised by drawing data from extant relatives *(Allen et al., 2021)*. Extending the rationale of using data on extant animals to inform on extinct taxa, the jumping capability of the extinct *Archaeopteryx* could be tested by driving a musculoskeletal model with kinematics and kinetics data of extant avians. Such an approach of biomechanically simulating the take-off leap and inferring the ability for a jumping take-off for *Archaeopteryx* has the potential to add evidence towards a ground-up hypothesis for the evolution of avian flight.

1.2 Organisation of the thesis

Chapter 1 provides an overview of the background and significance of the research and an outline of the organisation of the thesis.

Chapter 2 offers an introduction describing the key areas of research that this thesis explores. A summary of the evolution of avian flight, with a particular focus on the hind limbs, is presented followed by a description of the role of biomechanical analyses in the study of avian behaviour. Finally, an overview of approaches used to relate morphology from extant species to extinct is presented.

Chapter 3 outlines gaps in the subject knowledge and specific aims and objectives of the study.

Chapter 4 presents a computational biomechanical model of the magpie, *Pica pica*, to quantify the functional hindlimb anatomy in leaping birds. Here, comprehensive analyses considering key sources of uncertainty provided robust estimates for the moment-generating capacity of its pelvic muscles and demonstrated substantial capability for internal/external rotation as well as flexion/extension, revealing that avian hip muscle function is not limited to the sagittal plane. This chapter has been published in Frontiers in Bioengineering and Biotechnology:
Meilak, E.A., Gostling, N.J., Palmer, C., and Heller, M.O. (2021). **On the 3D Nature of the Magpie (Aves: Pica pica) Functional Hindlimb Anatomy During the Take-Off Jump**. Frontiers in Bioengineering and Biotechnology 9. DOI: 10.3389/fbioe.2021.676894

Chapter 5 describes how a computational musculoskeletal model of the zebra finch, *Taeniopygia guttata*, hindlimb was developed and driven with previously published take-off ground reaction forces and 3D kinematics. This first biomechanical model to study the internal biomechanics necessary for take-off used an inverse dynamics approach to calculate the external moments at the ankle, knee, and hip joints and contrasted these to the cumulative capacity of the hindlimb muscles to balance these moments across a range of take-off conditions. This chapter reports substantial external moments at the hip and ankle joints, reaching magnitudes of about two times the values previously reported during the running of a flightless bird. This chapter is under review in Royal Society Interface and has been submitted as a preprint:

Meilak, E.A., Provini P., Palmer C., Gostling, N.J., and Heller, M.O. (2021). **On the hindlimb biomechanics of the avian take-off leap**. bioRxiv, DOI: 10.1101/2021.11.19.469279

Chapter 6 tests the leaping ability of *Archaeopteryx* to become airborne. By carefully adapting a published model of *Archaeopteryx* to reflect the novel understanding of avian hindlimb kinematics and kinetics developed here, the capability of *Archeopteryx* to leap is confirmed, obtaining robust estimates of the maximum take-off velocity powered by their hind limbs. Using a conservative approach to integrate contributions of hindlimbs and wings we demonstrated that *Archaeopteryx*, taking successive leaps like a living bird, could generate sufficient velocity with its hindlimbs to reach the minimum sustainable flight speed within two to three hops. This chapter was prepared for submission to Nature Communications.

Chapter 7 offers a concise summary of the essential contributions of the thesis, its limitations, and recommendations for future research.

Chapter 2 Literature review

Chapter 2 An introduction describing the key areas of research that this thesis explores. A summary of the evolution of avian flight, with a particular focus on the hind limbs, is presented followed by a description of the role of biomechanical analyses in the study of avian behaviour. Finally, an overview of approaches used to relate morphology from extant species to extinct is presented.

2.1 Evolution of birds

The evolution of birds has been a subject of great debate since Darwin published "On the Origin of Species" in 1859 (Darwin, 1859). It is accepted that birds evolved from theropod dinosaurs and that the formation of the avian body plan occurred over millions of years whereby the key avian characteristics essential for flight (miniaturisation, lengthening of forelimbs and evolution of the flight feather) were gradually assembled (Gatesy and Middleton, 1997; Burgers and Chiappe, 1999; Brusatte et al., 2014; Brusatte et al., 2015). The evolutionary path of birds from their carnivorous bipedal ancestors to small feathered specialist fliers is now one of the most studied and best understood evolutionary transitions. With a new species of dinosaurs being discovered on average every week, it is currently the golden age of dinosaur discovery (Brusatte, 2017). Fossil characteristics of discoveries are fed into cladistical analyses which inform phylogenetic trees mapping the evolutionary path of dinosaurs.

Cladistics is a method of classifying taxa according to shared characteristics and has been used to produce phylogenetic trees (under parsimony) to map the evolution of theropods (Baron et al., 2017). It is well established in the scientific community that birds evolved from a clade of dinosaurs called the theropods (Chiappe, 2009; Brusatte et al., 2015; Brusatte, 2017). Theropods were bipedal carnivores that varied greatly in size from the gigantic tyrannosaurs to the smaller corvid-sized *Archaeopteryx* (Yalden, 1984; Brusatte et al., 2015).

The phylogenetic tree that maps the evolutionary path of theropods, and therefore modern-day birds, is continually being changed as new fossil discoveries are made and technology advances. For example, previously it was believed that dinosaurs were split into two sister groups; Saurischia (having a reptilian-like pelvis) which included theropods and sauropods (like *Diplodocus)*, and Ornithischia (having a bird-like pelvis, for example, *Stegosaurus*). However, a study by Baron et al. (2017) changed the dinosaurian phylogenetic tree by conducting a phylogenetic analysis of the largest and most complete dataset on basal dinosaurs. Theropods are now placed within a new group, Ornithoscelida, which includes the Ornithischians but not the Sauropods (Figure 1).

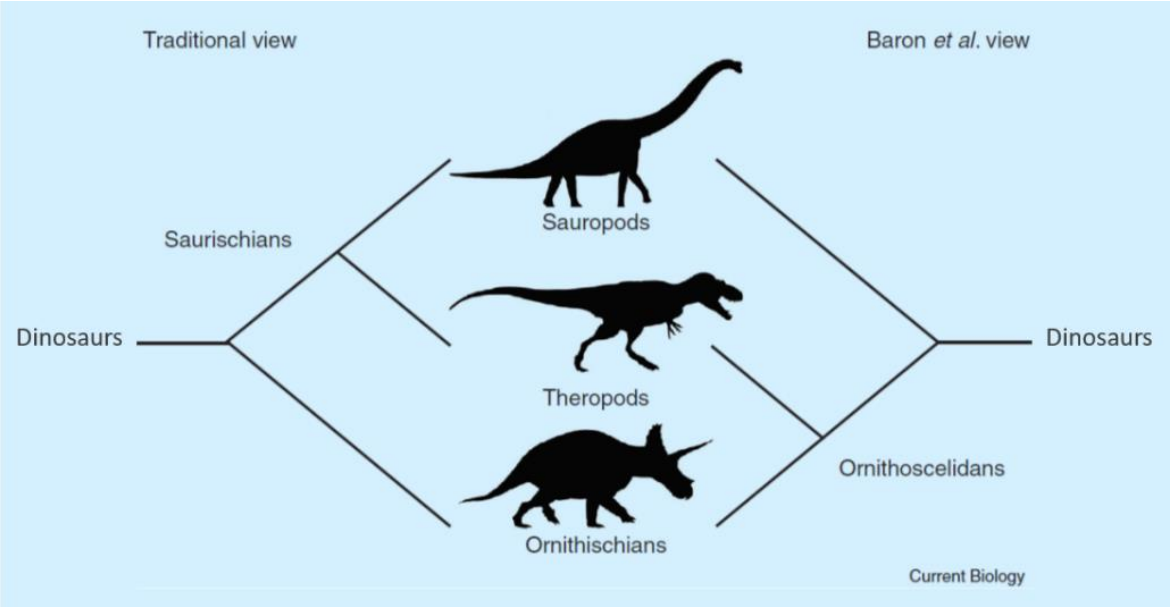

Figure 1 Differences between the 'traditional' phylogenetic tree of dinosaurs, grouping sauropods and theropods (saurischians) and the new tree rendered by Baron et al. (2017) grouping theropods and ornithischians (ornithoscelidans) (Brusatte, 2017). New fossil discoveries allow new data to feed into cladistical analyses that redefine the evolutionary path of birds. Figure adapted from Brusatte (2017).

Despite the updating phylogenetic tree, it is widely accepted that birds (Aves) belong within the clade of theropods, descending from smaller subgroups: the Coelurosauria, Maniraptora (Holtz, 1996) and Paraves (Figure 2). The avian body plan evolved gradually over millions of years (Figure 2), and once established allowed comparatively rapid evolution due to the success that flight brought to the family (Brusatte et al., 2014; Jarvis et al., 2014). *Archaeopteryx*, the first bird, recognised as such since the 1860s, by Thomas Henry Huxley (Huxley, 1868), and confirmed in 2013 by Godefroit et al. (2013) (although it remains in a position that is affected by each discovery), encompassed many of the key traits that define a bird (Ostrom, 1976; Sereno and Chenggang, 1992; Padian and Chiappe, 1998; Mayr et al., 2005; Brusatte et al., 2014; Foth et al., 2014). The avian characteristics, defining *Archaeopteryx* as the first bird, the bipedal posture, asymmetric vaned flight feathers, the furcula (wishbone) and wings evolved in its dinosaurian ancestors (Figure 2). However, *Archaeopteryx* lacks a keeled sternum; has a shoulder joint that would not allow dorsal elevation of the wings beyond the horizontal; has poor extensive pronation of the wing; and a relatively lower degree of feather asymmetry, when compared with extant birds (Olson and Feduccia, 1979; Poore et al., 1997; Senter, 2006; Zheng et al., 2014; Mayr, 2017; Voeten et al., 2018). Furthermore, the pygostyle (fused tail) and beak, both characteristics that make flying birds lightweight and well adapted for flying, evolved further down the avian lineage (Brusatte et al., 2015). However, *Archaeopteryx* could fly (Alonso et al., 2004), yet how proficient and powerful a flyer *Archaeopteryx* was, remains the topic of discussion (Burgers and Chiappe, 1999; Nudds and Dyke, 2010; Paul, 2010; Voeten et al., 2018).

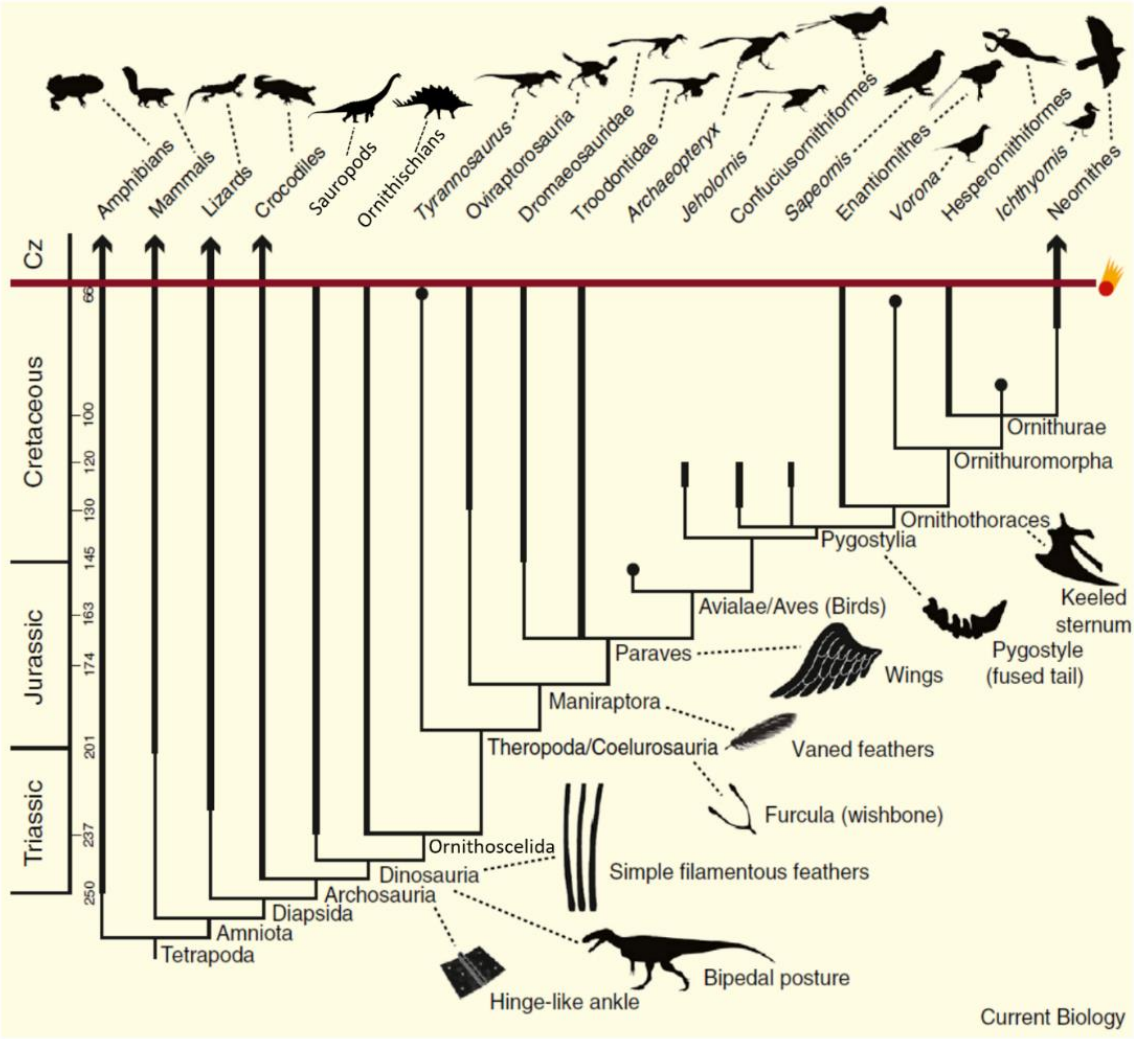

Figure 2 Summary phylogeny showing where birds fit into the vertebrate family tree. Many of the anatomical characteristics that define the bird and allow flight evolved gradually over millions of years for non-flight purposes. Timescale values are in millions of years; thick red line denotes mass extinction at the Cretaceous-Paleogene boundary caused by asteroid impact; arrows denote lineages that survived the extinction; circles represent species known from a particular point in time; thick line sections of branches indicate direct fossil evidence and thin lines are temporal distributions implied by phylogenetic ghost lineages; Cz, Cenozoic interval after the end-Cretaceous extinction. Figure adapted from Brusatte et al. (2015).

2.2 Evolution of avian flight

2.2.1 Hypotheses on the evolution of avian flight

One of the key morphological traits observed in *Archaeopteryx* fossils, which defines the bird is the avian wing, here defined as a feathered forelimb used to fashion aerofoils for flight purposes (Brusatte et al., 2015). The vaned feather and the wing evolved for non-flight purposes, probably for display, thermoregulation or egg brooding (Koschowitz et al., 2014; Brusatte et al., 2015). However, how basal birds such as *Archaeopteryx* used their wings to fly is a key question, intrinsically linked to the evolution of birds. Specifically, the take-off of basal birds, a crucial phase of flight requiring energy-intensive motion to accelerate into the air, is a subject of great debate (Burgers and Chiappe, 1999; Dyke et al., 2013; Heers, 2013; Voeten et al., 2018).

Many of the hypotheses on the evolution of avian flight focus specifically on the question of take-off (Ostrom, 1976; Cowen and Lipps, 1982; Padian, 1982; Caple et al., 1983; Padian and Chiappe, 1998; Burgers and Chiappe, 1999; Garner et al., 1999; Earls, 2000; Videler, 2000; Peters, 2002; Dial, 2003; Long et al., 2003; Zhang and Zhou, 2004; Zhou, 2004; Videler, 2006; Dial et al., 2008; Dyke et al., 2013). The ground-up and trees-down (cursorial and arboreal, respectively) theories have often been a common way of categorising the hypotheses. Cursorial hypotheses encompass those whereby the basal bird in which avian flight first evolved (be it *Archaeopteryx* or otherwise) was bipedal and took to the air from the ground through flapping. Arboreal hypotheses include those in which the nodal ancestor took to the air from the trees and glided, which is a behaviour observed in flying squirrels and reptiles (Garner et al., 1999; Russell et al., 2001; Bishop, 2008; Heers, 2013). The model suggests that the first birds jumped from higher elevations and glided to another lower place. There was a loss of altitude with each glide, eventually reaching the ground, forcing the bird to climb to another high point, tree, hill, or, cliff, to be able to glide between points again(Chatterjee and Templin, 2003; Dial, 2003; Long et al., 2003; Zhou, 2004; Longrich, 2006). However, the “ground-up vs. trees-down” dichotomy is increasingly viewed as outdated and “hindering research” as extant birds exhibit both behaviours, which are not mutually exclusive (Padian, 2001; Hutchinson and Allen, 2009; Martyniuk, 2012).

To make sense of the many hypotheses on the evolution of avian flight, the take-off behaviour of birds today is compared to the proposed take-off behaviour of basal avians (Heers, 2013). Although take-off strategies of many extant bird taxa are not well documented, those of a wide phylogenetic range of land birds, ranging from relatively more derived Passeriformes to the more basal Galliformes have been investigated (Figure 12). However, the take-off of large water birds such as

swans have not been scientifically studied and at best there is anecdotal evidence of their laboured take-off strategy.

Long powerful hindlimbs are a characteristic birds inherited from their theropod ancestors therefore it is hypothesised that basal birds would have used their well-developed hindlimbs to their advantage when trying to perform a ground take-off and therefore would require full engagement of the hindlimb. Ground take-off (as opposed to arboreal take-off) is considered likely because the ancestors of basal birds have anatomy adapted for cursorial locomotion, therefore it follows that they would take to the air from the ground (Hutchinson and Allen, 2009). Moreover, a recent phylogenetic study by Field and colleagues (2018) concluded that all modern birds evolved from taxa exhibiting predominately non-arboreal behaviours.

Table 1 Review of hypotheses on the evolution of avian flight, with a focus on the role of the hindlimb. Hypotheses in which the inherited, long powerful hindlimb is the primary take-off driver are highlighted; "Thrust generation for faster running", "Running on water", "Wings for stability" and "Jumping model". Table adapted from Heers (2013).

hypothesis		role of the hindlimbs	is the hindlimb the primary take-off driver?	proposed behaviour still observed in extant avians?
intraspecific fighting	Cowen and Lipps (1982)	legs have little to no essential role	✗	✗
flutter gliding	Long et al. (2003)		✗	✗
insect net	Ostrom (1976)	precise jump	✗	✗
predatory strike	Padian (1985)		✗	✗
thrust generation for faster running	**Burgers and Chiappe (1999)**	run at a specific speed	✓	✗
running on water	**Videler (2006)** **Videler (2000)**		✓	✗
wing assisted incline running (WAIR)	Dial (2003)	ground traction	✗	✓
controlled flapping descent	Dial et al. (2008)		✗	✓
forelimb propelled leaping biped	Padian (1982)	running jump	✗	✗
wings for stability	**Caple et al. (1983)**		✓	✗
ridge gliding	Peters (2002)		✗	✓
pouncing proavis	Garner et al. (1999)	two-footed standing jump	✗	✗
jumping model	**Earls (2000)**		✓	✓
arboreal gliding	Norberg (1985) (Chatterjee and Templin, 2003) Xu and Wang (2003) Jarvis et al. (2014) Zhou (2004) Dyke et al. (2013)	climbing tree	✗	✗

2.2.2 The role of the hindlimb in the evolution of avian flight and the importance of jumping

Of all the hypotheses on the evolution of avian flight (See Heers (2013) for review), four rely on the hindlimb as the primary driver for taking-off from the ground; thrust generation for faster running, running on water, wings for stability and the jumping model (Caple et al., 1983; Burgers and Chiappe, 1999; Earls, 2000; Videler, 2000) (Table 1). Considering that basal avians inherited long powerful hindlimbs from their theropod ancestors, and under the hypothesis that the first birds would have used their hindlimbs when taking to the air, we focus on the hypotheses which rely on the hindlimb as the primary locomotor, all involving running, jumping or a combination of both. What follows is a brief review of these hypotheses, with an additional review on wing assisted incline running (WAIR). Although WAIR does not rely solely on the hindlimb as the primary take-off driver, it describes a behaviour observed in extant avians to this day and is included for completeness (Dial, 2003; Heers et al., 2018).

2.2.2.1 Thrust generation for faster running

Burgers and Chiappe (1999) hypothesised that the flapping wings of *Archaeopteryx* were used to provide enough thrust to allow for faster running, eventually resulting in *Archaeopteryx* taking off as the residual lift from the wings could support its weight. The authors' hypothesis relies on the assumption that force migration occurs. It is assumed that, as velocity increases and the residual lift relieves the hindlimbs from supporting body weight, velocity would still increase, some thrust supplied from the legs and some from the wings. However, as the vertical force migration occurs, logic suggests that the hindlimbs would lose traction and velocity would decrease. No study on the biomechanics of its hindlimb has shown whether this motion could be sustained at take-off speed. Additionally, this hypothesis proposes a behaviour that has never been observed in extant birds today, no bird uses its wings to run faster (Heers, 2013). Nonetheless, a detailed study on the running capabilities of *Archaeopteryx,* especially at low levels of traction, would assist in crediting the assumption that the vertical force migration would result in running speed acceleration.

2.2.2.2 Running on water

The "running on water" hypothesis proposes that *Archaeopteryx* was able to slap its feet on the water in a similar method observed in the Jesus Christ lizard (common basilisk, *Basiliscus basiliscus*), so named for its ability to run across bodies of water (Videler, 2000; 2006). By slapping its feet rapidly against the water's surface, *Archaeopteryx* could have used its wings to provide some lift, allowing it to traverse further along the water. The hypothesis originated from the fact that all 12 *Archaeopteryx* fossil specimens were found in marine deposits, giving rise to the idea that

Archaeopteryx were shorebirds that crossed bodies of water. However, the fact that no specimens were found in non-marine deposits does not necessarily mean that all members of this species exclusively lived in marine habitats. Although the proposed evolutionary mechanism is named after extant common basilisk, this is a behaviour also observed in aquatic birds that slap their feet on the water's surface while they take off (Heers, 2013).

2.2.2.3 Wings for stability

Caple et al. (1983) hypothesised that animal flight requires a high degree of neuro-muscular control, therefore the transition of a feathered forelimb to a wing was to control lift, thrust and drag and that each stage of avian flight evolution was to better the animal's coordination. "Wings for stability" postulates that *Archaeopteryx* ran to take to the air, relying on the assumption that *Archaeopteryx* could run at its maximum speed, calculated by Taylor's model as a function of estimated mass and not its hindlimb anatomy (Taylor, 1973). The proposed take-off mechanism requires *Archaeopteryx* to jump from a single foot whilst running, which would part angular momentum onto the animal about the roll axis, resulting in incorrectly positioned feet for optimal landing. However, the author's reason that reports of a lizard that can jump from two feet after an initial run could mean that *Archaeopteryx* might have done the same and then would have used its wings to control the flight trajectory. However, the proposed behaviour of a running jump, followed by a gliding descent, controlled by the wings is not observed in extant birds today (Heers, 2013).

2.2.2.4 Wing assisted incline running (WAIR)

WAIR has been proposed as one way for the 'ground up' models to lead to flight (Dial, 2003; Baier et al., 2013). Adult partridges and their chicks can ascend a slope, more easily, by flapping their wings as they run. The model continues, with strong enough flapping and fast running, flight was achieved. The problem this model suffers with is a lack of intention to fly, flapping harder to get up the slope causes flight, but it is more than required simply to get up the hill, which is the desired outcome. In the case of the adult modern birds observed displaying the behaviour, they can already fly but are choosing not to. WAIR does not equal and does not lead to flight in modern birds either, it is instead actively *not flying*.

2.2.2.5 Jumping model

The jumping model, first proposed by Garner (1999) and expanded upon by Earls (2000), suggests that the first birds were jumping with enough velocity that they could use their feathered forelimbs to extend their jump trajectory (Garner et al., 1999; Earls, 2000). Earls reported on the ground take-

off jumps of small extant birds, starling *Sturnis vulgaris* and quail *Coturnix coturnix*, discovering that although they use different jumping techniques to take to the air (Figure 3), both taxa produce 80-90% of take-off velocity is with the hindlimb.

Earls was the first to hypothesise that jumping could have been the mechanism for the origin of avian flight: the nodal ancestor was jumping, no matter the reason, and any downward motion from a feathered forelimb after the start of a leap could add height or distance to the otherwise ballistic path of the leap. The direct ancestors of birds were small theropod dinosaurs which would have become prey items themselves unless they could evade capture.

More than 10 distinct mechanisms have previously been proposed to address the evolution of avian flight (Heers, 2013). Other than the jumping model, thrust generation for faster running, running on water and wings for stability are the hypotheses that rely on the hindlimb as the primary thrust generator. Both the thrust generating for faster running and the wings for stability hypotheses propose behaviours not observed in extant birds. The motion of slapping feet on the water, proposed in the running on water hypothesis, is seen in aquatic birds but these use specialised aquatic morphology, such as webbed feet, of which there is no evidence seen in *Archaeopteryx*.

The hypotheses most relevant to extant animals are wing assisted incline running (WAIR), gliding (trees down/arboreal hypothesis) and jumping models (Chatterjee and Templin, 2003; Dial, 2003; Long et al., 2003; Zhou, 2004; Longrich, 2006). The problem with which both of these models suffer is that there is some element to teleology, an intention to fly, flapping harder to get up the slope causes flight, but it is more than required simply to get up the hill, which is the desired outcome. Similarly, with the trees down hypothesis, flight evolves to avoid the resultant need for a climb. The problem is that neither model is evolutionarily testable.

The jumping model offers the most tangible, testable simplest, alternative to the WAIR and the gliding models, putting the least restrictions on the predicted behaviour of *Archaeopteryx*. Jumping to take to the air is a behaviour still commonly used by modern birds today, whilst explaining the evolutionary pressure for a more developed wing to evolve; the better the wing, the further the protobird could extend its trajectory, escaping predation, surviving to reproductive age, passing on better and more developed flight apparatus down the line. Additionally, we have a mechanism that supports this idea and has been tested for the last 162 years, Natural Selection. All organisms actively try to survive, and as such, a small, feathered animal, with powerful legs could jump out of the way of danger. Adding in a flap from its feathered forelimbs could extend the distance of the jump. As stated, this exact behaviour is seen in living birds as they take off from the ground. Is it a plausible mechanism for the evolution of flight in the earliest bird?

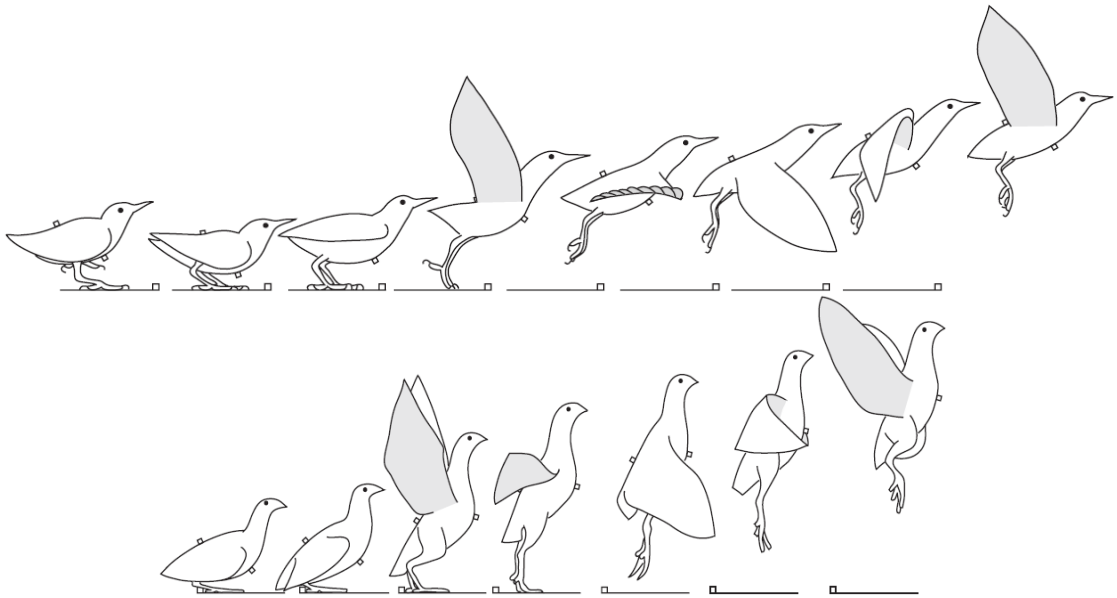

Figure 3 Different jump techniques of the starling Sturnis vulgaris and quail Coturnix coturnix. Top: body position of starling during the countermotion ground take-off jump with a peak jumping force of 4 times body weight. Bottom: quail during the squat ground take-off jump with a peak jumping force of 8 times body weight. Figures adapted from Earls (2000). However, in both take-offs, 80-90% of take-off velocity is powered by the hindlimb.

2.3 Biomechanical analysis methods

2.3.1 The biomechanics of jumping

Biomechanics is the study of anatomical and functional aspects of biological and physiological systems by using the principles of mechanics (Frankel and Nordin, 2001; Hall, 2007) and thus a biomechanical approach is an ideal method to investigate the avian take-off jump. There are three jumping techniques observed in the animal kingdom; the squat jump (legs are rapidly extended from a static crouching position), countermovement jump (legs are flexed before the extension) and the catapult jump (elastic energy is stored and then released) (Alexander, 1995). Birds, like all vertebrates, cannot perform the catapult jump however some (like the starling *Sturnis vulgaris*) do perform the countermovement technique to improve the otherwise less effective squat jump (used by e.g. quail Coturnix coturnix, Figure 3) (Alexander, 1995; Earls, 2000). The difference in efficiency between the two jump strategies is reflected in the maximum ground reaction forces applied; where the starling exerts a peak ground force of four times bodyweight (BW), the quail exerts eight BW. It is essentially unknown how *Archaeopteryx* took to the air therefore having access to a range of different avian take-off behaviours, and associated variation in take-off mechanics appears to be of critical importance for the investigation of the evolution of avian flight.

2.3.2 Assessing the musculoskeletal function of animals

Essential structures that determine the function of musculoskeletal systems are the bones, the muscles, and the joints that connect body segments. By characterising biomechanical aspects of these three elements and relating them to each other, subject-specific computational biomechanical musculoskeletal models can be developed and analysed, offering quantitative insight into the musculoskeletal function of animals (Nigg et al., 2000; Mow and Huiskes, 2005).

2.3.2.1 Methods for characterising the mechanics of bones

Although there are a few methods for characterising bone geometry such as surface scanning, Computed Tomography (CT) scanning or Magnetic Resonance Imaging (MRI), CT scanning offers a more accurate and precise identification of bone from image data. However, CT scanning is a method of utilising X-rays to non-destructively 3D image the internal structure of an object with a micron-level spatial resolution (Figure 4). Where the radiation is not a concern CT scanning is the preferred choice for characterising bone geometry for musculoskeletal analysis purposes (Taylor et al., 2006; O'Neill et al., 2013; Rankin et al., 2016; Charles et al., 2018).

When describing a 3D musculoskeletal model it is necessary to not only obtain detailed information about the morphology of individual bones but also to collect accurate data on the relative position and orientation of the bones to each other. Scanning a specimen with either all soft tissue attached or at least with joint cartilaginous and ligamentous tissue still intact serves to maintain the passive constraints to the joint to the maximum extent possible and is, therefore, the preferred approach to musculoskeletal imaging (Hutchinson et al., 2015; Otero et al., 2017; Manafzadeh and Padian, 2018).

Bone has a hierarchical structure, ranging from nanoscale to macroscale (greater than microscale) and within a single bone, the material properties vary greatly, for instance between the spongy cancellous bone and the mostly solid cortical bone where e.g. the elastic modulus is known to vary from as little as 1.0 to as much as 17 GPa (Speirs et al., 2007; Sharir et al., 2008; Currey, 2012).

Essential material properties such as Young's modulus and Poisson's ratio can be determined by subjecting a sample of the material to well-controlled loading conditions while recording the resulting deformation (Sharir et al., 2008). Once the material properties are known, computational models can be developed to estimate the mechanical behaviour of the entire bone which encompasses not only the material properties but the shape of the bone also (Rohlmann et al., 1980; Rohlmann et al., 1982; Duda et al., 1998; Speirs et al., 2007; Helgason et al., 2008; Trabelsi et al., 2011). However, given the rather small deformations of bone under load (Perillo-Marcone and Taylor, 2006; Speirs et al., 2007) compared to the much more substantial displacements of joints during locomotion, analyses that aim to determine muscle and joint forces typically consider bones as rigid bodies (Heller et al., 2001a; Heller et al., 2001b; Taylor et al., 2006; Arnold et al., 2009; Hutchinson et al., 2015; Rankin et al., 2016; Bishop et al., 2018a). This simplified rigid body assumption for the behaviour of bones will also be adopted for the musculoskeletal analyses in this thesis.

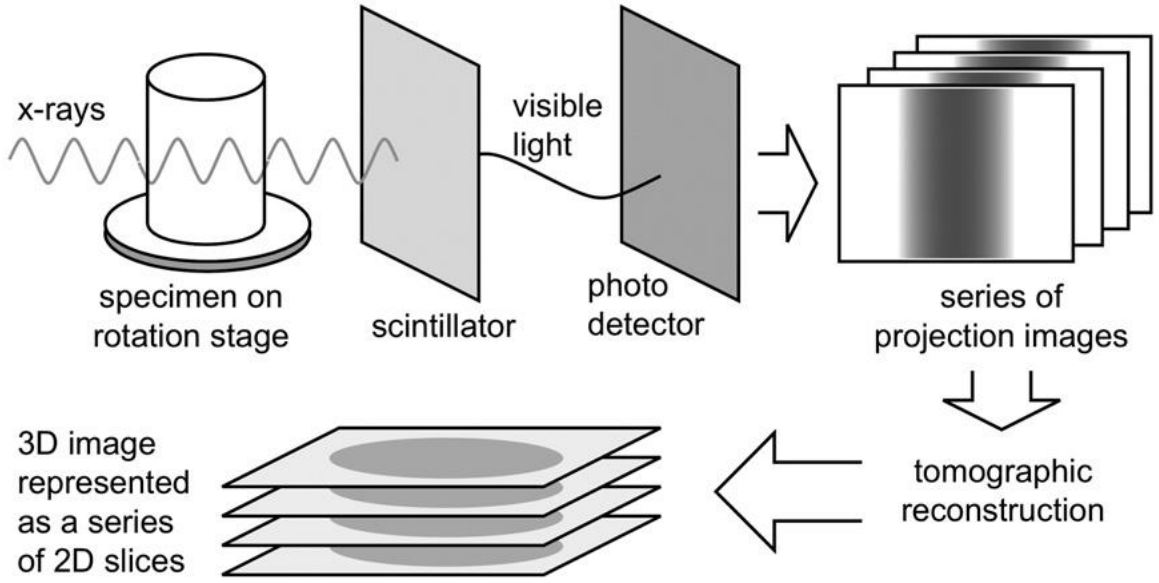

Figure 4 Diagram of X-ray CT acquisition and reconstruction processes. X-ray projection images are acquired and mathematically reconstructed to produce a 3D map of X-ray absorption in the volume. The 3D map is typically presented as a series of 2D slice images. Figure from (Landis and Keane, 2010).

2.3.2.2 Methods for characterising the biomechanical function of joints

In computational biomechanical musculoskeletal models, limbs are modelled by linking rigid body segments through functional joints and it is useful to characterize joints according to their movement capabilities (Hall, 2007). Freely moveable joints, also called synovial joints, (as opposed to immovable or slightly moveable joints) are formed by two or more articulating bone surfaces covered by articular cartilage, surrounded by an articular capsule containing lubricating synovial fluid (Hall, 2007). There are several types of synovial joints such as gliding, hinge, pivot, condyloid, saddle, and ball and socket joints which differentiate the number and nature (rotational or translational) of the degrees of freedom associated with them. These variations in type are brought about by variations in the geometry of the articular bone, cartilage, ligaments, muscles and tendons, which all interact to define the motion of a biological joint and their constraints (Frankel and Nordin, 2001; Hall, 2007). However, such requirements may be relaxed for conditions when the detailed articular motion of a joint has been measured directly (Brainerd et al., 2010; Kambic et al., 2014; Kambic et al., 2017; Provini and Abourachid, 2018) and the contribution of the passive forces to the internal loading conditions is expected to be small (Brand et al., 1986; Brand et al., 1994; Heller et al., 2001b; Taylor et al., 2006; Trepczynski et al., 2012; Trepczynski et al., 2018).

When developing computational musculoskeletal models, it is important to carefully balance the benefits of greater fidelity that would result from using models with a larger number of degrees of freedom against the challenges of accurately identifying small joint excursions. If for example, only limited (small number of markers) and very noisy motion data with large measurement uncertainty was available, a simplified model of the knee joint that only allowed 1 rotational degree of freedom, and no translation at all, could be the most appropriate as degrees of freedom with a small excursion (internal/external rotation, translation) cannot be robustly identified from such data (Delp et al.; Delp and Loan, 2000; Delp et al., 2007; Arnold et al., 2009). However, it is important to ensure that joint axes of rotation match as closely as possible to the functional physiological axes of rotation at the joint and robust methods to derive such axes are well-known in the literature (Taylor et al., 2005; Ehrig et al., 2006; 2007; Ehrig and Heller, 2019). In reality, joint centres and axes of rotation will be dynamic over the functional range of motion of a joint, therefore the mean position is often used to approximate the joint axes (Allen et al., 2017).

2.3.2.3 Methods for characterising the force and moment-generating capacity of skeletal muscles

Skeletal muscles apply moments about joints by contracting, resulting in moving or stabilising the joint. Muscles are the only tissue that can actively produce tension by contracting and pulling on bones (Hall, 2007). Muscles attach to tendons, which in turn attach to bone and the mechanical

behaviour of a muscle-tendon unit is often approximated by defining the units specific behaviours and properties (Hall, 2007).

A Hill–type model is commonly used to characterise a muscle-tendon unit with three elements; a Series Elastic Components (SEC), Parallel Elastic Component (PEC) and a Contractile Element (CE) (Figure 5). The elastic components describe the musculotendinous unit's extensibility and elasticity properties (Figure 5) (Hall, 2007). The PEC provides resistance when a muscle is passively stretched and SEC provides resistance due to the tendons which store elastic energy when a tensed muscle is stretched. The model requires four parameters (optimal fibre length, maximum isometric force, pennation angle and tendon slack length) to scale generic muscle property curves to predict the force generation of the muscle-tendon unit (Zajac, 1989; Arnold et al., 2009). Muscle fibre length and pennation angle (the angle the muscle fibres are oriented to the force-generating axis of the muscle) are often measured physically during dissection using digital callipers and protractors, respectively (Verstappen et al., 1998; Hutchinson et al., 2015).The maximum isometric force of a muscle is the maximum contractile force the muscle can exert and can be directly related to the physiological cross-sectional area (PCSA) (Hutchinson, 2004b; Nelson et al., 2004). PCSA can be calculated as a function of muscle mass, pennation angle, fibre length and muscle density, which can all be directly measured from the individual muscle (Hutchinson et al., 2015). One of the muscle parameters that musculoskeletal models are most sensitive to is tendon slack length (Charles et al., 2016). Tendon slack length can be measured physically from the dissected specimen (Verstappen et al., 1998) or a numerical optimisation method can be used based on joint range of motion (RoM) (Manal and Buchanan, 2004; Rankin et al., 2016).

To estimate their moment-generating capacity, muscles are often modelled as polylines spanning origin and insertion while via points are sometimes added to fully describe their 3D paths (Jensen and Davy, 1975; Duda et al., 1996; Heller et al., 2001b; Taylor et al., 2005; Delp et al., 2007; Arnold et al., 2009; Trepczynski et al., 2012; Trepczynski et al., 2018). The moment that a muscle applies about a joint axis is determined by the product of the contractile force it is applying and the instantons moment arm about that joint axis (Delp and Loan, 2000; Delp et al., 2007). The instantaneous moment arm can be defined as the minimum distance between the line of action of a muscle and the centre of rotation of the joint axis. A method for calculating muscle moment arms in a biomechanical model is by using a generalized force method (Sherman et al., 2010; Sherman et al., 2013) and is the method used in OpenSim, an open-source software for conducting biomechanical analysis on musculoskeletal models (Delp et al., 2007; Seth et al., 2018).

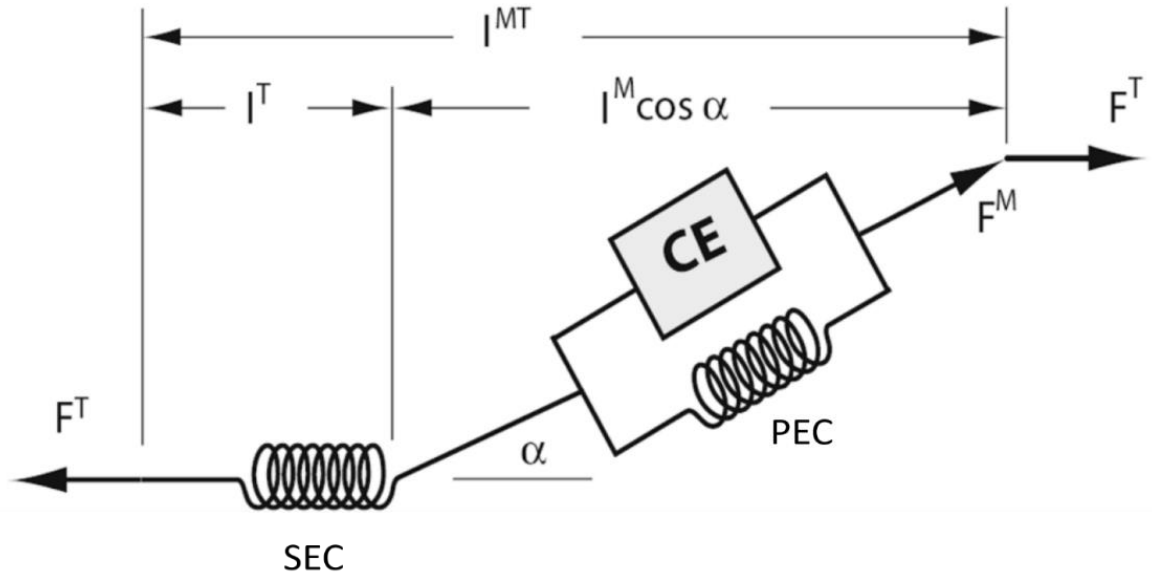

Figure 5 Hill-type model of a musculotendinous unit modelled as a configuration of elastic components and a contractile component to model how the unit mechanically behaves. This Hill-type model is used to estimate tendon and muscle force, comprising of a Series Elastic Component (SEC) and Parallel Elastic Component (PEC) with a contractile element (CE). The muscle-tendon length (l^{MT}) derived from the muscle–tendon geometry is used to compute muscle fibre length (l^{M}), tendon length (l^{T}), pennation angle (α) muscle force (F^{M}), and tendon force (F^{T}). Figure adapted from (Arnold et al., 2009).

The two main methods used to characterise the geometry of animal muscles are CT scanning stained tissue and anatomical digitisation (Duda et al., 1997a; Hutchinson et al., 2015; Allen et al., 2017; Charles et al., 2018). Irrespective of the method, the geometry of a muscle can be described by its attachment sites on the bone surface and its 3D path between its origin and insertion (Jensen and Davy, 1975; Duda et al., 1997a).

Anatomical digitisation utilises a digitizing probe that will record points in relation to a defined coordinate system (Figure 6). A local coordinate system is defined for each bone and the probe is used to digitise the circumference of muscle attachment sites and the path of muscles (Duda et al., 1997a; Hutchinson et al., 2015). This method can only be conducted if the hindlimb is dissected to allow access to the bone and the muscle tissue. CT scanning in comparison is a non-destructive process to visualise bone and soft tissue. However, due to the limited soft-tissue contrast, identification of individual muscles is improved by contrast enhancement through e.g. diffusible iodine solution (Figure 7) (Gignac and Kley, 2014; Vickerton et al., 2014). Such contrast-enhanced CT imaging of soft tissues is often preferred over MRI scanning in particular in small animals due to the more limited spatial resolution of MRI scans and their potential for geometric distortion (Sullivan et al., 2019).

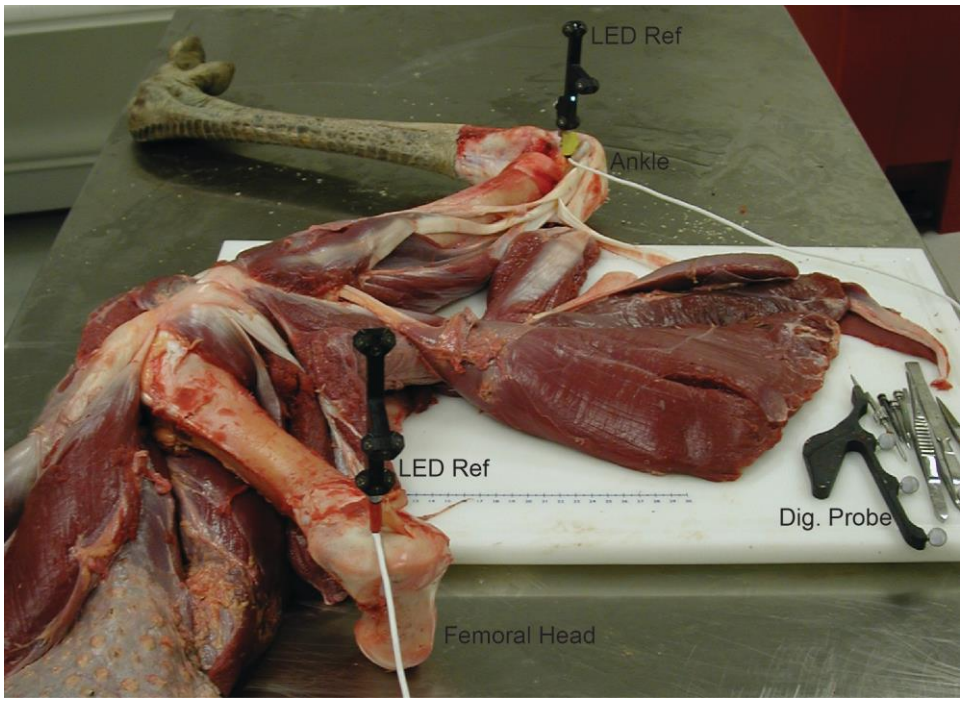

Figure 6 Digitizing apparatus used during anatomical dissection of ostrich. "LED Ref" indicates the proximal and distal reference frames, "Dig. Probe" indicates the digitizing probe used to collect landmarks used to measure muscle geometry. Figure adapted from Hutchinson et al. (2015).

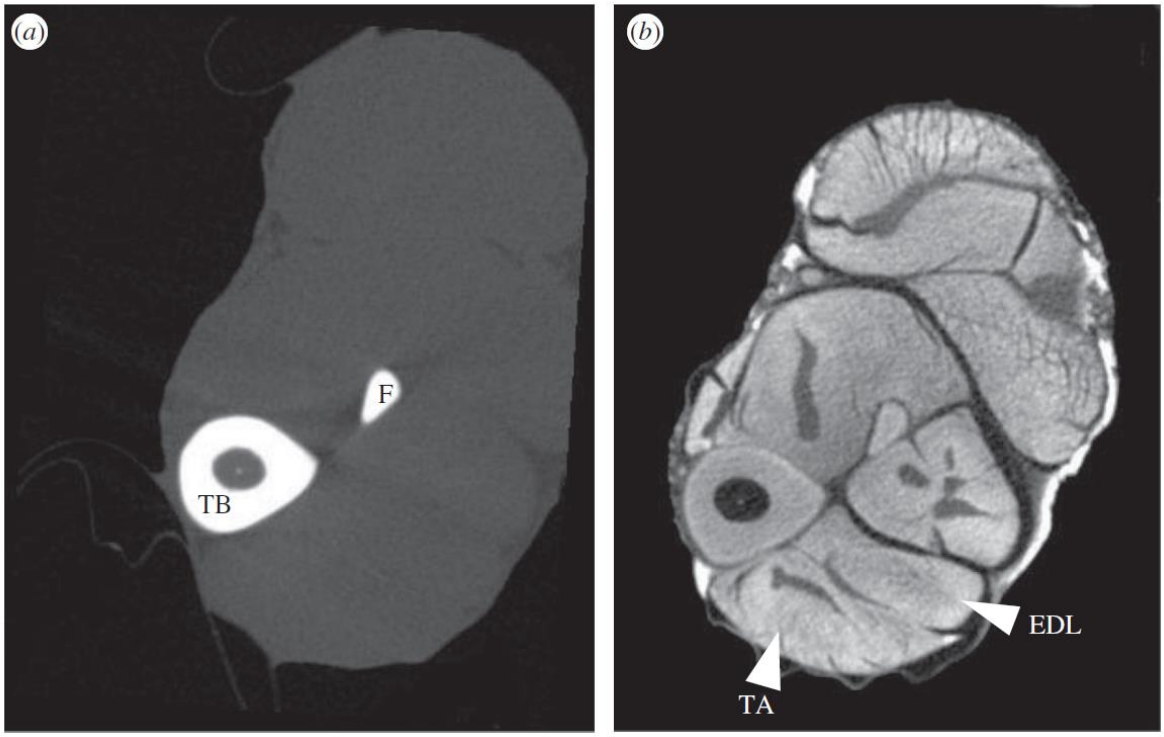

Figure 7 Mid-tibial transverse microCT scans of the rat hindlimb illustrating the difference between imaging without (a) and with (b) contrast agent (I2KI). When contrast is added individual muscles can be distinguished and segmented more easily. EDL, extensor digitorum longus; F, fibula; TA, tibialis anterior; TB, tibia. Figure adapted from Vickerton et al. (2014).

2.3.3 Computational biomechanical analysis

Key analyses of interest which are enabled by musculoskeletal models as described previously are studies into the kinematics and the internal musculoskeletal loading conditions during dynamic activities (Brand et al., 1986; Brand et al., 1994; Heller et al., 2001a; Heller et al., 2001b; Heller et al., 2003; Trepczynski et al., 2012; Trepczynski et al., 2018). Kinematics and kinetics are fields of biomechanical study essential to the analysis of the avian take-off jump. Kinematics is the quantitative study of motion, which is often broken down into the motion of individual body segments of a biological system. The field of kinetics is the study of the forces associated with motion, which in its application to the musculoskeletal system includes the study of forces applied to bone through muscles (Nigg et al., 2000; Mow and Huiskes, 2005; Hall, 2007) and the bone-on-bone contact forces at the joints which result from the interaction of external forces together with the concerted action of muscle forces (Bergmann et al., 2001; Heller et al., 2001b).

2.3.3.1 Methods for assessing animal kinematics

When capturing animal kinematics, the aim is to capture independent motions of linked rigid body segments. Such kinematic data might be acquired by methods that use directly observable visual information available which can be obtained with and without markers, or more invasive, X-ray imaging methods. Where video cameras can effectively capture kinematics measured from surface markers, X-ray imaging methods, such as biplanar fluoroscopy can capture detailed kinematics of bone motion beneath the skin, thereby avoiding issues associated with skin artefacts (Taylor et al., 2005; Brainerd et al., 2010; Lu et al., 2020). Whilst single-camera systems can typically obtain 2D kinematics information only, calibrated stereoscopic or multi-camera systems allow the reconstruction of 3D kinematic data (Pfister et al., 2014). High-speed cameras have been used to record 2D and 3D animal kinematics of various motions, including gait, running, jumping and hopping (for example Verstappen et al. (2000), Rubenson et al. (2007) and). Studies into the kinematics of birds have recorded using a range from 200Hz (Tobalske and Dial, 2000; Berg and Biewener, 2010) up to 1000Hz (Earls, 2000; Tobalske, 2004), the only trend being the larger the animal, the lower the sampling rate tended to be. To effectively capture avian take-off kinematics, which can vary in duration between 60 ms to 120 ms (zebra finch and guineafowl respectively), with sufficient data points, camera shutter frequency is an important factor to consider.

Motion capturing in animals using video-based systems has often been limited to 2D analyses, including work on the take-off behaviour of birds. Here, Verstappen and colleagues (2000) recorded the terrestrial locomotion of the magpie using high-speed cameras (500 Hz) to derive sagittal joint motion of the hind limbs (flexion/extension). An overlay 2D stick model was used to reduce errors in the manual digitising of hindlimb joint locations when the joints were not visible such as during

periods when covered by wings. The authors note that there were larger errors for joints most obscured by soft tissues and the wings (i.e. the hip and knee) compared with other body points but suggested that the errors were not large enough to invalidate the results (Verstappen et al., 2000) although no formal corroboration of that suggestion was provided.

To effectively capture 3D body segment motion, a minimum of three markers must be tracked for each segment (Taylor et al., 2006; Provini and Abourachid, 2018). Both reflective tape and paint have been used as skin markers when recording animal kinematics, with no reported advantage for either method. For example, Earls (2000) used small reflective markers to measure the take-off kinematics of the starling and quail, while Charles and colleagues (2016, 2018) used white paint to mark the joint locations on mice. Retro-reflective markers (illuminated and recorded with infrared (IR) light) are used almost exclusively on large animals such as sheep, dogs, and horses, where kinematics are often recorded using dedicated multi-camera motion capture systems (Besier et al., 2003; Taylor et al., 2005; Taylor et al., 2006; Rubenson et al., 2010; Lu et al., 2020; Byström et al., 2021; Söhnel et al., 2021). A key problem shared by all approaches that attach markers on the skin of a subject is that the skin can move relative to the skeletal structure underneath, resulting in an error in the skeletal kinematics derived from such noisy skin-mounted markers (Cappozzo et al., 1996; Alexander and Andriacchi, 2001; Taylor et al., 2005).

Fluoroscopy is a method using X-rays to image the skeletal structures of a moving object and biplanar fluoroscopy, as a stereoscopic variant of the technology, has been used to record the 3D kinematics of avian gait (Kambic et al., 2014) and ground take-off (Provini and Abourachid, 2018). The X-Ray Reconstruction of Moving Morphology (XRoMM) process involves recording animal kinematics using multiple x-ray videography systems, merged with skeletal morphology data from bone scans (Brainerd et al., 2010). The process allows the recording of detailed skeletal kinematic data using implanted tantalum bead markers. By rigidly attaching markers to the bone, soft tissue artefacts are minimized. When bones cannot be implanted with at least three markers, the positions and orientations of bones cannot be tracked directly and are derived by methods such as scientific rotoscoping, where 3D surface models of the bones are interactively fitted to the fluoroscoipy data (Brainerd et al., 2010; Gatesy et al., 2010; Provini and Abourachid, 2018). To obtain detailed models of skeletal anatomy that can be fit to the X-Ray video kinematic data CT scans are often obtained after euthanising the animals (Brainerd et al., 2010; Gatesy et al., 2010).

The 3D kinematic data can then be used to drive a biomechanical model of the musculoskeletal system of the animal. This process of linking the recorded motion to the degrees of freedom available in the computational model is called inverse kinematics (Delp et al., 2007). For marker-based studies, the 3D position of such markers through time is matched to similar positions defined

on the musculoskeletal model while surface-based studies match vertex positions across the entire bone surface. The placement of markers and the degrees of freedom of the joints in the biomechanical model interact to define the accuracy of the kinematics derived from the inverse kinematics method. For marker-based fluoroscopy procedures, metallic markers are attached directly to the skeleton to reduce error from soft tissue movement (e.g. Provini and Abourachid (2018)) and thus increase the accuracy of the derived skeletal kinematics data. However, the secure attachment of markers to the bone is achieved through surgical procedures. Although animals are given enough time to recover from surgical procedures it has been suggested that the implantation of markers may be associated with a limp (Provini, 2021) suggesting that there may be a trade-off between obtaining accurate bone kinematics and capturing unimpaired locomotion.

2.3.3.2 Methods for assessing ground reaction forces in animals

The method most commonly used in assessing the external kinetics (the ground reaction forces and moments) during the locomotion of animals, small and large, are force platforms. Different technologies (strain gauges, piezoelectric elements) are available to measure external kinetics and the most developed products allow for the measurement of the time-varying 3D forces, their location in space (centre of pressure, CoP) and the free moment acting between the animal and its environment (Figure 8). The measurement of such data suggests that the external forces during leaping of birds reach values of multiples of body weight (Earls, 2000; Tobalske and Dial, 2000; Tobalske, 2004; Provini et al., 2012) and therefore form an essential input into more detailed analyses of the internal musculoskeletal loading conditions (Hall, 2007; Lund and Hicks, 2012a; 2015).

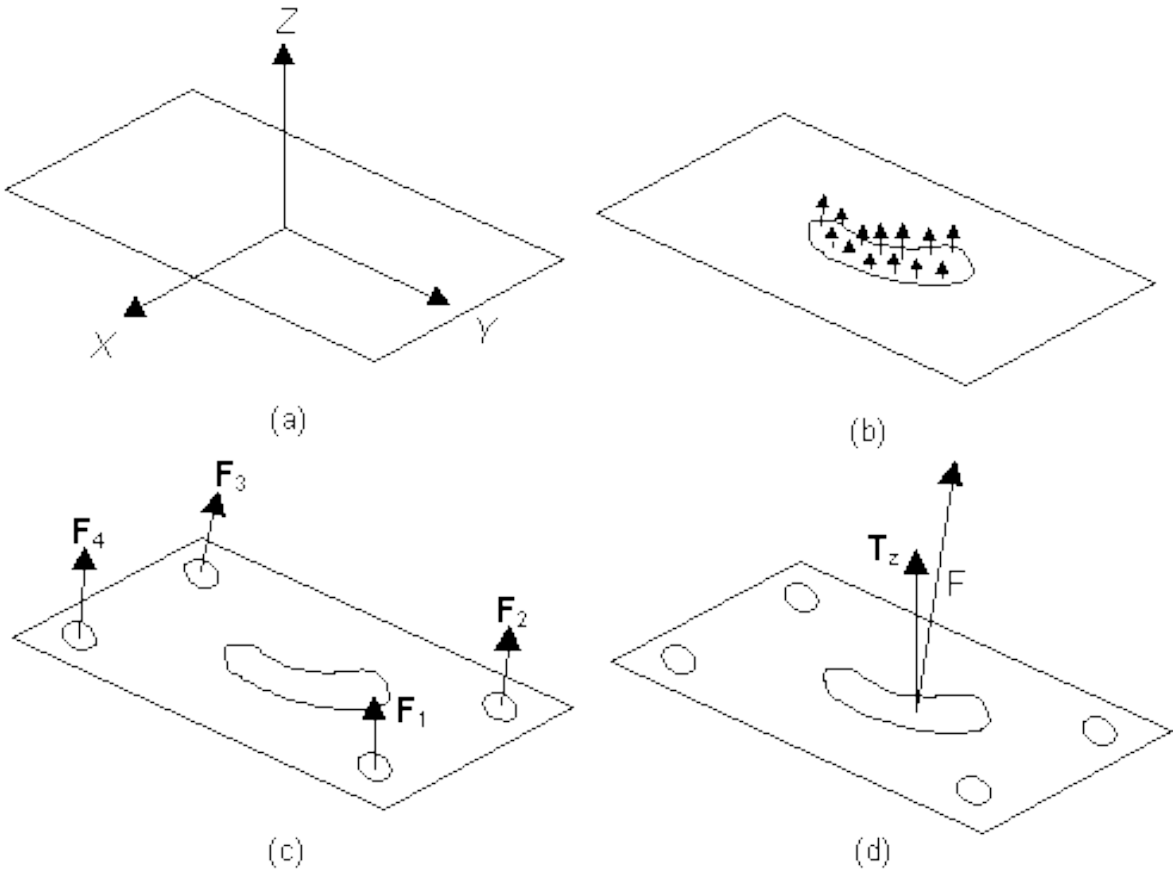

Figure 8 Diagram illustrating the function of a force plate with four strain gauge force transducers positioned in the corners of the device (c). All the forces acting between the foot and the ground are summed to produce a single ground reaction force vector (F) and a free torque vector (Tz) (d) with respect to the force plate origin (a). The point of application of the ground reaction force on the plate is the centre of pressure (CP). All the small reaction forces collectively exert on the surface of the plate at the CP (b). Figure from (Kwon, 2018)

2.3.3.3 Internal moment and force analyses

2.3.3.3.1 Inverse kinematics

An inverse kinematic (IK) analysis matches experimental kinematic data to a constrained biomechanical model to produce joint and body kinematic data (i.e. a pose) that best matches the kinematic data (Grochow et al., 2004; Lund and Hicks, 2012b). There are many methods used for IK analysis (see Aristidou and Lasenby (2009) for review), including the Newton methods, (based on second order Taylor series expansion method (Kwan Wu et al., 1997; Fletcher, 2013), Sequential Monte Carlo methods (Courtny and Arnaud (Courty and Arnaud, 2008)) and Jacobian Inverse methods . The latter family of methods is utilised by the OpenSim (an open-source software that allows the computational biomechanical analyses of musculoskeletal models including IK (Pizzolato et al., 2017; Seth et al., 2018)) IK tool through a weighted least squares approach to minimize errors between experimental markers and those attached to the model at each time step. Certain markers can be weighted differently to determine which ones are to be considered more important or reliable than others. The goodness of fit is reported by the maximum and RMS marker errors that can guide the optimisation of the marker weighting values (Lund and Hicks, 2012b).

2.3.3.3.2 Inverse dynamics

Dynamics is the study of systems where acceleration is involved and also covers kinematics and kinetics (Nigg et al., 2000; Mow and Huiskes, 2005; Hall, 2007). When external kinematics and kinetics are used to drive a simulation, to calculate internal joint moments and forces, this is an inverse dynamics (ID) approach. Inverse dynamics takes the prescribed motion (e.g. IK data), mass and inertia of a biomechanical system along with experimental ground reaction forces to predict the forces and moments that cause said motion. Equations of motion (derived from the mathematical musculoskeletal model) are used to iteratively solve for the resulting net forces and moments at the joints (Chao and Rim, 1973). Where the analysis is dependent on acceleration of the bodies, derived from differentiated noisy position data, the outcome of the analysis is sensitive to sufficient smoothing of the input data (Cahouët et al., 2002). The results of ID analysis can be used to estimate how muscles are used to produce the prescribed motion (Erdemir et al., 2007). The ID tool incorporated into the OpenSim software reports the joint moments that muscles need to produce to balance the external moments being applied by the external kinetics. The analysis works on the assumption that at each point in time the biomechanical system is in static equilibrium, i.e. the muscles need to produce equal moments at the joints acting in the opposite directions as the joint moments being applied by the external kinetics (Duda et al., 1997a; Taylor et al., 2006; Goetz et al., 2008; Lund and Hicks, 2012a; Pizzolato et al., 2017).

2.3.3.3.3 Muscle optimisation

An extension to the inverse dynamics approaches that further resolves the external net joint moments into individual muscle forces is offered by static or dynamic optimization techniques (Crowninshield, 1978; Challis, 1997; Heller et al., 2001b; Seth et al., 2011; Lund and Hicks, 2015). Static optimisation considers the forces and moments acting on the biomechanical system at each time point and calculates the muscle activation and contractile force to balance the external moments being applied to each joint degree of freedom as calculated through inverse dynamics analysis (Crowninshield, 1978; Brand et al., 1986; Brand et al., 1994) Static optimization finds the solutions that will balance the biomechanical system whilst attempting to find the solution that requires e.g. the minimum amount of activation across muscles. The results of a static optimization analysis are used to estimate muscle forces at any moment in time and bone-on-bone contact forces. Static optimization techniques have been used to estimate muscle forces in the hind limbs of large animals (Duda et al., 1997a; Taylor et al., 2005; Taylor et al., 2006) and to estimate muscle activation profiles and muscle forces for a prescribed motion in small rodents (Rankin et al., 2016), confirming their usefulness to gain quantitative insight into the musculoskeletal loading conditions across a range of species.

The forces of all muscles spanning a joint are key contributors to the surface-on-surface contact forces occurring at each joint. Here, directly measured joint forces using advanced implants can provide critical information about the validity of the joint forces predicted by the computational models (Bergmann et al., 2001; Heller et al., 2001a; Kutzner et al., 2011; Trepczynski et al., 2012; Trepczynski et al., 2018). Limitations in diminishing the size of the measurement devices have so far precluded their use for such validation purposes except select large animal studies (Taylor et al., 2006). Although the calculation of actual muscle and joint contact forces offers a most comprehensive picture of the internal loading musculoskeletal conditions (Duda et al., 1997b; Heller et al., 2001a), the solution of the associated optimisation problem not only requires an appropriate choice of the optimisation criterion (Dul et al., 1984; Kaufman et al., 1991; Glitsch and Baumann, 1997; Prilutsky et al., 1997; Heintz and Gutierrez-Farewik, 2007; Rode et al., 2016; Sohn and Ting, 2016; Trepczynski et al., 2018; Afschrift et al., 2019) but may also necessitate the subject-specific identification of numerous parameters for each musculo-tendon unit such as the tendon slack length, the contractile velocity, pennation angle, optimal fibre length and maximum isometric force before the accurate estimation of joint contact forces becomes possible (Manal and Buchanan, 2004; Modenese et al., 2016; Serrancolí et al., 2016; Bishop et al., 2021a; Bishop et al., 2021b). As a result, the estimation of muscle and joint forces requires estimating a much more substantial number of parameters than an analysis focussing on a comparison of the external joint moments to the muscle's moment-generating capacity (Rankin et al., 2016). Especially for

conditions when the validation of predicted muscle and joint forces against direct measurements is not possible, focussing on a less muscle optimisation methods is preferable.

2.3.3.3.4 Sensitivity analysis of estimates of a muscles' moment-generating capacity

When characterising the musculoskeletal anatomy of an animal through a model, it is important to be aware of errors in the estimated geometry, i.e. errors in determining the locations of the origin and insertion areas and in describing the 3D muscle paths, and to quantify how sensitive model predictions are to such errors (O'Neill et al., 2013; Charles et al., 2016). Although it has been noted that estimates of a muscles' moment arms are most sensitive to errors in the identification of the insertion site as opposed to the origin (O'Neill et al., 2013) and the need for robust sensitivity analyses to establish musculoskeletal models has been recognised, Hutchinson et al. (2015) comment on how the accuracy of avian musculoskeletal models remain unresolved and how no sensitivity analysis on the avian hindlimb has been carried out.

A musculoskeletal model comprises many factors and sensitivity analyses have been conducted to measure the model sensitivity to force-generating parameters (Charles et al., 2016) and indeed the optimization techniques used to assess said model (Rankin et al., 2016). Charles and colleagues (2016) reported that the maximum isometric muscle moment is most sensitive to tendon slack length and coordinates of the muscle insertion, therefore in agreement with O'Neill and colleagues (2013). To date, there has been no reported sensitivity analysis on the musculature of the hindlimb muscles of any flying or flightless bird.

2.3.4 Extant avian hindlimb functional anatomy and biomechanics

2.3.4.1 Long bones of the hind limbs

The long bones of the avian hind limbs are the femur, tibiotarsus, fibula, and tarsometatarsus (Figure 9). Although research has been conducted on the relative leg lengths of avian hindlimb bones, the bulk of research has focussed on birds that possess terrestrial locomotor styles presumably similar to their ancestral state (Gatesy and Biewener, 1991; Hutchinson, 2004b; Hutchinson, 2004a; Doube et al., 2012). For those birds, Gatesy and Biewener (1991) suggest that the femur comprises a smaller percentage of the overall pelvic (hind) limb length in larger birds than in smaller ones (e.g. 20% for the ostrich *Struthio camelus* vs. 30% in the Chinese painted quail E*xcalfactoria chinensis*). However, the study was grossly weighted towards larger terrestrial birds (flightless and burst fliers composing of 77% of the study and fliers only 10%) and in how far the results can be generalised to avians more generally remains to be determined.

Passeriformes (passerines) includes over 5000 species of bird, making up approximately 60% of all bird species (Ricklefs, 2012; Selvatti et al., 2015), and within this larger group, the Corvidae (corvids) have been extensively studied, from behaviour to biomechanics and more. Data from research documenting the osteology of European corvids shows that within a single phylogenetic family the relative length of hindlimb long bones do not change, despite the overall leg lengths within the family varying by more than a factor of 2 and, mass a quantity by over an order of magnitude (Figure 10) (Tomek and Bochenski, 2000). A very recent study that took the crown group Otidmorphae and plotted the range of hindlimb indices (where the hindlimb index is defined das (tarsometatarsus length + tibiotarsus length)/femur length) found that arboreal species had comparatively smaller hindlimb indices compared with non-arboreal ones with typical values for the former found to be in range of 2.2 to 2.6 while values for the latter varied from 2.6 to 3.8 (Zeffer, 2003; Field et al., 2018). Species which exhibited mixed cursorial and arboreal habits had hind limb indices ranging between 2.3 to 2.8. The hindlimb indices of European corvids appear to the observations that corvids show both arboreal and non-arboreal behaviours (Hudson, 1937; Hayes and Alexander, 1983; Verstappen et al., 2000; Field et al., 2018). For example, the crow *Corvus Corone* (440 g) and raven *Corvus corax*, (1.1 kg) have hindlimb indices of 2.75 and 2.63 respectively. By extending the analysis further to other passerines, for example, the zebra finch *Taeniopygia guttata*, 15.4 g and starling *Sturnis vulgaris* (77.3 g) (Earls, 2000), with hindlimb indices of 2.64 and 2.84 respectively, we notice a consistency in relative leg morphology that spans across the order of Passeriformes, despite a large range in mass. As there is a constancy in relative leg morphology across Passeriformes, there could also be correlations between take-off style and bony morphology which could be used to infer the possible behaviour of extant and extinct taxa whereby the only

information available is bony anatomy. Biomechanical analyses of the take-off of flying birds would aid in corroborating this hypothesis. There is a gap in the knowledge documenting the relative leg segment lengths of flying birds that take to the air from a take-off leap.

Figure 9 Emu (Dromaius novaehollandiae) hindlimb anatomy showing the functional joints (hip, knee, ankle, and subtalar joints). The avian hindlimb comprises of a primarily horizontally orientated femur and vertically orientated tibiotarsus and tarsometatarsus. This uniquely avian posture results in a primarily knee-based limb kinematics Figure adapted from Goetz et al. (2008).

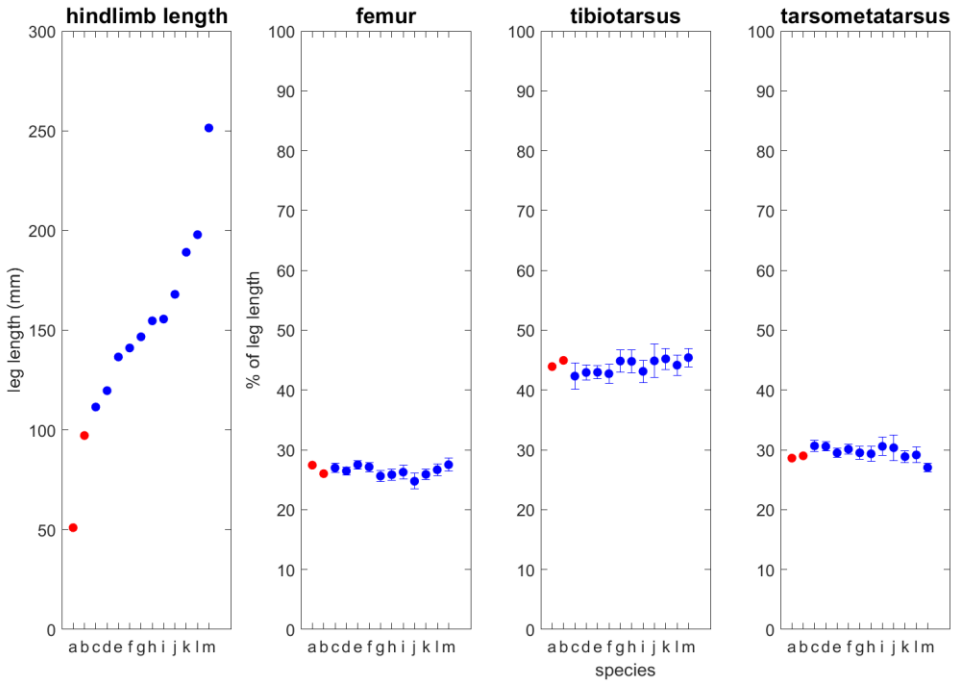

*Figure 10 Comparative hindlimb long bone lengths of European corvids (blue) with zebra finch (*Taeniopygia guttata*) starling (*Sturnus vulgaris*) (red) for comparison. Leg length varies by more than a factor of 2 within the corvid clade however no significant change in relative hindlimb segment length between species is seen. Hindlimb segment lengths as percentage of overall leg length show the mean value ± 1 standard deviation. Species in ascending order of leg length (femur + tibiotarsus + tarsometatarsus): a) zebra finch (*Taeniopygia guttata*) b) starling (*Sturnus vulgaris*) c) Cyanopica cyanus (azure-winged magpie) d) perisoreus infaustus (Siberian jay) e) nucifraga caryocatactes (Eurasian nutcracker) f) garrulus glandarius (Eurasian jay) g) corvus monedula (jackdaw) h) pyrrhocorax graculus (Alpine chough) i) Pica pica (Eurasian or common magpie) j) pyrrhocorax pyrrhocorax (chough) k) corvus frugilegus (Rook) l) corvus corone (carrion crow) m) corvus corax (Raven). Corvid data from Tomek and Bochenski (2000). Number of measurements per bone per corvid species varied, typically n=39, min n=6, max n=74. Data for the zebra finch and starling from Provini and Abourachid (2018) and Earls (2000) respectively.*

2.3.4.2 Avian myology

The myology (defined as the study of the geometry and properties of skeletal muscle) of the avian hindlimb has been explored in literature. Birds have been dissected and their hindlimb musculature qualitatively described and scaled anatomical drawings reported (Figure 11) (Hudson, 1937; Raikow, 1987; McKitrick, 1991; Verstappen et al., 1998). Detailed drawings of muscle morphology are described through images of muscle attachment sites on bones (Figure 11) and histological samples of hindlimb cross-sections taken at known locations along the hindlimb. By digitizing images of muscle attachment sites and cross-sections, the detailed 3D paths of muscles can be reconstructed with respect to bones using data available in the literature.

Myology across species of birds are largely similar. For example, the ostrich *Struthio Camelus* (Gangl et al., 2004; Hutchinson et al., 2015) shares approximately 90% of its myology with the magpie *Pica pica (Hudson, 1937; Verstappen et al., 1998),* which sits on the opposite side of the phylogenetic tree of Aves and differs largely in size, locomotion and habitat (Figure 12). Passeriformes are the largest order of birds, containing over half of all bird species (Raikow, 1987). However, there is broadly similar hindlimb musculature across all species of passerines, all following the characteristic hindlimb morphology of passerine birds (Raikow, 1987).

Quantitative parameters of particular muscles have also been measured including the PCSA, pennation angle and fibre length, although this area remains largely understudied as inter and intra-species variation has not been investigated (Bennett, 1996). Few studies have investigated the force-velocity and force-length properties of avian hindlimb muscles (Daley and Biewener, 2003; Nelson et al., 2004). Results of the force-velocity investigation yielded that shortening velocities were within the ranges published for reptilian and mammalian muscles. However, Daley and Biewener (2003) report that while the tendon morphology differs greatly between species, the stretch of the tendon relative to muscle fibre length at loads experienced during locomotion are similar across species. However, tendon behaviour during locomotion is different compared with tendon behaviour during a take-off jump. Additionally, the countermotion leap relies on the elasticity of the hindlimb tendons to improve jump performance.

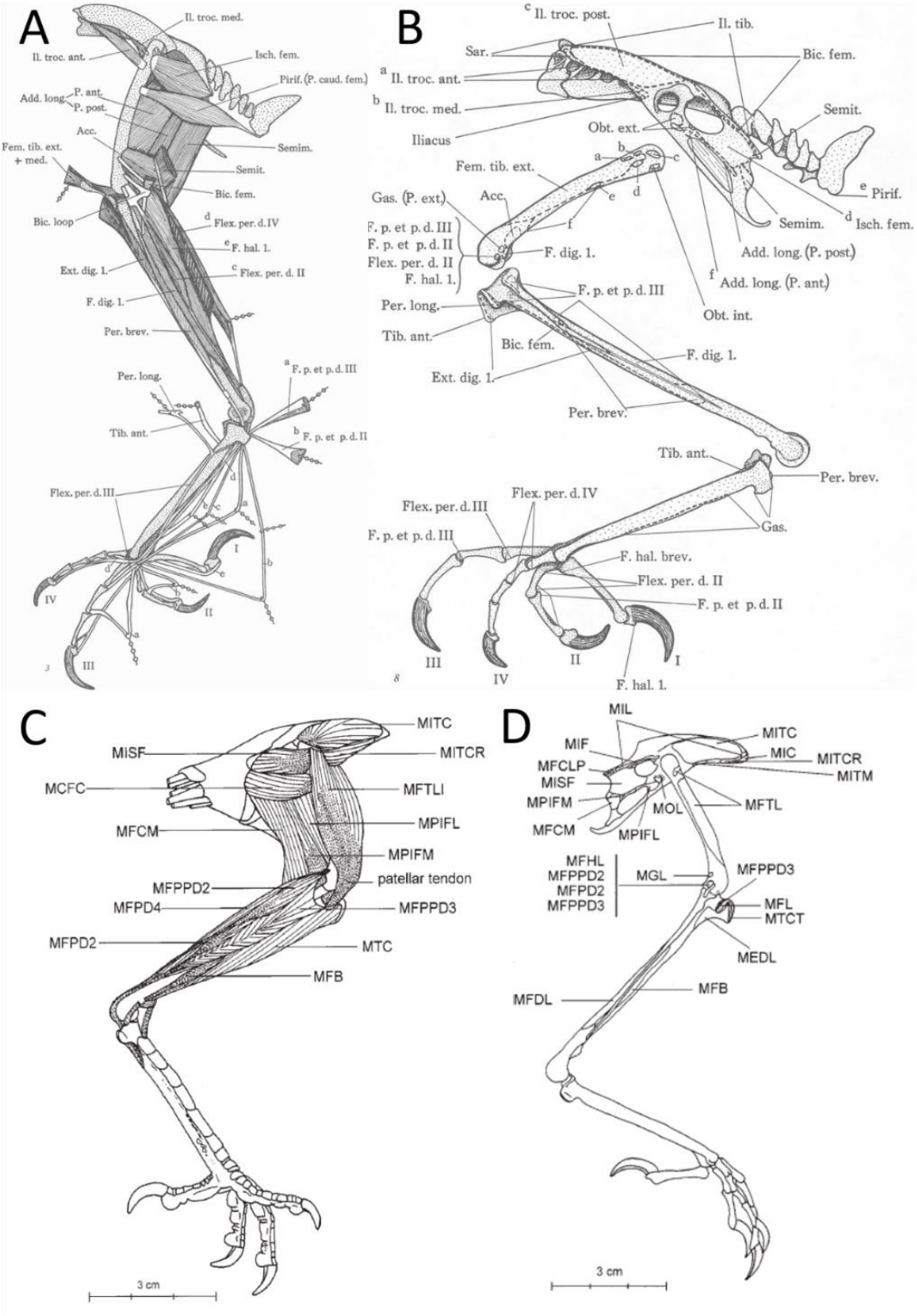

Figure 11 Example anatomical drawings of the avian hindlimb available in literature. Scaled drawings can be digitised and used to inform the geometry of a biomechanical musculoskeletal model of the avian hindlimb. A) hindlimb musculature of the crow. B) hindlimb muscle attachment sites of the crow (Hudson, 1937). C) hindlimb musculature of the magpie. D) hindlimb muscle attachment sites of the magpie (Verstappen et al., 1998).

2.3.4.3 Extant avian kinetics and kinematics

Kinematics and kinetics of the avian hindlimb jump and terrestrial locomotion have been recorded over a wide phylogenetic range of birds (Figure 12). Ground reaction forces are the most easily attainable biomechanical data, requiring relatively little work to process post-acquisition and therefore is the most available data across species. Ground reaction forces of the take-off leap of zebra finch *Taeniopygia guttata,* starling *Sturnus vulgaris,* pacific parrotlets *Forpus coelestis,* rufous hummingbird *Selasphorus rufus,* diamond dove *Geopelia cuneate,* rock dove *Columba Livia,* European migratory quail, *Coturnix coturnix* and guineafowl *Numida meleagris* are available in literature (Heppner and Anderson, 1985; Earls, 2000; Tobalske, 2004; Henry et al., 2005; Provini et al., 2012; Chin and Lentink, 2017). Of these studies, all report that the majority of the initial flight velocity is produced by the impulse imparted by the hindlimbs e.g. in small birds (starling *Sturnis vulgaris* and zebra finch *Taeniopygia guttata*) the hindlimb is responsible for 80 and 95% of take-off velocity respectively (Earls, 2000; Provini et al., 2012). Even in the smallest avian (the hummingbirds) which have disproportionally small hindlimbs and fly with an insect-like wingbeat, the hindlimb produces up to 59% of take-off velocity (Tobalske, 2004; Provini et al., 2012).

Hindlimb kinematics throughout the avian take-off leap has been recorded with skin markers on the starling and quail, revealing ankle and subtalar joint angles about flexion/extension (Earls, 2000). However, only a single study quantifying the range of motion about three rotational degrees of freedom of the hip, knee and ankle joints of the avian take-off leap has been conducted ((Provini et al., 2012)). The authors used biplanar fluoroscopy techniques (XRoMM) to record the hindlimb kinematics of the take-off of the diamond dove and zebra finch take-off leaps, tracking tantalum beads implanted on the hindlimb bones of the animal subjects. XRoMM analyses have also been used to quantify the hindlimb kinematics of the predominately ground welling guineafowl (Kambic et al., 2014; Allen et al., 2017; Kambic et al., 2017). However, whereas there is data available on the kinematics and kinetics of the avian ground take-off leap, any biomechanical musculoskeletal analyses have primarily focussed on terrestrially based birds run and gait.

There are three main joints in the avian hindlimb; the hip, knee and ankle (see Figure 9). At the end of the hindlimb, the subtalar joints link the digits to the tarsometatarsus. The horizontally orientated femur means during avian locomotion most rotation in the sagittal plane occurs at the knee instead of the hip (Carrano, 1998). Although avian hindlimb joints have been modelled as being pivotal (i.e. one degree of freedom, e.g. see Verstappen et al. (2000)) the reality is that the joints all allow at least three rotational degrees of freedom (DoF), allowing flexion/extension (FE),

internal/external rotation (IER) and abduction/adduction (ABAD), however, some are more constrained than others.

For example in the ostrich model by Hutchinson and colleagues (2015) the hip and knee are modelled to have 3 rotational DoF and the ankle 1 DoF. Studies have been conducted to observe the ranges of motion during gait and running (Hutchinson et al., 2015; Kambic et al., 2017) but are also informed by joint passive motion tested on the cadavers and conclude that when biomechanically modelling avian hindlimb joints taking 1D or 2D measurements will always be incomplete. Using external kinetics ascertained from force plates and kinematics from markers attached to the skin, simulations have been made of the flightless ostrich *Struthio camelus and* emu *Dromaius novahollandiae* (Goetz et al., 2008; Hutchinson et al., 2015; Rankin et al., 2016). In both cases, computational biomechanical musculoskeletal models of the hindlimb were used to calculate the internal moments and forces acting at the hindlimb joints. By using static optimisation methods the models predicted muscle activation and force patterns resulting in the measured kinematics and kinetics. Additionally, a biomechanical musculoskeletal model of the chicken *Gallus gallus* was characterised and static optimisation conducted to ascertain which muscles are used during normal stance (Bishop et al., 2018a).

A more recent study, investigating the ranges of motion of the hip, knee and ankle joints of the zebra finch and diamond dove throughout their take-off leaps revealed that there is a substantial range of motion about all three rotational degrees of freedom about the hip, knee and ankle joints (Provini and Abourachid, 2018). However, a large range of motion about all three rotational degrees of freedom may be based on an artefact of the definition of the joint centre. If the joint centre or axis is estimated to be significantly offset to the real functional joint centre then the resulting range of motion will be in three degrees of freedom even if the joint is only moving about one axis (Ehrig and Heller, 2019). Care must be taken to ascertain functionally accurate joint centres and axes of rotation to reduce misinterpretation of joint motion.

The antitrochanter, patella and hypotarsus are passive structures that aid in generating moments about the hip, knee and ankle joints respectively. The antitrochanter, located ventrodorsal to the acetabulum on the pelvis, provides a surface for the trochanter to articulate against. Due to the predominately flexed position of the femur, the antitrochanter passively provides an adduction moment to the hip joint (Hutchinson et al., 2015; Rankin et al., 2016; Bishop et al., 2021a).

As in humans, the avian knee joint includes a patella, which acts as a gear between the extensor muscles and patella tendon, especially during deep knee flexion. Allen et al. (2017) report that the avian patella allows relatively greater extension force but relatively lesser extension velocity than in the human knee. The posterior side of the ankle includes the hypotarsus, guiding the tendons

through constrained ossified channels, keeping them away from the joint axis of rotation and ensuring the moment arms required (Hudson, 1937; Verstappen et al., 1998). Where possible these passive structures should be incorporated in to the musculoskeletal models, especially when modelling the jump which uses a wide range of angular range of motion t the hip, knee and ankle.

However, only a single study has investigated the biomechanics of the avian jump, focussing on a predictive simulation of the ground-dwelling elegant-crested tinamou *Eudromia elegans (Bishop et al., 2021a).* However, due to the scarcity in kinematics and kinetics of the tinamou leap, which an inverse analysis would rely on, the authors opted for a forward approach to predict the leaping behaviour. To date, there has been no study into the internal hindlimb joint mechanics of a flying bird as it leaps into the air.

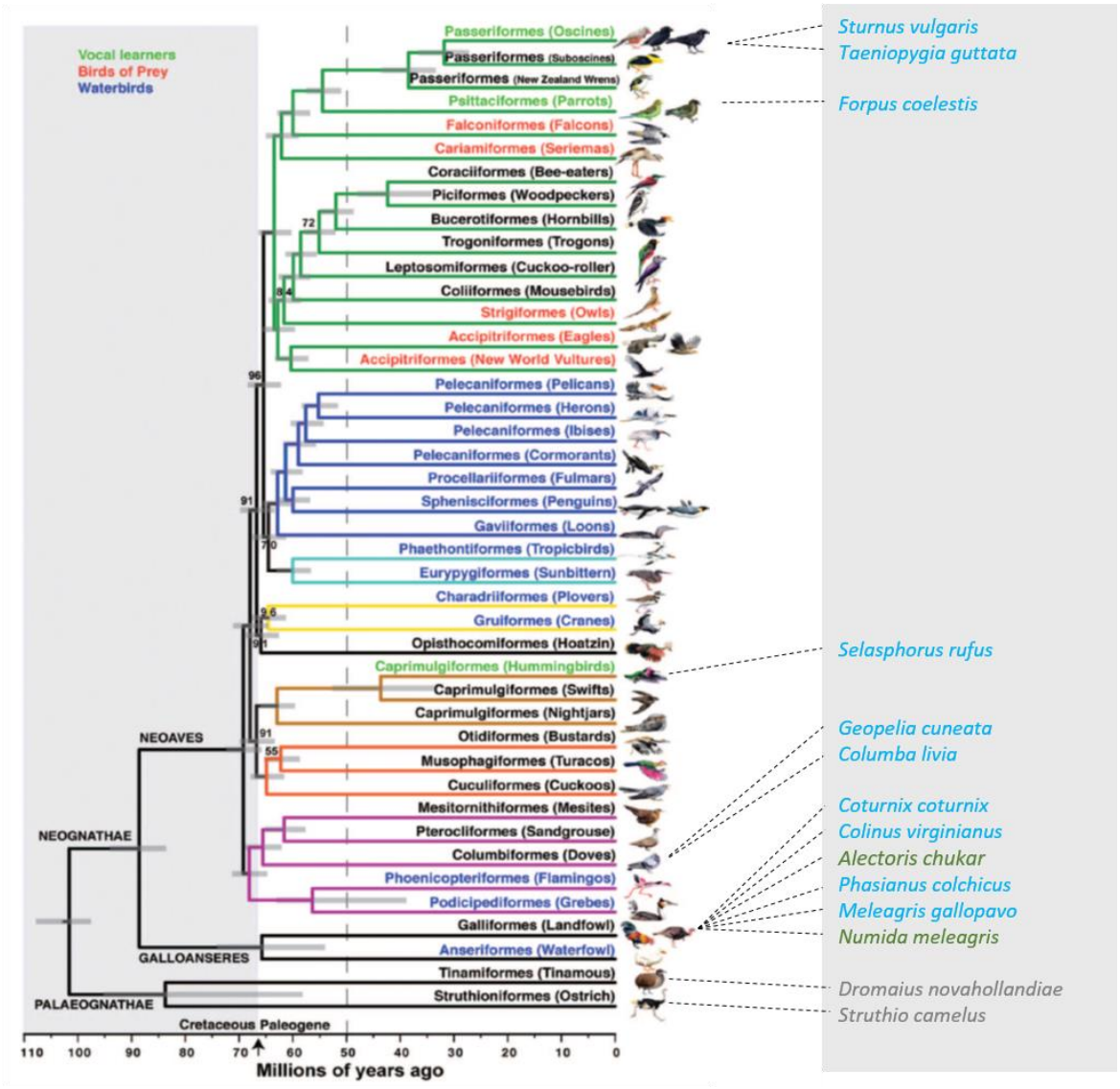

Figure 12 Genome scale phylogeny of birds to demonstrate which avian taxa hindlimb biomechanics (kinematics and kinetics) have been investigated in literature (right hand column). Pale blue indicates taxa where leaping has been investigated; grey indicates taxa where terrestrial locomotion has been investigated and green indicates taxa where both leaping and terrestrial locomotion have been investigated. From highest to lowest; Sturnus vulgaris (European starling) (Bonser and Rayner, 1996; Lee et al., 1996; Earls, 2000), Taeniopygia guttata (zebra finch) (Provini et al., 2012; Provini and Abourachid, 2018), Forpus coelestis (Pacific parrotlets) (Chin and Lentink, 2017), Selasphorus rufus (rufous hummingbird) (Tobalske, 2004), Geopelia cuneata (diamond dove) (Provini et al., 2012; Provini and Abourachid, 2018), Columba livia (rock dove) (Heppner and Anderson, 1985; Berg and Biewener, 2010), Coturnix coturnix (European migratory quail) (Earls, 2000), Colinus virginianus (northern bobwhite), Alectoris chukar (chukar) (Heers et al., 2018), Phasianus colchicus (ring-necked pheasant), Meleagris gallopavo (wild turkey) (Tobalske and Dial, 2000; Tobalske, 2004), Numida meleagris (guineafowl) (Henry et al., 2005; Kambic et al., 2014; Allen et al., 2017; Kambic et al., 2017), Dromaius novahollandiae (emu) (Goetz et al., 2008), Struthio camelus (ostrich) (Gangl et al., 2004; Rubenson et al., 2007; Hutchinson et al., 2015; Rankin et al., 2016). Figure adapted from Jarvis et al. (2014)

2.3.5 Extinct dinosaur biomechanics

2.3.5.1 Archaeopteryx lithographica

Data from fossils of extinct basal avialans within Paraves, such as *Archaeopteryx*, offer detailed data on bony morphology, however, often little to no soft tissue is preserved. The preservation quality of *Archaeopteryx* varies between specimens. Small fossils of basal avialans are particularly vulnerable to flattening and consequently, bone preservation can be poor and some long bones are flattened or fractured (Rauhut et al., 2018). With advanced imaging techniques (e.g. synchrotron X-ray tomography) crushed 3D fossils can be virtually reconstructed and analysed (e.g. see Voeten et al. (2018)). All specimens of *Archaeopteryx* were found in Solnhofen lithographic limestone, of Bavaria where this particular Lagerstätte allows exceptionally good preservation of fossils (Wellnhofer, 2010). As a result, some specimens of *Archaeopteryx* show little to no flattening of the bones (e.g. the London Specimen, Figure 13) and details of the skeleton beyond simply the length of bones can be discerned (Ostrom, 1976). The London specimen shows the hindlimb and pelvic appendage in superb detail, revealing the ilium, femur, tibiotarsus and tarsometatarsus. However, finer details are missing from the specimen including sesamoid bones such as the patella and parts of the pelvis including the pubis and ischium (Figure 13).

The London specimen is one of the largest specimens of *Archaeopteryx,* with a femoral length measuring 61 mm and weighing approximately 400 g (Wellnhofer and Haase, 2009). By documenting the take-off velocities of a variety of birds ranging in mass (2.5 g humming bird to the 6.5 kg wild turkey) Tobalske and colleagues (2004) published a model correlating the take-off velocity of a bird as a function of mass (Figure 14). Using this model and applying it to a 400 g *Archaeopteryx Lithographica,* the estimated take-off velocity of *Archaeopteryx* was 2.7 m/s (Figure 14). Although the authors noted that only 43% of the variation in take-off velocity was due to a variation in mass, the rest coming from morphology, motivation and take-off performance, it serves as a tool to get an initial estimation of the take-off velocity for *Archaeopteryx*.

For modern birds, the transition period from take-off to the minimal sustainable flight speed relies on powerful flapping strokes to keep airborne and accelerate (Klein Heerenbrink et al., 2015; Chin and Lentink, 2017). The minimum sustainable flight speed for *Archaeopteryx* has been estimated to be approximately 7 m/s (Rayner, 1988; Burgers and Chiappe, 1999; Longrich, 2006), and to achieve it, *Archaeopteryx* would have needed to engage the use of its wings. However as previously stated, there are many contentions as to the flapping ability of *Archaeopteryx.* Analyses on the aerodynamics of a flapping *Archaeopteryx* by Burgers and Chiappe (1999) predicted that at an airspeed of 2.71 m/s (similar to the predicted take-off velocity), *Archaeopteryx* could produce thrust and lift equivalent to 0.19 and 0.17 bodyweights (BW) (Burgers and Chiappe, 1999). A

biomechanical analysis estimating the jumping capability of *Archaeopteryx* followed by a subsequent analysis of its projectile path is needed to calculate the achievability of *Archaeopteryx* taking to the air as birds do today.

Figure 13 The London specimen of Archaeopteryx lithographica*, showing the skeletal bones embedded in the rock. The fossil contains the well-preserved pelvis, femur, tibiotarsus, tarsometatarsus and digits of Archaeopteryx. The dimensions of the slab are approximately 60x40 cm. Figure from (Wellnhofer and Haase, 2009).*

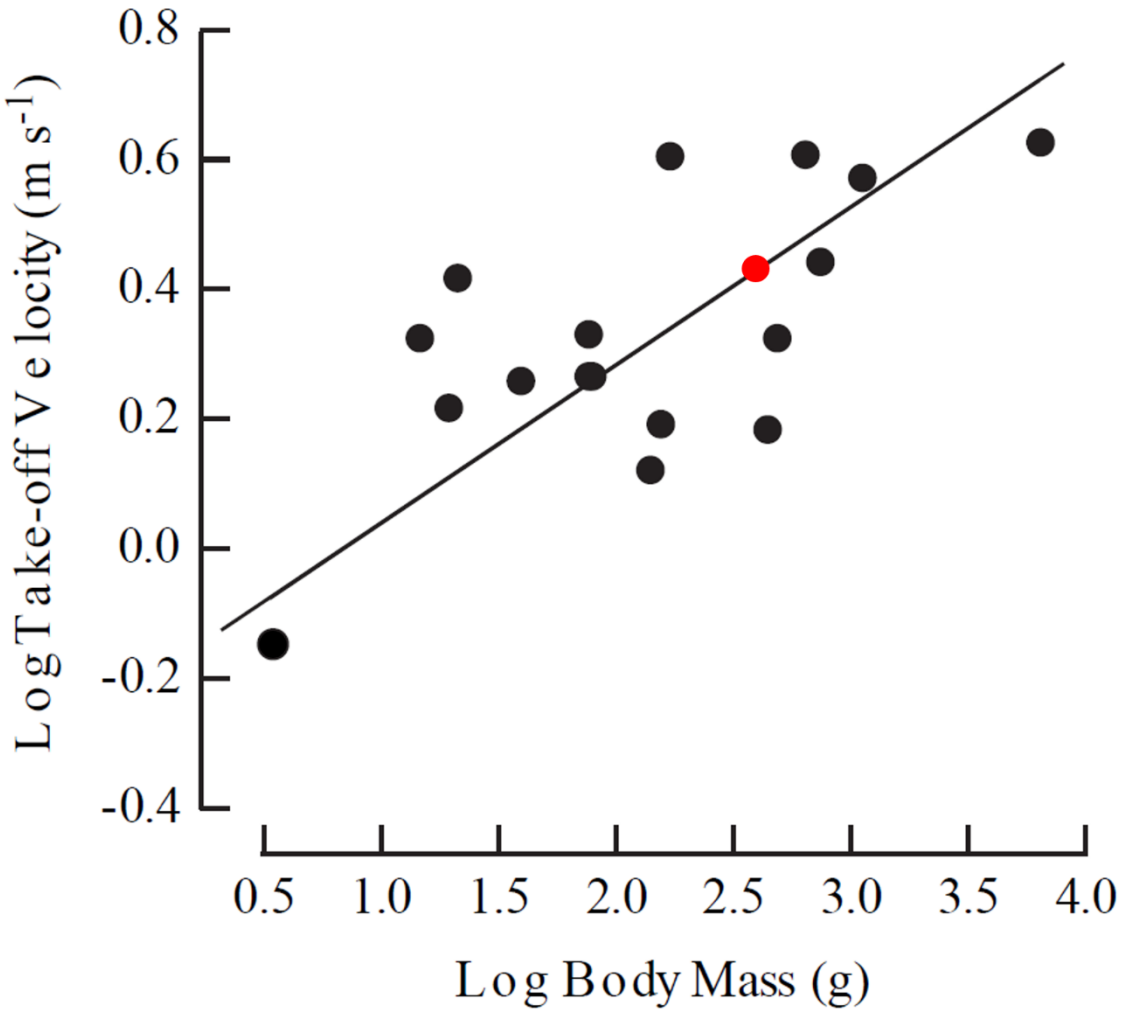

Figure 14 Take-off velocities versus mass in 17 bird species (shown as black dots) including, in order of increasing body mass: rufous hummingbird (Selasphorus rufus); zebra finch (Taeniopygia guttata); dark-eyed junco (Junco hyemalis); house finch (Carpodacus mexicanus); diamond dove (Geopelia cuneata); American robin (Turdus migratorius); European starling (Sturnus vulgaris); western scrub jay (Aphelocoma californica); northern flicker (Colaptes auratus); ringed turtle-dove (Streptopelia risoria); European migratory quail (Coturnix coturnix); American crow (Corvus brachyrhynchos); rock dove (Columba livia); black oystercatcher (Haematopus bachmani); ring-necked pheasant (Phasianus colchicus); herring gull (Larus argentatus); wild turkey (Meleagris gallopavo). Regression line of log-transformed data. The red dot represents the estimated take-off of a 400g Archaeopteryx lithographica. *Figure adapted from (Tobalske, 2004).*

2.3.5.2 Mapping extant myology to extinct dinosaur osteological morphology

Little data on soft tissue, including muscle tissue, is preserved on fossils (Witmer, 1995). However, muscles leave scars on the bone showing where they attach. These are not always distinguishable on fossils and almost no muscle scars have been described for any of the *Archaeopteryx* fossils. Occasionally an exquisitely preserved fossil means that muscle attachment sites are readily distinguishable. A well-preserved fossil such as *Tyrannosaurs rex* (FMNH PR 2081 "Sue") along with detailed analysis of extant archosaurs, allowed Carrano and Hutchinson (2002) to recreate the pelvic and hindlimb musculature of the non-avian dinosaur behemoth which differed greatly in detail and placement of several important muscles from previous reconstructions of *Tyrannosaurus Rex* hindlimb musculature (Romer, 1923; Tarsitano, 1983). The preservation of the fossil and sheer size meant that although no soft tissue was preserved, muscle scars could be distinguished which gave some indication of the myology of the theropod.

The authors use the Extant Phylogenetic Bracket (EPB) technique (Witmer, 1995) which reconstructs the soft tissue attributes of extinct vertebrates by relating information from the living representatives of at least the first two outgroups of the fossil taxon. In the case of dinosaurs, the clade that encompasses the closest two groups of extant taxa is the archosaurs which comprise *Crocodylia* and *Aves* (Figure 15).

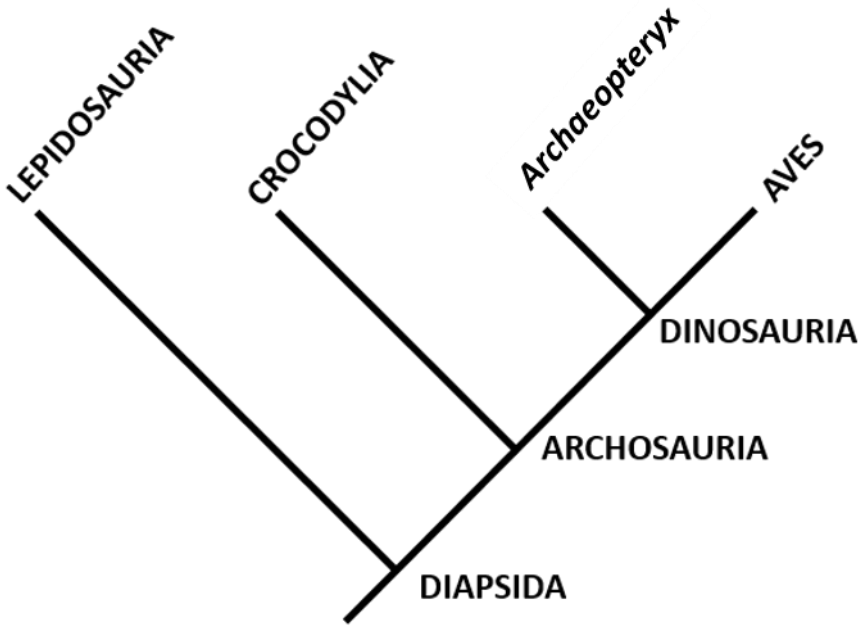

Figure 15 Phylogenetic framework showing the first two living outgroups of dinosaurs, Crocodylia and Aves. Figure adapted from Carrano and Hutchinson (2002).

A similar approach has also been used in mapping the pelvic and hindlimb musculature of *Archaeopteryx*. The pelvic girdle of *Archaeopteryx* still holds characteristics of its theropodan ancestry, including a pubis that has not reached the caudal pointing position of the avian lineage (Hutchinson, 2001). Differences such as these and the application of the EPB method means that data used to inform a model of the *Archaeopteryx* hindlimb are drawn not only from extant avians but also the Archosarian sister group – Crocodylia.

2.3.5.3 Computational biomechanical musculoskeletal models of extinct dinosaurs

Attempts have been made to estimate hindlimb locomotor abilities of various theropods based on their estimated mass and derived patterns seen in extant animals today (e.g. Gregory (1998) and Taylor (1973)). However, only a handful of studies have attempted to reconstruct the musculoskeletal structure of extinct dinosaurs to estimate biomechanical abilities (Sellers et al., 2017) investigated the running abilities of T-rex using a simplified (4 DoF) musculoskeletal model adapted from Hutchinson et al. (2005), demonstrating the effectiveness of using biomechanical modelling to derive insight in the abilities and behaviour of extinct taxa.

A recent, seminal study investigating how the pelvic muscles of bird-line archosaurs evolved (2021) made computational biomechanical musculoskeletal models of the hindlimb of avian and non-avian theropods, including *Archaeopteryx lithographica,* freely available to enable further study *(Allen et al., 2021)*. The authors used the well established EPB method, using a combination of avian and crocodilian muscles, to develop a representation of the musculature of the basal bird with 32 musculotendon units and seven joint degrees of freedom (Figure *16*). However, the authors opted to model a rather small individual which does not appear to be most representative of the species with a femoral length of 35.8 mm and weighing 99 g where femoral length in *Archaeopteryx* specimens has been reported to vary from 37 to 67 mm and similarly weight has been estimated to range from 0.2 to 0.6 g (Burgers and Chiappe, 1999; Chatterjee and Templin, 2003; Wellnhofer and Haase, 2009). Moreover, although the hip joint in a manner consistent with reasonable expectations for the movement of that joint (3 rotational degrees of freedom), the knee and ankle joints were modelled by 1 DoF joints only, a simplification that appears at least questionable considering the joint range of motion reported for modern birds (Kambic et al., 2014; Kambic et al., 2017; Provini and Abourachid, 2018) Addressing these limitations it seems possible to develop the musculoskeletal model of *Archaeopteryx* so it can be driven with the external kinematics and kinetics of the extant avian take-off leap to assess the capability of *Archaeopteryx* to take-off as birds do today.

Figure 16 *Computational biomechanical musculoskeletal model of Archaeopteryx lithographica from Allen and co-workers (2021), characterised using the extant phylogenetic bracketing technique. The model includes 32 musculotendon units and allows 3 rotational DoF motion at the hip and 1 DoF at the knee and ankle (Allen et al., 2021).*

Chapter 3 Aims and Objectives

Chapter 3 Outlines gaps in the subject knowledge and specific aims and objectives of the study.

3.1 Gaps in the research and project aim

The research presented in this thesis concerns the investigation of the biomechanical ability of the take-off leap of *Archaeopteryx*, by investigating the biomechanics of the take-off leap of extant birds, to shed light on the evolution of avian flight. Following a literature review to identify current gaps in the research, the following essential, previously unmet research needs have been identified:

1. Need for developing a quantitative understanding of the functional role of the hindlimb muscles of a flying bird.
2. Need for developing an understanding of the sensitivity of muscle moment-generating capacity to computational musculoskeletal modelling of a bird.
3. Need for developing quantitative knowledge regarding the biomechanical requirements associated with a take-off leap and the avian hind limb muscles' ability to meet these requirements.
4. Need for a quantitative biomechanical investigation into the leaping ability of the extinct basal bird, *Archaeopteryx,* to test the jumping hypothesis of the evolution of avian flight.

Therefore the study aims to develop a quantitative understanding of whether *Archaeopteryx* could have taken off like modern birds, with a bipedal take-off leap. The research approach to address this aim was to collect data and glean understanding on the take-off leap of modern extant birds and to apply this understanding to investigate the leaping ability of *Archaeopteryx.*

3.2 Project objectives

1. Use computational biomechanical musculoskeletal modelling to analyse the 3D functional roles of the pelvic muscles of the magpie *Pica pica* and investigate the sensitivity of the muscle moment-generating capacity to the modelling approach.
2. Investigate the internal mechanics of the zebra finch *Taeniopygia guttata* hindlimb by simulating the take off *in silico* and using the inverse dynamics approach to quantify the biomechanical requirement of the muscles and their capacity to meet these requirements
3. Simulate the take-off leap of the extinct avian *Archaeopteryx*, informed by external kinematics and kinetics data of the zebra finch take-off leap to ascertain its biomechanical ability to leap into the air. Use this understanding to expand on the jumping hypothesis on the evolution of avian flight.

Chapter 4 On the 3D nature of the magpie (Aves: Pica pica) functional hindlimb anatomy during the take-off jump

Chapter 4 presents a computational biomechanical model of the magpie, *Pica pica*, to quantify the functional hindlimb anatomy in leaping birds. Here, comprehensive analyses considering key sources of uncertainty provided robust estimates for the moment-generating capacity of its pelvic muscles and demonstrated substantial capability for internal/external rotation as well as flexion/extension, revealing that avian hip muscle function is not limited to the sagittal plane.

4.1 Citation

In this chapter the full manuscript titled “On the 3D nature of the magpie (Aves: Pica pica) functional hindlimb anatomy during the take-off jump”, published in Frontiers in Bioengineering and Biotechnology is presented. Supplementary information is provided in Appendix A. The citation is provided below:

Meilak, E.A., Gostling, N.J., Palmer, C., and Heller, M.O. (2021). **On the 3D Nature of the Magpie (Aves: Pica pica) Functional Hindlimb Anatomy During the Take-Off Jump**. Frontiers in Bioengineering and Biotechnology 9. DOI: 10.3389/fbioe.2021.676894

4.2 Abstract

Take-off is a critical phase of flight and many birds jump to take to the air. Although actuation of the hindlimb in terrestrial birds is not limited to the sagittal plane and considerable non-sagittal plane motion has been observed during take-off jumps, how the spatial arrangement of hindlimb muscles in flying birds facilitates such jumps has received little attention. This study aims to ascertain 3D hip muscle function in the magpie (*Pica pica*), a bird known to jump to take off.

A musculoskeletal model of the magpie hindlimb was developed using µCT scans (isotropic resolution of 18.2µm) to derive bone surfaces while 3D muscle path definition was further informed by the literature. Function was robustly characterised by determining the 3D moment generating capacity of 14 hip muscles over the functional joint range of motion during a take-off leap considering variations across the attachment areas and uncertainty in dynamic muscle geometry. Ratios of peak flexion-extension (FE) to internal-external rotation (IER) and ab-adduction (ABD) moment generating capacity were indicators of muscle function.

Analyses of 972 variations of the 3D muscle paths showed that 11 of 14 muscles can act as either flexor or extensor, while all 14 muscles demonstrated the capacity to act as internal or external rotators of the hip with the mean ratios of peak FE to IER and ABD moment generating capacity were 0.89 and 0.31, respectively.

Moment generating capacity in IER approaching levels in FE moment generating capacity determined here underline that avian hip muscle function is not limited to the sagittal plane. Together with previous findings on the 3D nature of hindlimb kinematics our results suggest that musculoskeletal models to develop a more detailed understanding of how birds orchestrate the use of muscles during a take-off jump cannot be restricted to the sagittal plane.

4.3 Introduction

Take-off is a critical phase of flight and many land birds perform some form of jump to take to the air. Although recent work strongly indicates that the hindlimbs are a key contributor to providing the initial take-off velocity, (Heppner and Anderson, 1985; Bonser and Rayner, 1996; Earls, 2000; Tobalske and Dial, 2000; Tobalske, 2004; Henry et al., 2005; Berg and Biewener, 2010; Provini et al., 2012; Chin and Lentink, 2017; Provini and Abourachid, 2018), how exactly birds use their hindlimbs to take to the air has received little attention. Through their contraction, muscles act as "motors" driving hindlimb motion, and therefore understanding avian muscle function during the take-off jump is a first step to understand how the hindlimb contributes to taking to the air.

Current understanding of the functional anatomy of the avian hindlimb is informed by pioneering work that provides detailed, but primarily qualitative, characterizations of muscle function based on anatomical dissection (Hudson, 1937; Wilcox, 1952; Verstappen et al., 1998; Smith et al., 2006). Whilst methods to quantitatively describe a muscles' function based on analyses of their 3D moment arms and moment generating capacity are well established (Jensen and Davy, 1975; Murray et al., 1995; Hutchinson et al., 2005; Arnold et al., 2009; O'Neill et al., 2013; Charles et al., 2016), few studies applied these techniques to the avian hindlimb. Hutchinson and co-workers (2015) determined ostrich (*Struthio camelus*) muscle function based on the moment arms throughout the range of motion (RoM), defined by osteological joint congruency, a measure of how bones articulating at a joint relate to each other. Using that quantitative approach, the major function of the M. Obteratorius medialis (MOM) was identified to be that of a flexor muscle. *Contra* this view, Smith et al. (2006), whose definition of muscle function was determined by anatomical dissection, suggested that the main function of the MOM was that of an extensor. These opposing functional definitions for the same muscle in the same species demonstrate how the methodology for determining muscle function significantly affects the outcome. Additionally, investigation into muscle function of theropods, the wider clade that avians belong to, yielded that all muscles in the hindlimb essentially act in all three rotational degrees of freedom therefore highlighting their inherent multi-functionality (Hutchinson et al., 2005; Hutchinson and Allen, 2009). Taken together these findings suggests that robust identification of muscle function in the avian hindlimb requires the use of comprehensive sensitivity analyses in 3D (Modenese and Kohout, 2020).

Although a first description of essential muscle function for the magpie (*Pica pica*), a bird known to jump to take to the air, is available in the literature (Verstappen et al., 1998) muscle function was estimated for only a limited number of muscles based on a 2D moment arm analysis in the sagittal plane. Initial analyses to characterise avian hindlimb motion used surface markers and investigated sagittal plane motion only (Earls, 2000; Kambic et al., 2017). The introduction of novel technology

has enabled the capture of 3D motion (Rubenson et al., 2007; Rubenson et al., 2010; Kambic et al., 2014; Kambic et al., 2017; Provini and Abourachid, 2018). Such analyses have shown substantial motion not only in the sagittal plane, but also in the transverse and frontal planes during the avian take-off leap. It is therefore reasonable to assume that such motion must be either actively generated or at least controlled by muscles. The 3D nature of avian take-off kinematics, along with the finding that theropod musculature is 3D and multifunctional, described in the literature (Hutchinson and Allen, 2009; Provini and Abourachid, 2018; Allen et al., 2021) supports the hypothesis that avian hindlimb musculature is multifunctional throughout the take-off jump. However, no quantitative analysis of the 3D moment generating capacity of the avian hindlimb for this important motion is available in the literature to substantiate this hypothesis.

This study aims to robustly ascertain muscle function based on the 3D moment generating capacity of the pelvic muscles in the magpie. Based on the evidence that the kinematics of avian locomotion in general and specifically during the take-off jump is not restricted to the sagittal plane, the hypothesis here is that pelvic muscles will not only be able to flex/extend the hip but be substantially three-dimensional. Specifically, the extent of the capacity to produce moments about the ab/adduction and int/external rotation axes was expected to be similar to the one about the flex/extension axis.

4.4 Materials and Methods

4.4.1 Model Development

A musculoskeletal model of the magpie hindlimb was developed based on dedicated CT scans performed for this study, histological samples of muscle cross-sections (Hudson, 1937) and bone attachment site sketches available from the literature (Verstappen et al., 1998). The CT data provided the basis for establishing a 3D surface model of the skeletal anatomy of the hindlimb, the definition of joint centres and axes and local bone coordinate systems are available in the supplementary information. Muscles were modelled by 3D lines of action (Heller et al., 2001b; Seth et al., 2011; Trepczynski et al., 2012) by relating the cross-sectional and attachment data to the bone surfaces. Muscle function was then robustly characterised by determining 3D muscle moment arms and moment generating capacity over the functional joint RoM during a take-off leap, whilst considering key sources of uncertainty in the definition of static and dynamic muscle geometry. The study was approved by the University of Southampton Ethics Committee (ERGO ID 21781).

4.4.2 Skeletal model

A magpie *Pica pica* cadaver (190g), mounted in a perched position in a clear acrylic cylinder, stabilised by floral foam (OASIS, Kent, OH, USA) was CT scanned at an isotropic resolution of 18.2µm (225kVp/450kVp Nikon/Metris (Tokyo, Japan)), in a custom designed micro-focus computed tomography scanner (housed within the µ-VIS X-ray Imaging Centre, University of Southampton, UK) to capture bone geometry. A threshold based semi-automatic segmentation followed by a marching cubes algorithm surface reconstruction (Hege et al., 1997) was used to obtain bone surfaces for the right hindlimb (Avizo 9.0.1, Thermo Fisher Scientific, Waltham, MA, USA). All surfaces were re-meshed using the isotropic re-meshing tool (Open Flipper 3.1 (Möbius and Kobbelt, 2012)) to a target mean triangle edge length of 0.1 mm. The skeletal structures identified in that manner included the pelvis, femur, patella, tibiotarsus and fibula, tarsometatarsus, and all phalangeal bones.

In order to establish a musculoskeletal model for further analysis, a linked rigid body model with 6 segments including the pelvis, thigh, shank, tarsometatarsus and digits was defined in OpenSim v4.0 (Seth et al., 2018). Here, body segments were linked by 4 joints (hip, knee, ankle, and subtalar joints) with 3 rotational degrees of freedom each (Figure 17).

4.4.3 Muscle geometry

Fourteen key hip muscles were modelled as polylines spanning origin and insertion while via points were added to fully describe their 3D paths (Figure 18). Outlines of the muscle attachment areas on the pelvis and femur, as known from the literature, (Verstappen et al., 1998) were re-traced on the surface models of the bones of the magpie specimen scanned here (Figure 19). To that end, between 30 to 35 landmarks were defined for each attachment area (MorphoDig v 1.5.3, Lebrun (2018)). At the proximal femur in particular, prominent ridges on the bone surface further guided the delineation of the muscle attachments. The locations of the landmarks delineating the muscle attachment boundaries were imported into Rhino (v7; Robert McNeel & Associates, Seattle, USA, (McNeel, 2020)) where closed polylines were created and rebuilt to obtain smooth curves. The triangulated bone surfaces were fitted by subdivision surfaces using the QuadRemesh function in Rhino before converting them to Non-uniform rational basis spline (NURBS) surfaces. The smooth curves outlining the muscle attachments on femur and pelvis were then projected on the respective NURBS surface providing a detailed description of muscle attachment geometry (Figure 20A). Further attachment patches on the shaft of the long bones were digitised from the literature (Verstappen et al., 1998) and projected on to the 3D bone surfaces of the specimen using polar coordinate system mapping techniques. The shaft of the long bones was approximated by a cylinder onto which the medial and lateral sketches of the attachment sites were projected.

The use of via points is considered important to better replicate a muscle's curved path as differences in a muscle's moment arms by up to 50% compared to being modelled as a straight line have been reported (Jensen and Davy, 1975; Modenese and Kohout, 2020). Histological slice images of the crow (Corvus corone, being a closely related member of the same family as the magpie, within which hindlimb morphology is very conserved (Verstappen et al., 1998)) hindlimb, from which such via points could be derived, were thus digitised and mapped on to the magpie hindlimb to establish the 3D muscle path. Registration of the histological slices to the bone was carried out by determining their relative location along the long bone axis and registering the cross-sections by fitting circles to both the crow and magpie data (Figure 19). For each slice, the histological soft tissue contours were scaled by the ratio of the radius of the crow to the magpie femoral radius in the respective cross-sections. The mapped data was further orientated with respect to the femur by Iterative Closest Point (ICP) registration of the distal slices containing the distal femoral condyles (Figure 19). Centroid locations of registered muscle contours were used to define the 3D muscle paths (Jensen and Davy, 1975; Duda et al., 1997a; Taylor et al., 2006; Allen et al., 2017). Wrapping cylinders and ellipsoids were added to define 3D paths throughout the RoM to ensure muscles do not intersect bones. Axes directions and radii of these wrapping objects were determined by least-squares fitting to selected regions of the bone surfaces (Figure 18).

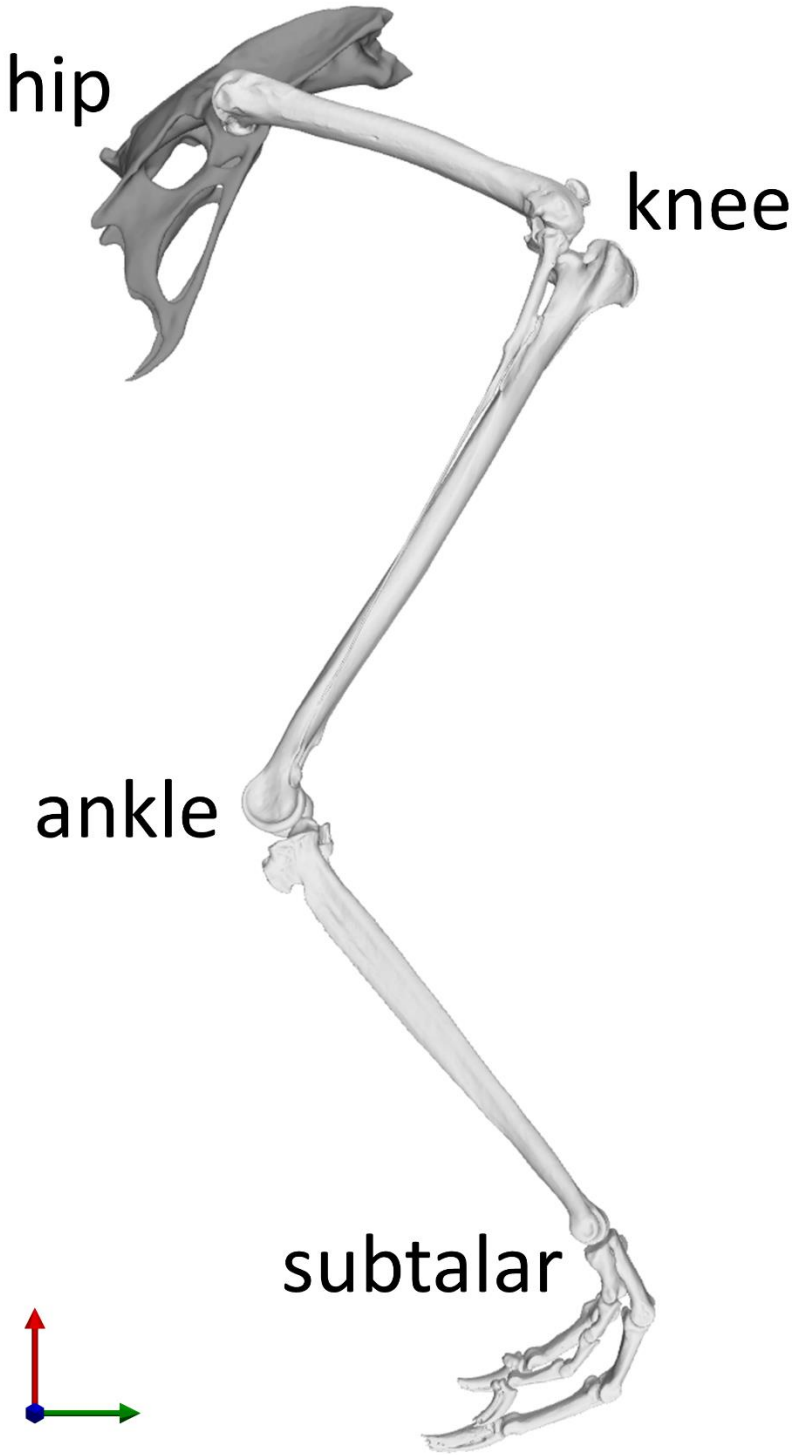

Figure 17 Skeletal model of the right hindlimb of the magpie in the reference position of the joints taken as the mean RoM of every joint degree of freedom (DoF). Each of the 4 joints (hip, knee, ankle, subtalar) possesses 3 rotational DoFs. The knee joint incorporated patella-femoral kinematics which were expressed as a function of knee flexion (Trepczynski et al., 2012). The x axis direction (green) points from caudal to cranial, the y axis direction (red) points from ventral to dorsal, and the z axis direction (blue) points from left to right.

4.4.4 Muscle moment generating capability analysis

In order to ascertain muscle function, the study focused on the 3D moment generating capacity of 14 pelvic muscles at the hip during the take-off jump. Moment arms of each muscle were assessed over the RoM of each rotational degree of freedom (DoF) at the hip (hip flexion/extension, adduction/abduction, and internal/external rotation). The RoM studied was based on 3D skeletal kinematics of the take-off jump obtained from XROMM of the Diamond Dove and Zebra Finch (Provini and Abourachid, 2018). Here, the joint neutral pose was matched to the joint orientation published by Provini and Abourachid (2018). The RoM was calculated by taking the upper and lower limits of the mean joint angles of the take-off jumps of both species. The RoM about flexion/extension (FE), internal/external rotation (IER) and abduction/adduction (ABD) axes derived in that manner were 54° (-62° to -8°), 20° (18° to 38°) and 8° (-33° to -25°), respectively. Moment arms were determined in 1° increments analysing a single DoF at a time while the two DoFs which were not being assessed were set at their mean value of the RoM.

In order to derive the moment generating capacity for each muscle, maximum isometric force ($F_{max,i}$) of the muscles was estimated first by relating physical cross-sectional area (PCSA) to the maximum isometric stress under maximal activation (equation 1). Here, σ_{max} was taken as $3.0 \times 10^5 Nm^{-2}$ (Hutchinson, 2004a; Nelson et al., 2004; Hutchinson et al., 2015; Rankin et al., 2016).

$$F_{max,i} = PCSA_i \times \sigma_{max} \qquad \text{(equation 1)}$$

The moment generating capacity of each muscle was then estimated using the PCSA data of a magpie (Verstappen et al. (1998), equation 2) matched to the current specimen by scaling by mass. For the purpose of the study, these moments were evaluated for each muscle *i (where i=1..14)* for the muscle maximum isometric force (F_{max}) at the mean moment arm ($\overline{MA}$) determined over the RoM for each rotational DoF *j (where j=1..3)* of the hip joint.

$$M_{i,j} = F_{max,i} \cdot \overline{MA}_{i,j} \qquad \text{(equation 2)}$$

Attribution of muscle function was based on the moment generating capacity of a muscle expressed as a percentage of the sum of the moments of all muscles acting in the same direction of the respective degree of freedom:

$$\frac{M_{i,j}}{\sum_{i=1}^{14} M_{i,j}} \qquad \text{(equation 3)}$$

Muscles were considered to contribute to a certain function (flexion, extension, abduction, adduction, internal or external rotation) if a lower bound on their muscle moment generating

capacity, defined as mean moment across all conditions minus 1 standard deviation, was greater than 2% of the sum of the mean moments of all muscles acting in the same direction.

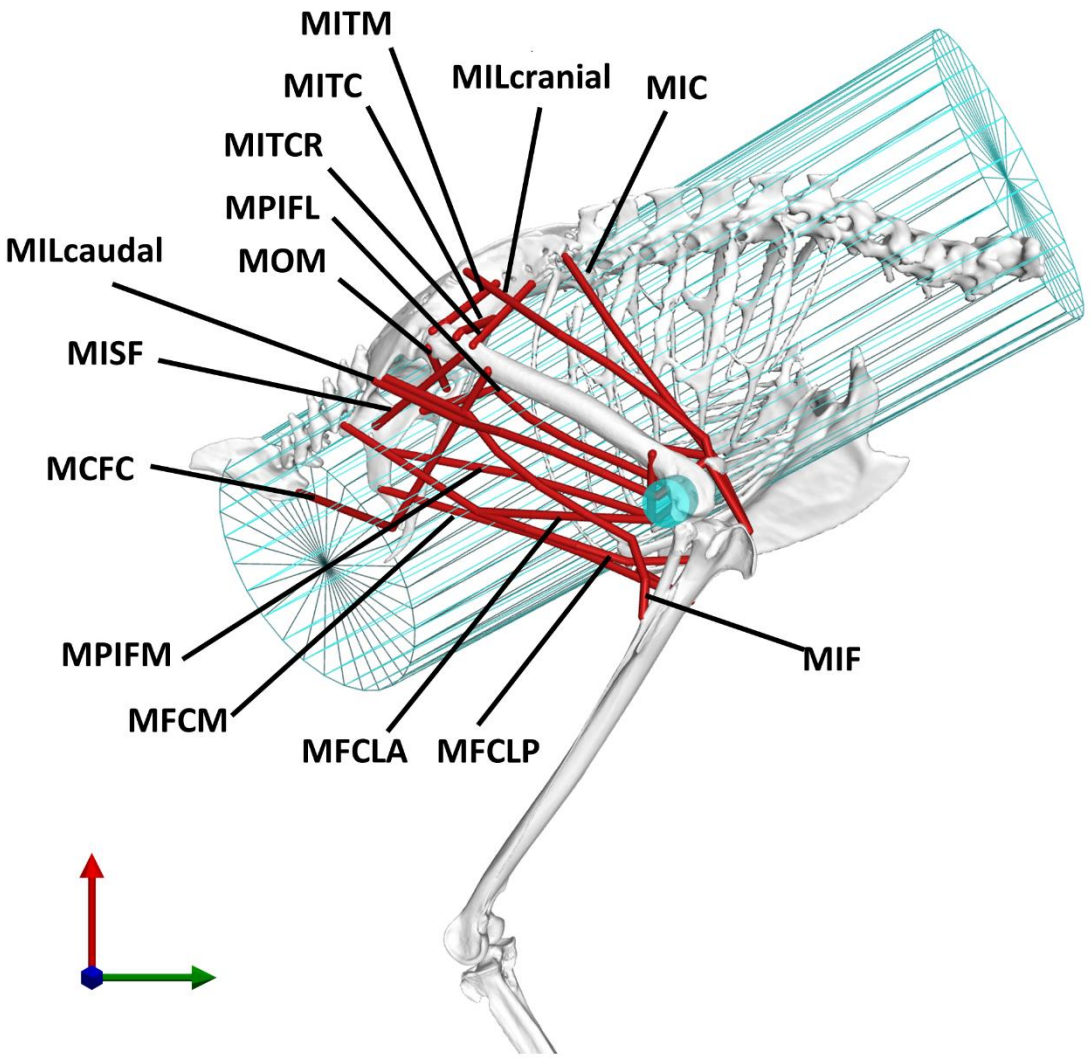

Figure 18 The analysis considered 14 key pelvic muscles of the magpie. To approximate the 3D paths of the muscle between origin and insertion, two wrapping cylinders (shown in blue) were introduced. The wrapping cylinder used for the MIC, simulating the action of the rib cage, is shown in wireframe representation while the wrapping object used to simulate the interaction with the distal femoral condyles is shown by a solid cylinder. For an explanation of the abbreviations of the muscles used here please refer to the key provided in Table 2.

Table 2 This study considered 14 key pelvis muscles for further analysis, listed here in alphabetical order.

abbreviation	muscle name
MFCLA	*m. flexor cruris lateralis pars accessoria*
MFCLP	*m. caudofemoralis pars caudalis*
MFCM	*m. flexor cruris medialis*
MIC	*m. iliotibialis cranialis*
MIF	*m. iliofibularis*
MILcaudal	*m. iliotibialis lateralis caudalis*
MILcranial	*m. iliotibialis lateralis cranialis*
MISF	*m. ischiofemoralis*
MITC	*m. iliotrochantericus caudalis*
MITCR	*m. iliotrochantericus cranialis*
MITM	*m. iliotrochantericus medius*
MOM	*m. obteratorius medialis*
MPIFL	*m. puboischiofemoralis pars lateralis*
MPIFM	*m. puboischiofemoralis pars medialis*

4.4.5 Sensitivity analysis

In order to ascertain robust estimates of muscle function when representing muscles by single lines of actions, two key sources of variability were considered in a sensitivity analysis, the location of muscle attachments and the position of the via points. The sensitivity analyses firstly considered a selection of possible attachment locations for each attachment site. The selection was informed by the general shape and size of the muscle attachments. Circular attachments (Table 3) were represented by a single location at the position of the projection of the geometric centroid of the attachment onto the respective surface. Eight additional points were added on the perimeter placed at cardinal and intercardinal positions (Table 3). For larger muscle attachments with a more triangular or rectangular shape, the respective edges as well as the projection of the geometric centroid of the attachment patch onto its surface were all considered in the analyses (Table 3). For the largest attachment, (MITC pelvis attachment) two additional, equidistantly distributed positions between the edges were considered while for the pelvic attachment of the MISF the midpoints between edges were additionally considered. Most attachments on the pelvis were of a rectangular shape with a rather small height (ventro-dorsal) compared to their width (cranio-caudal) (Table 3). For these attachment surfaces a medial axis was first determined (Rhino v7; Robert McNeel & Associates, Seattle, USA, (McNeel, 2020)) along which then a total of 7 equally distant points were defined that were considered for the analyses (Figure 20A).

To assess how uncertainty in the definition of path points affected moment generating capacity, via points could vary radially and circumferentially from their initial position at the centroid of the muscle cross-sections. Estimates of the variation in muscle paths across a wide range of bird species were obtained to derive informed limits on how much the via point locations could vary circumferentially. For 11 muscles of the hip, histological slices covering the cross-sectional musculoskeletal anatomy of a variety of bird species (sparrow hawk *Falco sparverius*, Screech owl *Otus asio*, Green heron *Butorides virescens* and Lesser yellowlegs *Totanus flavipes*) (Hudson, 1937) were digitised and related to the bones as described above. The centroids of the muscle cross-sections were transformed to polar coordinate systems with the origin located at the centroid of the femoral cross-section of the magpie specimen to then determine the standard deviation of their angular positions. The standard deviation of the angular position of these 11 muscles across five species was 10 degrees. Therefore, via point locations were varied circumferentially by ± 10 degrees.

The intraspecies variation in physiological cross-sectional area (PCSA) was used to derive an upper limit for how much the locations of the via points could vary radially. Based on the consideration that the radial distance of the centroid of a muscle with a larger PCSA would be further away from

the bone, the extent of PCSA variation was taken as a proxy for the extent of variation in radial position. A study into the variability in muscle architecture of the Monk Parakeet (*Myiopsitta monachus*) showed that the maximum coefficient of variation in PCSA of a muscle was approximately 10% (Carril et al., 2014). Therefore, a variation in the radial direction of the via point location of ±10% of the reference value was considered (Figure 20B).

For each muscle, the mean, standard deviation, and coefficient of variation of its moment generating capacity were computed at each joint angle increment (1°) for all possible combinations of origin, via point and insertion locations as appropriate. From these, the mean moment and coefficient of variation (CV) were calculated across the entire RoM and used as a measure of the muscle moment generating capacity and how robustly the function of a muscle was ascertained, respectively. As an overall measure of change in muscle moment generating capacity throughout the functional RoM, the percentage change of each muscle's moment arm over the RoM per DoF was further calculated.

In order to assess the influence of the way in which the 3D muscles paths were modelled, muscles were classified to belong to either of two categories based on the mean CV of their moment arms throughout the functional RoM. With a view to differentiate modelling artefacts from genuine changes in muscle moment arms throughout the RoM, muscles with a substantial CV (operationally defined here to be greater than 50%) were considered further (Heller et al., 2001b; Heller et al., 2005; Trepczynski et al., 2012; Charles et al., 2016; Trepczynski et al., 2018). A single muscle's moment arm can differ by up to 50% depending on whether it is modelled as a straight line, spanning origin and insertion site, or follows the 3D curved centroid line of the muscle (Jensen and Davy, 1975; Modenese and Kohout, 2020). Therefore, a CV of over 50% indicates that a muscle's variation in moment arms is not only due to the modelling approach but due to actual changes in muscle moment arms over the RoM. To quantify the contribution of modelling individual path points to the sensitivity of the muscle moment arms, locations of origins sites and via points were varied independently and CVs were calculated for each condition and compared. The peak value of the ratios comparing moment arms in internal/external rotation and ab/adduction to flexion/extension were determined as a measure to quantify a muscle's potential to actuate degrees of freedom outside of the sagittal plane. Moments of all muscles acting in the same direction were summed before calculating the respective ratios.

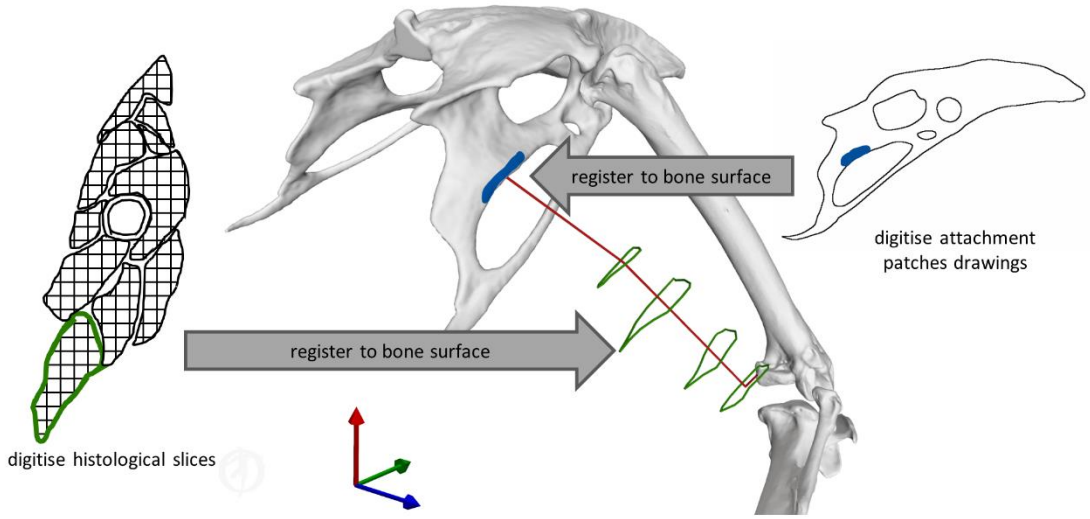

*Figure 19 Illustration of the key principles for defining muscle geometry using literature data to support the definition of both muscle attachments and 3D muscle path geometry. Right: muscle attachment patches from the literature (Verstappen et al., 1998) were digitised, and then registered to the respective bone surface. Left: histological slices of the crow (*Corvus corone*) hindlimb from the literature (Hudson, 1937) were digitised, and then registered to the magpie bone surfaces. For each of these cross-sections the centroids of the muscle contours were determined to inform the definition of the 3D muscle path spanning origin and insertion.*

4.5 Results

The moment generating capacity of 14 muscles was successfully analysed over the functional hip joint RoM of a take-off leap for a total of 972 variations of 3D muscle paths. Nine muscles were found to have functions about all three rotational DoFs, and the remaining 5 about only 2 DoF (Table 4, Figure 21). No muscle had a function restricted to just the saggital plane (flex/extension action). Moreover, 3 muscles (MITM, MITCR and MISF) produced significant moments only about the ab/adduction axis and int/external rotation axis and not about the flex/extension axis (Table 4, Figure 21). Every muscle had the ability to generate either internal or external rotations to the femur. All of the 11 muscles with capability to act as flexor or extensor had a similar capability to act as internal/external rotators, evidenced by a mean ratio of peak internal/external rotation to flexion/extension moments of 0.89±0.33. Conversely, the ability of flexors and extensors to act as abductors and adductors was considerably less, with a mean ratio of peak ab/adduction to flexion/extension moments of 0.31±0.19. Moments that acted to extend and externally rotate the hip made up most of the sum of the moment generating capacity of all pelvic muscles (36% and 30%, respectively). The largest moment generating capacity was observed for the extensors and external rotators, with values of 57.5±4.5 and 50±5.1 Nmm for the MPIFM and MISF respectively, (Figure 22).

Throughout the RoM, the mean change in moment arms for most muscles was 24% ±20% excluding the MOM and MIC for which maximum moment arm changes around the flexion/extension axis and abduction/adduction of up to 106% and 150% respectively were observed.

The largest CVs of all muscles were observed for the MITC, MISF, MILcaudal, MILcranial, MFCLP/MFCLA with values ranging between 59%-85% (Table 5). The CVs for the MISF and MITC were largest with mean CVs of 85% and 77% about the ab/adduction and flex/extension axes, respectively. The MILcranial had a mean CV of 70% about int/external rotation axis whereas the MFCLP and MFCLA, both originating from the same location on the pelvis and possessing an adjacent initial via point on the femur, exhibited a mean CV of 62% about the ab/adduction axis. Similarly, the MILcaudal had a mean CV of 59% about the ab/adduction axis. Upon further investigation of the contribution of modelling individual path points to the sensitivity of the muscle moment arms it was revealed that the moment arms of the MITC, MISF, MILcaudal and MILcranial muscles were most sensitive to variations in the location of the origin sites. Here mean CVs ranged between 61-316% due to the variability of the origin site compared to 40-99% mean CVs from varying the via point (Table 6). The moment arms of the MFCLP and MFCLA were most sensitive to how the path point was varied, with mean CVs ranging from 16% and 41-43% due to the variability

in origin sites and via points respectively (Table 5). The CVs for the remaining eight muscles (MFCM, MIC, MIF, MITCR, MITM, MOM MPIFL, MPIFM) remained between 6-37% (Table 4).

Table 3 Muscle attachment sites were grouped by their shape which determined how they were was discretized (number of points) for the sensitivity analysis. Subscripts denote to which bone a muscle is attached to. For muscles with a larger perimeter (indicated by asterisk), a larger number of points was considered.

shape	muscle	number of points
thin rectangular		
	$MFCLA_{pelvis}$	7
	$MFCLP_{pelvis}$	7
	MIC_{pelvis}	7
	MIF_{pelvis}	7
	$MILcaudal_{pelvis}$	7
	$MILcranial_{pelvis}$	7
	$MITCR_{pelvis}$	7
	$MITM_{pelvis}$	7
	$MPIFL_{pelvis}$	7
	$MPIFM_{pelvis}$	7
rectangular		
	$MFCM_{pelvis}$	7
	$*MISF_{pelvis}$	15
	$*MISF_{femur}$	9
triangular		
	$*MITC_{pelvis}$	19
	$MITC_{femur}$	7
	$MITCR_{femur}$	7
circular		
	$MITM_{femur}$	9
	MOM_{pelvis}	9
	MOM_{femur}	9

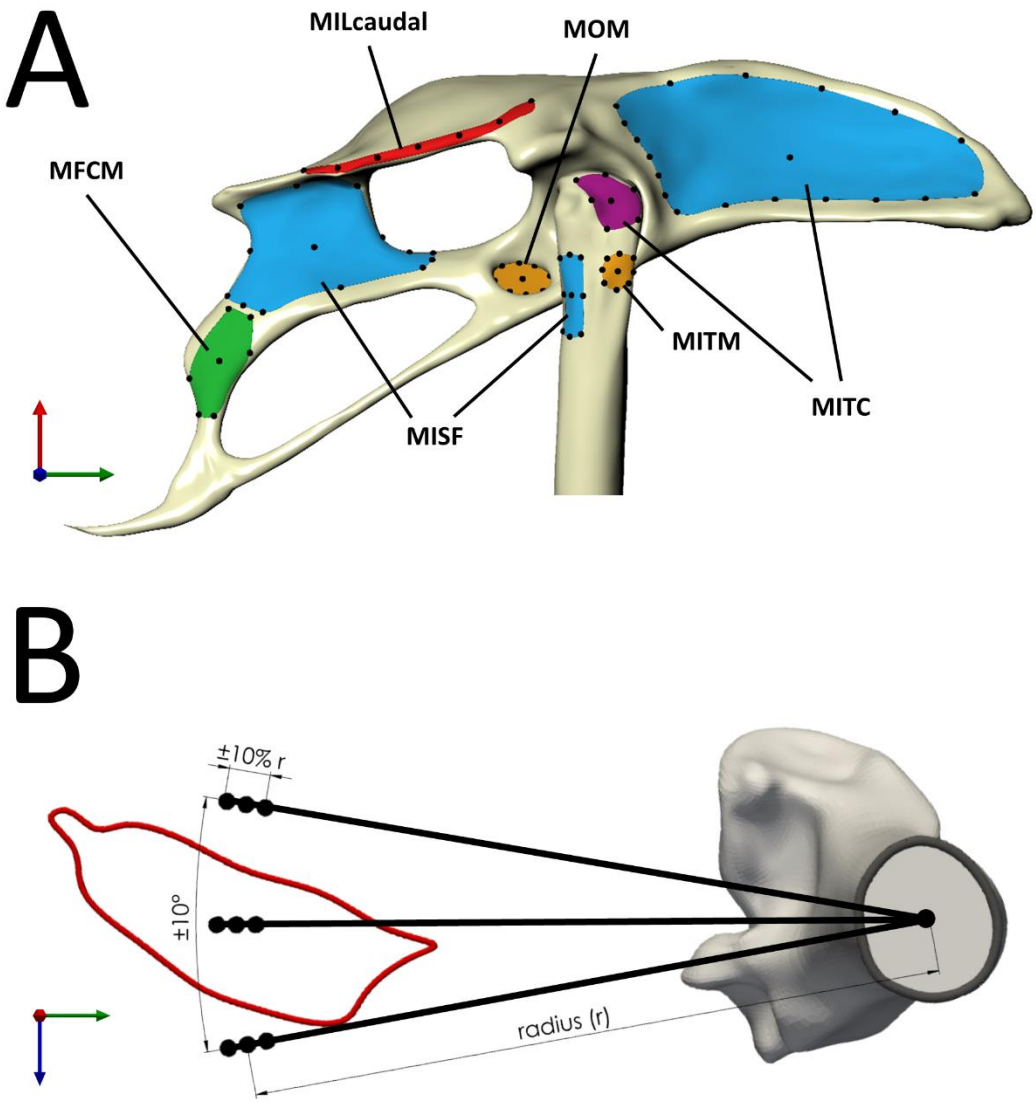

Figure 20 Sensitivity of the moment generating capacity of the pelvic muscles was investigated with respect to uncertainty in the definition of muscle attachments and via points. A) Muscle attachment shape was classified as either thin rectangular (red attachment area, $MILcaudal_{pelvis}$), rectangular (green, $MFCM_{pelvis}$), triangular (violett, $MITC_{femur}$), or circular (orange, MOM_{pelvis}, $MITM_{femur}$) (Table 2). Long thin attachments were discretised using 7 points ($MILcaudal_{femur}$, black dots) along the medial axis of the attachment surface, while for attachments with other shapes the discretisation considered the perimeter and centroid of the attachment area. For muscles with a larger perimeter (blue attachment area, $MITC_{pelvis}$, $MISF_{pelvis}$, $MISF_{femur}$) a larger number of points was defined on the perimeter. B) Uncertainty in the definition of via points, as exemplified here for a via point for $MFCLP_{femur}$, considered circumferential variation around the long bone axis by ±10° and radial variation by ±10% of the distance of the muscle contour centroid from the associated centroid of the bone cross-section (radius r).

Table 4 Function of key pelvic muscles of the hindlimb of the magpie as ascertained in this study for flexion/extension (F/E), abduction/adduction (AB/AD), and internal/external rotation (Int/Ext) were compared to data from the literature (Verstappen et al. (1998)). The letter O indicates conditions where Verstappen and co-workers attributed a muscle a function about a joint other than the hip.

muscle	F/E		AB/AD	Int/Ext
	this study	literature	this study	this study
MFCLA	E	E	AD	E
MFCLP	E	E	AD	E
MFCM	E	E	AD	E
MIC	**F**	**O**	**AB**	**I**
MIF	E	E	AB	E
MILcaudal	**E**	**O**	**AB**	**E**
MILcranial	**F**	**O**	**AB**	**I**
MISF		O	AB	E
MITC	**E**	**F**		**I**
MITCR		**F**	**AD**	**I**
MITM		**F**	**AD**	**I**
MOM	F	F		E
MPIFL	E	E	AD	E
MPIFM	E	E	AD	E

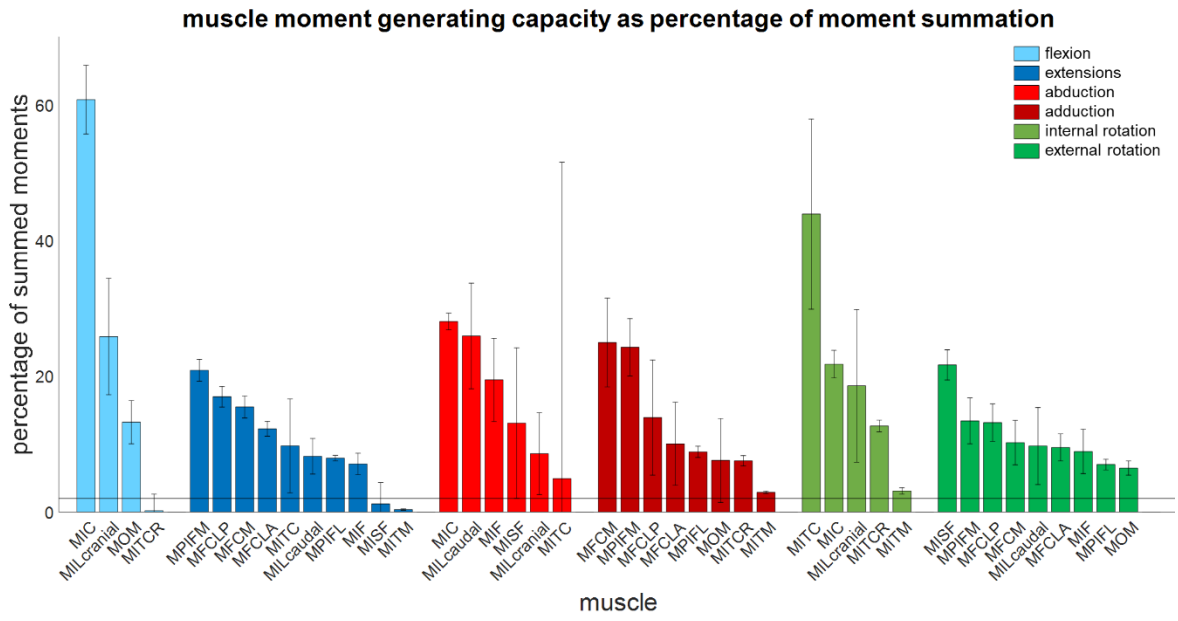

Figure 21 Muscle moment generating capacity as a percentage of the sum of all moments acting in the same direction. Error bars show ±1 standard deviation. Muscles for which the mean moment generating capacity minus 1 standard deviation was less than 2% of the sum of all moments were not considered to have a function about that axis.

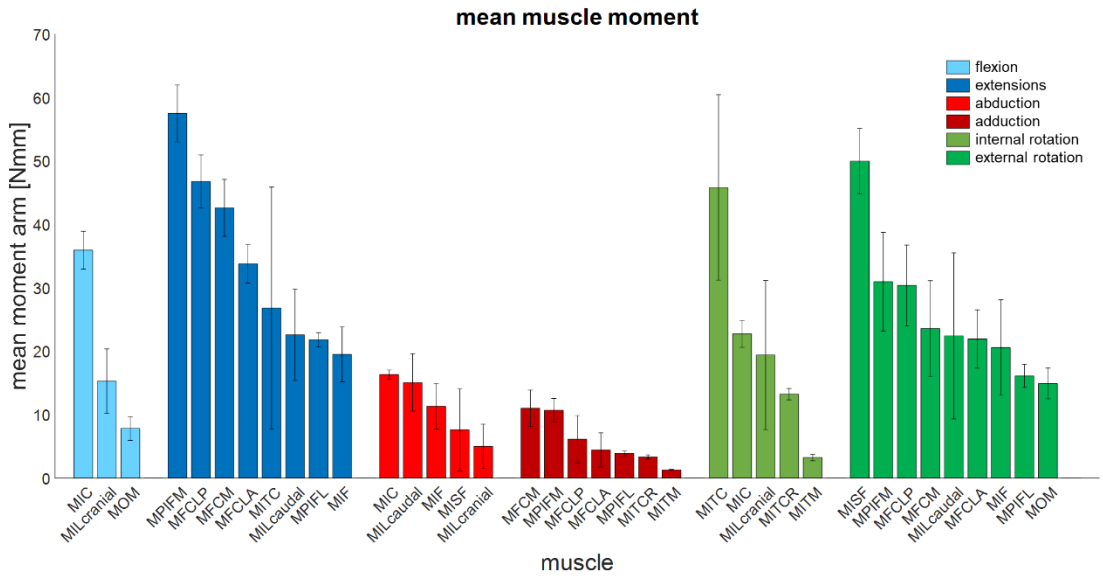

Figure 22 Mean muscle moment generating capacity of 14 key pelvic muscles of the magpie about all 3 rotational degrees of freedom of the hip. Error bars show ±1 standard deviation.

Table 5 The mean coefficient of variation (CV) of each muscle's moment generating capacity computed at each increment of joint angle from all possible combinations of origin, via point and insertion locations as appropriate. Blank cells indicate conditions where a muscle does not have a function with respect to the respective degree of freedom.

muscle	*F/E*	*AB/AD*	*Int/Ext*
MFCLA	*9%*	*62%*	*21%*
MFCLP	*9%*	*62%*	*21%*
MFCM	*11%*	*26%*	*33%*
MIC	*9%*	*4%*	*9%*
MIF	*23%*	*32%*	*37%*
MILcaudal	*33%*	*30%*	*59%*
MILcranial	*33%*	*70%*	*61%*
MISF		*85%*	*10%*
MITC	*77%*		*32%*
MITCR		*10%*	*7%*
MITM		*6%*	*15%*
MOM	*25%*		*16%*
MPIFL	*5%*	*9%*	*11%*
MPIFM	*8%*	*17%*	*25%*

Table 6 Mean coefficient of variation (CV) of the muscle moment generating capacity in response to varying origin site and via point locations. Only muscles for which the mean CV was particularly large (over 50%) were investigated further (MFCLA, MFCLP, MILcaudal, MILcranial, MISF, and MITC). For these muscles further analyses revealed whether the moment generating capacity was most sensitive to varying either the origin site or via point locations. Subscripts denote the axis about which the moment generating capacity was most sensitive.

	mean CV	
muscle	*origin*	*via point*
$MFCLA_{AB/AD}$	*16%*	***41%***
$MFCLP_{AB/AD}$	*16%*	***43%***
$MILcaudal_{Int/Ext}$	***61%***	*40%*
$MILcranial_{AB/AD}$	***72%***	*45%*
$MISF_{AB/AD}$	***81%***	*63%*
$MITC_{F/E}$	***316%***	*99%*

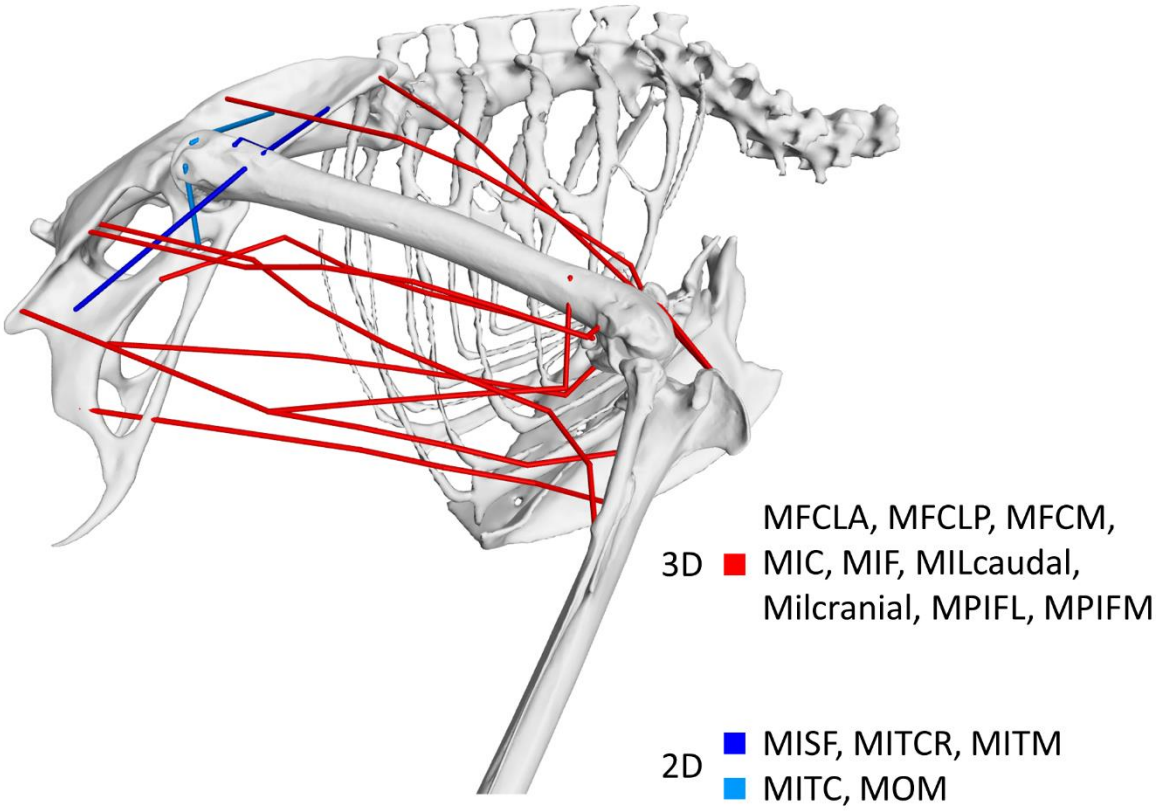

Figure 23 Visual representation of the nature of 3D muscle function identified in this study. Muscles shown in red were found to possess dominant moment arms in 3D while those shown in blue had functions around 2 axes only. Muscles shown in dark blue represent those whose functions are about the ab/adduction and int/external rotation axes while the function of muscles depicted in light blue is about the flex/extension and int/external rotation axes.

4.6 Discussion

This study aimed to quantify 3D function of the pelvic muscles of the magpie (*Pica pica*) based on the muscle moment generating capacity throughout the take-off jump. Based on a previous description of the 3D nature of the kinematics of bird jumping take-offs (Provini and Abourachid, 2018), the underlying hypothesis was that pelvic muscles were multi-functional rather than acting solely in the sagittal plane. Our analyses show that although 11 of 14 key pelvic muscles investigated here do indeed act in the sagittal plane where they function as either flexors or extensors, all 14 muscles also act as either internal or external rotators (Figure 23). The 3D muscle moment generating capacities determined here indeed reveal that internal/external moments are of similar magnitude to those in flexion/extension with the mean ratio between a muscles' peak internal/external rotation and flexion/extension of 0.89±0.33. This capacity of the pelvic muscles to actuate 3D moments reported here is consistent with kinematic analyses that characterise the motions as 3D rather than planar (Provini and Abourachid, 2018). Additionally, our findings agree with the notion that theropod hindlimb muscles more generally are multifunctional (Hutchinson and Allen, 2009), possessing moment generating capacity about all 3 joint degrees of freedom. The 3D nature of the kinematics and the moment generating capacity of the muscles suggest that in order to develop a detailed understanding of avian take-off mechanics hindlimb anatomy should be considered in 3D.

In the past, muscle function in birds has been ascertained primarily through anatomical dissection of muscle-tendon paths (Hudson, 1937; Wilcox, 1952; Verstappen et al., 1998; Smith et al., 2006) and remained limited to function about the flexion extension axis for single joints, including muscles which cross multiple joints. Muscle function about flexion/extension determined by the quantitative approach here agreed with the literature for all muscles except for the MITC which had previously been defined as a flexor but was defined here as an extensor (Table 4). The MITC is a muscle with a large attachment area at its pelvic origin, inserting proximal to the femoral neck. Depending on the level of ab/adduction and internal/external rotation, the muscle line of action could be either above or below the flexion/extension axis of rotation. Therefore, it is possible for the function of the muscle about the flexion/extension axis to swap depending on the orientation of the femur. Although the MITC's moment generating capacity was sensitive to the modelling process (Table 4), the function never swapped from extensor to flexor in our analyses when considering the joint RoM for a take-off leap previously determined by 3D fluoroscopy (Provini and Abourachid, 2018). The current study thus provides evidence that throughout the jump, the activity considered here, the MITC acts exclusively as a hip extensor.

The literature describes three muscles attaching at the pelvis (MIC, MILcaudal and MILcranial) to have a function about the knee but does not report about their role at the hip (Table 4, Verstappen et al. (1998)). Our analyses showed that the MIC and MILcranial contributed substantially to the moment generating capacity in hip flexion, accounting for 61 and 26% respectively, to the overall capacity (Fig. 5, Table 4) and thus point towards a crucial role of these muscles also for hip function. On the other hand, the MILcaudal accounted for only 8% of the total extensor moment generating capacity, suggesting a more limited role for its hip function during a jump.

During the take-off jump all joints of the hindlimb, including the knee, are extended through activation of the muscles. The hip flexors MIC and MILcranial also have the capacity to extend the knee (Verstappen et al., 1998) and if activated during take-off, would work against the hip extensors. Such seemingly paradoxical muscle function may add to hip joint stability during the jump by active co-contraction, a mechanism that has been described for human hindlimb (Herzog and Binding, 1993; Ait-Haddou et al., 2000; Jinha et al., 2006a; Jinha et al., 2006b; Correa et al., 2010; Trepczynski et al., 2018). Further studies using computational modelling approaches to either estimate muscle activation patterns (Rankin et al., 2016)) or work to directly measure muscle activation (Higham et al., 2008) are required to further elucidate the nature of avian hindlimb muscle coordination patterns during a take-off leap.

It is well established that the muscle moment generating capacity determined by a model is sensitive to how 3D muscle lines of actions are described (Jensen and Davy, 1975; Blemker and Delp, 2005; Heller et al., 2005; O'Neill et al., 2013; Charles et al., 2016). The current study took a rigorous approach to estimate the extent of uncertainty in defining 3D muscle paths considering likely morphological variation in muscle attachments and via points within the family of corvids and more widely across extant birds (Hudson, 1937; Verstappen et al., 1998; Carril et al., 2014). Our sensitivity analysis considering 972 different configurations of the 3D muscle paths demonstrated modest variation in the moment generating capacity for eight of the 14 hip muscles (mean CV below 50%) suggesting that modelling their function by a single line of action is appropriate (Monti et al., 2001; O'Neill et al., 2013; Charles et al., 2016; Modenese and Kohout, 2020).

In contrast, the moment generating capacity of the MITC, MISF, MILcranial, MILcaudal, MFCLP and MFCLA varied between 59 to 85% (Table 5). The MITC, MISF, MILcranial and MILcaudal are muscles that have large attachment areas on the pelvis with substantial cranio-caudal extent and, depending on the location of a modelled muscle line of action, their moment generating capacity at the hip may vary considerably. Modelling muscles with large attachment sites with multiple lines of action is common practice when modelling the biomechanics of the human hip, where the glutei are typically modelled by three distinct lines of action (Arnold et al., 2009; Higham and Biewener,

2011; Modenese and Kohout, 2020). The analyses here suggest that a similar approach would also be beneficial to capture the varied function of the MITC, MISF, MILcranial and MILcaudal in the avian hindlimb. On the other hand, the large moment arm sensitivity of the MFCLP/MFCLA was mainly due to the extent of the variation of the via points considered here, with circumferential variation of 10 degrees, a value determined from the variation of 11 hip muscles across the 5 species considered. However, for these specific muscles, the actual variation between species was considerably smaller with only 2 degrees suggesting that the sensitivity determined here represents a safe upper bound for the likely effect.

Muscle function in the avian hindlimb has previously been examined using similar, quantitative techniques throughout the full RoM of the joints of the ostrich, an extant flightless bird (Hutchinson et al., 2015). Whilst the exact details and extent to which pelvic muscles in the ostrich take on 3D function appear to vary somewhat from the data reported here, Hutchinson and co-workers (2015) provided strong evidence for the function of pelvic muscles in the ostrich to be 3D in nature rather than being limited to the sagittal plane, where all pelvic muscles were found to have functions about all three rotational degrees of freedom and four muscles (IC, ILp, FCLP and OM) were found to have substantial capacity to act about multiple degrees of freedom at the hip. Even though the ostrich and magpie sit on opposite ends of the phylogenetic tree (Jarvis et al., 2014), the functional demand from their habitual locomotor activities (running, jumping) appears to necessitate hip muscle function in flightless and flying birds alike to be 3D in nature.

Extending the methodology established here to robustly quantify 3D muscle function at the hip to muscles crossing the knee and ankle constitutes a stepping stone to establishing a more advanced musculoskeletal model (Heller et al., 2001a; Heller et al., 2001b; Heller et al., 2003; Heller et al., 2005; Arnold et al., 2009; Trepczynski et al., 2012; Hutchinson et al., 2015; Trepczynski et al., 2018) of the hindlimb in extant and extinct avians to elucidate how birds orchestrate the use of muscles to take to the air by a jump. The current study highlighted the capability for all pelvic muscles to act as an internal/external rotator throughout the RoM of the take-off jump along with the previously described and undoubtedly essential flexion/extension (Verstappen et al., 1998). Developing such musculoskeletal models would also offer a means to further explore the hypothesis that internal/external rotation is indeed a crucial motion that needs to be powered or at least controlled to take to the air which is supported by the data provided here and previous studies supporting a 3D muscle function of the avian pelvic hindlimb more generally (Hutchinson et al., 2015; Rankin et al., 2016; Allen et al., 2021).

The study conducted here had limitations. Bone scans were based on one specimen of a magpie to inform the skeletal system of the biomechanical model. However, the length of the femur of the

scanned specimen (38.8 mm) places its size well within one standard deviation of the mean femoral length (40.2±1.5 mm) measured from a population of 81 magpies in the literature (Tomek and Bochenski, 2000). Furthermore, the mass of the specimen used here (190 g) was very close to the mean mass (188±20 g) of the 7 magpie specimens analysed by Verstappen and co-workers (1998) and thus the data used here appears to be reasonably representative of a typical magpie. Although muscle attachment sites were not obtained from the specimen itself, they were informed by the literature (Verstappen et al., 1998) following a careful approach to map attachments on the surfaces of the 3D CT scanned specimen. Moreover, although the crow, the species informing the locations of the via points, is a different species to the magpie, they are closely related and belong both to the family of Corvidae within which hindlimb morphology is very conserved (Verstappen et al., 1998). Furthermore, a detailed sensitivity analysis considering the uncertainty presented by using data from different sources, analysing 972 variations of 14 muscles, ensured that pelvic muscle function was ascertained in a robust manner.

The approach developed here combines state-of the art 3D CT imaging and computer graphics and visualisation techniques with detailed anatomical descriptions of musculoskeletal anatomy of birds obtained in the past (Hudson, 1937) to efficiently establish 3D representations of musculoskeletal anatomy. Maximum isometric force of the muscle was calculated from PCSA described in literature (Verstappen et al., 1998) and was scaled by mass to the scanned specimen. This study investigated muscle function throughout of the RoM during the take-off jump which was informed by data from the literature rather than information for the specimen for which the 3D skeletal anatomy was derived. However, the data used to inform the RoM was determined using biplanar fluoroscopy (XRoMM) (Provini and Abourachid, 2018), a method currently deemed to constitute the gold-standard for determining accurate 3D skeletal kinematic data (Brainerd et al., 2010; Gatesy et al., 2010).

This is the first investigation into the 3D moment generating capacity of the hindlimb muscles during the take-off jump of a flying bird. Through the sensitivity analysis, 8 of 14 muscles were found to be modelled sufficiently with a single line of action whereas 4 of the remaining 6, owing to their large origin sites, should be modelled with multiple lines of action. Using robust quantitative analysis our study revealed that while most (11 of 14) muscles acted as either flexor or extensor of the hip, all key pelvic muscles studied here also have the capacity to act as either internal or external rotators. Similarly, 12 muscles possessed at least some ab/adduction capability, thereby revealing the function of the avian hip to be essentially 3D in nature. The ability for all pelvic muscles to act as an internal/external rotator implies that internal/external rotation might be a crucial motion that needs to be powered or at least controlled to take to the air. Advanced musculoskeletal models of the hindlimb can now use the quantitative evidence on essential hindlimb muscle function obtained

here to reveal in detail how birds orchestrate their muscles to generate the forces necessary to take to the air by a jump.

4.7 Acknowledgments

This work was supported by the Natural Environmental Research Council [grant number NE/L002531/1].

Chapter 5 On the hindlimb biomechanics of the avian take-off leap

Chapter 5 describes how a computational musculoskeletal model of the zebra finch, *Taeniopygia guttata*, hindlimb was developed and driven with previously published take-off ground reaction forces and 3D kinematics. This first biomechanical model to study the internal biomechanics necessary for take-off used an inverse dynamics approach to calculate the external moments at the ankle, knee, and hip joints and contrasted these to the cumulative capacity of the hindlimb muscles to balance these moments across a range of take-off conditions. This chapter reports substantial external moments at the hip and ankle joints, reaching magnitudes of about two times the values previously reported during the running of a flightless bird.

5.1 Citation

In this chapter the full manuscript, titled "On the hindlimb biomechanics of the avian take-off leap" submitted as a preprint to Bioarchive and in review in the Royal Society Interface is presented. Supplementary information is provided in Appendix B. The citation for the preprint is provided below:

Meilak, E.A., Provini P., Palmer C., Gostling, N.J., and Heller, M.O. (2021). **On the hindlimb biomechanics of the avian take-off leap**. bioRxiv, DOI: 10.1101/2021.11.19.469279

5.2 Abstract

Although extant land birds take to the air by leaping, generating the initial take-off velocity primarily from the hindlimbs, the detailed musculoskeletal mechanics remain largely unknown. We therefore simulated *in silico* the take-off leap of the zebra finch, *Taeniopygia guttata,* a model species of passerine, a class of bird which includes over half of all extant bird species. A 3D computational musculoskeletal model of the zebra finch hindlimb, comprising of 43 musculotendon units was developed and driven with previously published take-off ground reaction forces and kinematics. Using inverse dynamics, the external moments at the ankle, knee, and hip joints were calculated and contrasted to the cumulative muscle capability to balance these moments. Mean peak external flexion moments at the hip and ankle were 0.55 bodyweight times leg length (BWL) each whilst peak knee extension moments were about half that value (0.29 BWL). Muscles had the capacity to generate 146%, 230%, and 212 % of the mean peak external moments at the hip, knee, and ankle, respectively. Similarities in hindlimb morphology and external loading across passerine species suggest that the effective take-off strategy employed by the zebra finch may be shared across the passerine clade and therefore half of all birds.

5.3 Introduction

Take-off is a crucial part of avian flight, requiring energy-intensive motion to accelerate into the air. Understanding how birds make the transition from standing statically to being airborne is one of the key components necessary for understanding how avian flight evolved. Previous work on the take–off of a variety of land birds demonstrated that the hindlimb plays a major role in propelling the bird in to the air, and suggests that the bipedal leap generates approximately 80-90% of the take-off velocity (Heppner and Anderson, 1985; Bonser and Rayner, 1996; Earls, 2000; Tobalske, 2004; Provini et al., 2012; Provini and Abourachid, 2018). The group Passeriformes (passerines) includes over 5000 species of bird, making up approximately 60% of all bird species (Raikow, 1987; Ricklefs, 2012; Selvatti et al., 2015). Among them, the zebra finch (*Taeniopygia guttata*), a frequently utilised model species, is also known to primarily use its hindlimbs to take to the air: previous studies showed that the hindlimb is responsible for producing 94% of their take-off velocity (Provini et al., 2012). To date however, the detailed internal hindlimb mechanics necessary to produce a successful take-off remain largely unknown. This lack of knowledge in extant birds not only limits our understanding about how they master the feat of taking to the air but also presents an obstacle to accurately infer the capacity of fossil birds to be airborne, thus blurring our understanding of the origin of flight more generally.

Computational biomechanical modelling is a useful tool for calculating the internal mechanics occurring within a biomechanical system which are otherwise very difficult if not impossible to directly measure (Bergmann et al., 2001; Heller et al., 2001b; Heller et al., 2003; Taylor et al., 2006; Delp et al., 2007; Meilak et al., 2021a). Moreover, the application of such computational analysis methods to extant animals is seen as a key strategy to systematically develop the sound biomechanical basis on which to further our understanding also of the conditions in extinct species (Hutchinson et al., 2005; Bishop et al., 2018b; Allen et al., 2021). The inverse analysis approach is one such computational method that takes measured kinematics and kinetics to drive a biomechanical model to calculate the external moments at each degree of freedom of each joint (Duda et al., 1997a; Taylor et al., 2006; Goetz et al., 2008; Lund and Hicks, 2012a; Pizzolato et al., 2017). Detailed, 3D models of the musculoskeletal anatomy allow relating these external moments to the moment generating capacity of the internal force generating structures, i.e. the muscles, and to develop a more detailed understanding of internal avian hindlimb kinetics during the take-off leap. However, few studies have reported on the detailed external kinetics (ground reaction forces) (Heppner and Anderson, 1985; Bonser and Rayner, 1996; Tobalske, 2004; Provini et al., 2012) associated with the avian take-off leap and even fewer studies have investigated 3D hindlimb kinematics for these activities (Provini and Abourachid, 2018). The authors are aware of only a single study that has investigated the biomechanics of the avian jump, focussing on a predictive

simulation of the ground dwelling elegant-crested tinamou *Eudromia elegans* (Bishop et al., 2021a). However, due to the scarcity in ground reaction forces and kinematic data of the tinamou leap, data on which an inverse analysis would rely on, the authors opted for a forward approach to predict the leaping behaviour. In how far the simulations reflect kinetics and kinematics that are consistent with actual conditions that can be observed and measured in this bird therefore remains to be established. Although computational analyses in birds are available and have shown the value of such analyses to further our understanding of avian hindlimb biomechanics with respect to e.g. the critical role of the ankle muscles in the take-off leap of the tinamou and the function of the antitrochanter as a passive mechanism to stabilise the hip of the running ostrich (Rankin et al., 2016; Bishop et al., 2021a), to date no study has determined the internal hindlimb joint kinetics of a flying bird as it leaps into the air using detailed measurements of external forces and hind limb kinematics. With the application of X-ray reconstruction of moving morphology (XROMM) technology to capture detailed 3D bone kinematics of the avian take-off leap, in combination with computational biomechanical analyses, the technology is finally available to accurately simulate the internal mechanics of the extant avian take-off (Rubenson et al., 2007; Rubenson et al., 2010; Kambic et al., 2014; Kambic et al., 2017; Provini and Abourachid, 2018; Allen et al., 2021; Meilak et al., 2021a).

The current study therefore combines external forces and detailed bone kinematics that feed into computer simulations into the biomechanics of the hindlimb throughout the take-off leap of the zebra finch. In doing so we aim to address the following hypotheses that help to develop a comprehensive understanding of the mechanical requirements birds need to meet to propel themselves into the air. We firstly hypothesised that in order to generate the motion of the avian take-off leap, characterised by the hip, knee, and ankle joints all extending until the bird is airborne (Earls, 2000; Provini and Abourachid, 2018), net external flexion moments of similar peak magnitudes act at all these joints which the muscles balance by exerting extension moments. Consistent with the observation that predicative simulations of the tinamou predict the ankle to be most critical in determining the success of the take-off leap in a ground-dwelling bird (Bishop et al., 2021a), we further hypothesised that the ankle extensors of the zebra finch possess the largest capacity to balance the external moments. Finally, considering the avian hips' powerful capacity to generate internal/external rotation (IER) moments and a poor capacity to generate abduction/adduction (ABAD) moments (Rankin et al., 2016; Allen et al., 2021; Meilak et al., 2021a) in the presence of the antitrochanter, we hypothesise that external moments of similar peak magnitudes act in IER/ABAD on the hip joint of the zebra finch and that the bird possess powerful ability to actively balance the IER moments.

5.4 Materials and methods

To address our hypotheses, we built upon previously published detailed kinetics and kinematics data of the take-off leap of the zebra finch as input to a biomechanical simulation of the avian take-off leap (Provini et al., 2012; Provini and Abourachid, 2018) as explained in more detail below.

5.4.1 Overview

Key steps of our analysis methodology included the use of CT scans of the same individual, together with additional morphological data in the literature to characterise the bone and musculature respectively, from which a detailed 3D musculoskeletal model of the zebra finch hindlimb was developed. Here, muscles were mapped from a previously published magpie musculoskeletal model on to the zebra finch skeleton (Hudson, 1937; Verstappen et al., 1998; Meilak et al., 2021a). In addition, previously published 3D kinematics and ground reaction forces were used to drive the musculoskeletal model in inverse dynamics analyses to estimate external joint moments (Provini et al., 2012; Provini and Abourachid, 2018). The combination of these unique datasets, collected from the same species and even the same individual, offered a unique opportunity to generate an accurate simulation of the zebra finch take-off biomechanics.

The external joint moments were compared against the moment generating capacity of the muscles to document the biomechanical requirements and to assess the zebra finch's capability to actively balance the hindlimb joint moments experienced throughout the take-off leap. Here, moments about hip flex/extension (FE), ab/adduction (ABAD), int/external rotation (IER) and moments about FE at both the knee and ankle joints were considered. In addition, by comparing the hindlimb morphology and ground reaction forces of a variety of passerines ranging in mass (zebra finch *Taeniopygia guttata*, 15.4 g, starling *Sturnis vulgaris*, (77.3 g), crow *Corvus corone* (440 g) and raven *Corvus corax*, 1.1 kg) it was possible to explore the take-off mechanics of passerines more generally.

5.4.2 Materials, model building, and musculoskeletal analysis approach

The computational biomechanical musculoskeletal model of a zebra finch (15.4 g) was developed based on CT scans and muscle data of corvids from previously published works (Verstappen et al., 1998; Provini and Abourachid, 2018; Meilak et al., 2021a). The CT data was used for establishing the 3D skeletal model. In order to describe the spatial relationships between bones, local coordinate systems were established based on shape fitting techniques and functional analyses of the joints (Ehrig and Heller, 2019), as detailed in the supplementary information (Appendix B3). Muscles were modelled by 3D lines of action (Heller et al., 2001b; Seth et al., 2011; Trepczynski et al., 2012) by mapping muscles from the magpie skeleton to the zebra finch using elastic registration

(Schlager, 2015), while muscle maximum isometric force was scaled by body mass. Detailed kinematics derived from previously published XROMM data (Provini and Abourachid, 2018) were then used together with ground reaction forces (Provini et al., 2012) of zebra finch take-off leaps to drive the model in inverse dynamics simulations to calculate the external moments acting at the hindlimb joints. Nine sets of ground reaction forces obtained from 9 jumps of 4 birds (15.4±1.8g), were temporally synchronised with two sets of kinematics trials (taken from 1 bird with a mass of 15.4 g), resulting in 18 simulations analysed. Muscle moment arms were measured and used to calculate the maximum moment generating capacity about hip flexion/extension, ab/adduction and internal/external rotation, and knee and ankle flexion/extension. The muscle moment generating capacity was compared to the external joint moment to ascertain the zebra finch's ability to balance the external joint moments.

5.4.3 Skeletal model

The skeletal model was derived from CT scans (isotropic resolution 0.04 mm) of a zebra finch *Taeniopygia guttata* specimen (15.4 g), obtained in previously published studies (for full details please refer to (Provini and Abourachid, 2018)). For the current study, bones were segmented using ITK-SNAP (Yushkevich et al., 2006), and imported in to Rhino (v7; Robert McNeel & Associates, Seattle, USA) (McNeel, 2020) where triangulated bone surfaces were obtained after fitting subdivision surfaces using the QuadRemesh function. Bones which were treated in this way were the pelvis, femur, patella, tibiotarsus and tarsometatarsus. The detailed definition of joint centres and axes and local bone coordinate systems are available in the supplementary information (Appendix B1.2).

A linked rigid body model with 4 segments including the pelvis, thigh, shank and tarsometatarsus was defined in OpenSim v4.1 (Seth et al., 2018). Here, body segments were linked by 3 joints (hip, knee and ankle joints) with 3 rotational degrees of freedom (DoF) at the hip (allowing flexion/extension, internal/external rotation and ab/adduction) and 2 DoF at each of the knee and ankle joints (allowing flexion/extension and internal/external rotation). Because the foot remained stationary on the perch and motion of the trunk was largely due to the extension of the hip, knee and ankle joints, the foot was not included as a dedicated structure of the musculoskeletal model. In order to better capture the mechanics of hindlimb extension, a biomechanical model of the patella-femoral joint was incorporated in to the model. Here, the motion of the patella was defined by a 3D spline curve following approximately the trochlear surface of the femur. The patella was allowed to move along that spline as a function of the knee angle, with details of the motion informed by a musculoskeletal model of the helmeted guineafowl *Numida meleagris* (Cox et al., 2019). In order to map patellar motion from the guineafowl to the zebra finch model, the femoral

surface of the guineafowl model was elastically registered to the zebra finch femur (Manu, 2021a). The parameters of the elastic registration were then used to map the spline defining patellofemoral motion from the guineafowl to the zebra finch model using the R-package MesheR (Schlager, 2015).

5.4.4 Muscle geometry

The musculoskeletal model of the zebra finch included 43 muscles crossing the hip, knee and ankle, which were modelled as 3D polylines spanning origin and insertion using via points to fully describe their curved paths (Figure 24). Magpies (*Pica pica*) and zebra finch, share broadly similar hindlimb myology both following the characteristic hindlimb morphology of passerine birds (Raikow, 1987). Muscle attachment sites and via points were therefore mapped from a previously established model of the magpie (Meilak et al., 2021a) to the zebra finch hindlimb. Using a non-rigid iterative closest point (ICP) registration (Manu, 2021a) the magpie femur, tibiotarsus and tarsometatarsus were elastically registered to the corresponding long bones of the zebra finch hindlimb (Schlager, 2015) (Figure 25). Using 3D Slicer 4.11 (Fedorov et al., 2012), the pelvis of the magpie and zebra finch were first split in to the ilium, ischium and pubis before elastically registering them onto each other following the same approach as described for the long bones above. Following non-rigid registration, the rigid transformation and isotropic scaling parameters were recovered using Ordinary Procrustes Analysis (OPA) (Veldpaus et al., 1988) computed between the vertices of the original magpie bone surface and the vertices of the magpie bone surface that was elastically registered to the respective zebra finch bone (Matlab (2019b, The Mathworks, Nantucket, USA). This step was encoded in a 4x4 homogeneous transformation matrix. The remaining difference between the positions of the OPA mapped vertices and their elastically registered counterparts was captured in a dense deformation field. The homogeneous transformation matrix and the dense deformation field were then applied to all attachment and via points of the magpie muscles associated to the respective bone surface using the R-package MesheR (Schlager, 2015), and in so doing mapping muscles from the magpie hindlimb to the zebra finch (Figure 25). Wrapping cylinders and spheres were added with positions, orientations and radii individually adjusted to define the 3D muscle paths throughout the jumping RoM that avoided any intersection of muscles with bones.

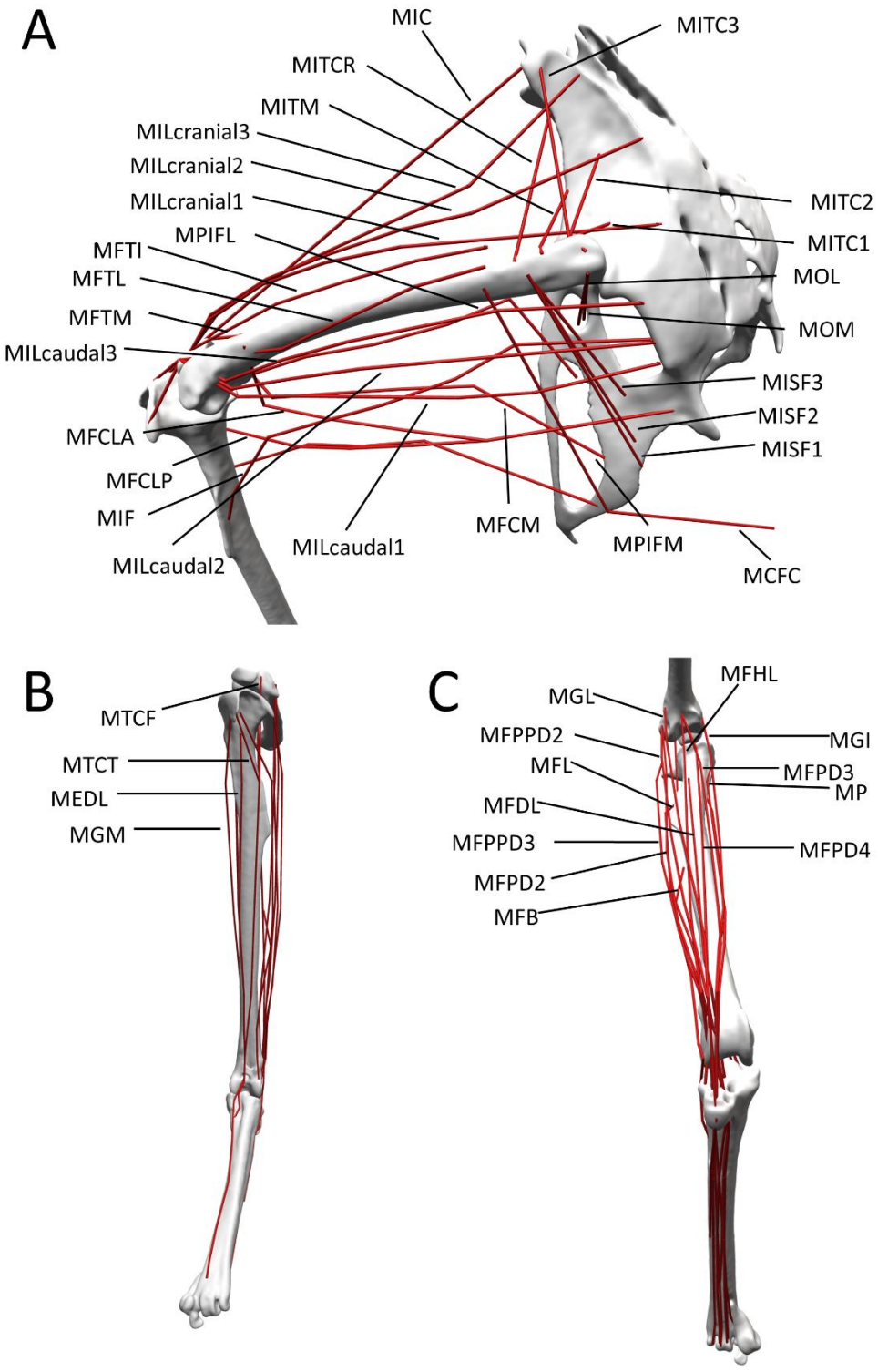

Figure 24 The musculoskeletal model of the left zebra finch hindlimb included 43 musculotendon units. A) Muscles that either cross the hip or knee joint and biarticular muscles crossing both hip and knee joints are shown in a caudo-lateral view. B) Anterior and C) posterior view of muscles crossing the ankle joint and biarticular muscles crossing both knee and ankle joints. For an explanation of the abbreviations of the muscles used here, please refer to Table 7.

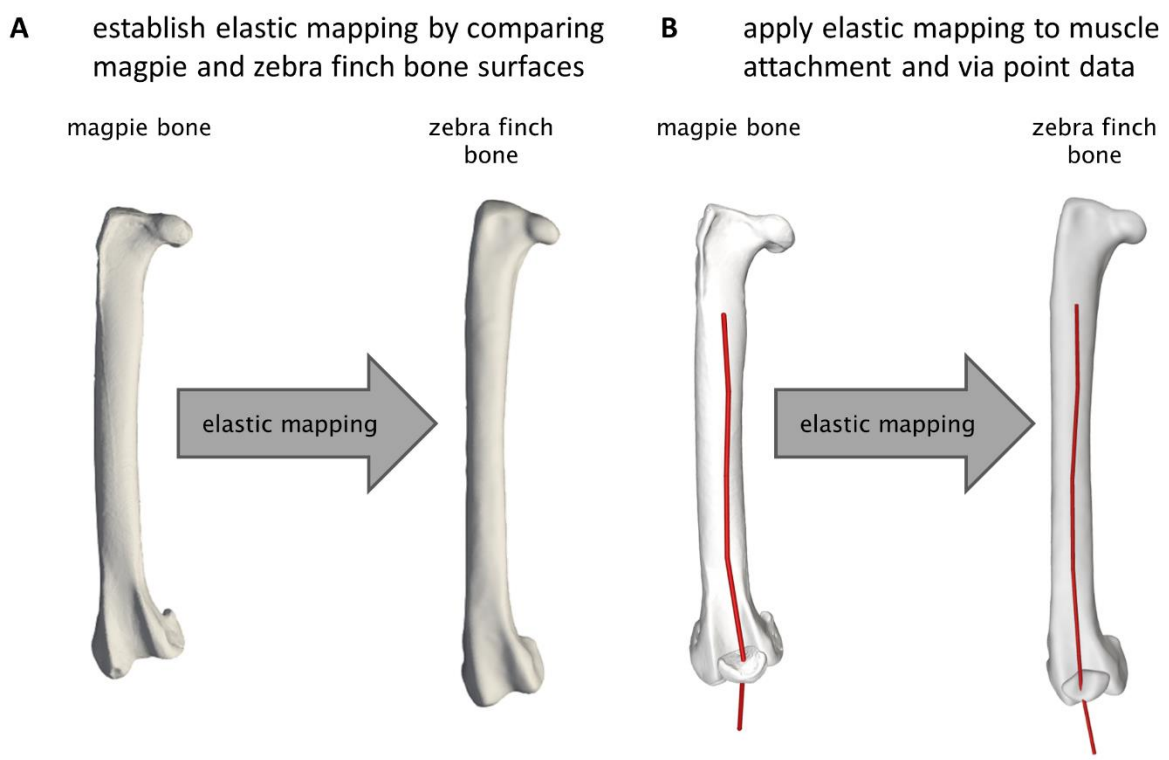

Figure 25 Schematic demonstrating the process of morphing the musculature from the magpie to the zebra finch hindlimb. To allow for a better visual comparison of the bones which differ by almost a factor of two in size, the bone surfaces depicted here are isotopically scaled by the reciprocal of the square root of their respective surface area. ***A*** *Establishing an elastic mapping by comparing magpie and zebra finch bone surfaces. Here, magpie bones were first registered to the corresponding zebra finch bone using non-rigid iterative closest point (ICP) registration (Manu, 2021a). Following non-rigid registration, the rigid transformation and isotropic scaling parameters were recovered using Ordinary Procrustes Analysis (OPA) computed between the vertices of the original magpie bone surface and the vertices of the magpie bone surface that was elastically registered to the respective zebra finch bone. This step was encoded in a 4x4 homogeneous transformation matrix. The remaining difference between the positions of the OPA mapped vertices and their elastically registered counterparts was captured in a dense deformation field.* ***B*** *Application of the elastic mapping to muscle attachment and via point data. The homogeneous transformation matrix and the dense deformation field were then applied to all attachment and via points of the magpie muscles associated to the respective bone surface, resulting in an elastic registration of these structures to the zebra finch model.*

Table 7 Musculotendon units included in the musculoskeletal model of the zebra finch, grouped by which joints they cross; H, K and A denote the hip, knee and ankle joints, respectively. Muscles which are categorised under two joints are biarticular. Maximum isometric force was calculated by scaling the maximum isometric force of the corresponding muscles of the magpie by mass (Meilak et al., 2021a).

Abbreviation	Muscle name	Joints	Maximum isometric force [N]
MCFC	*M. caudofemoralis pars caudalis*	H	0.154
MFCLA	*M. flexor cruris lateralis pars accessoria*	H	0.250
MISF1	*M. ischiofemoralis 1*	H	0.259
MISF2	*M. ischiofemoralis 2*	H	0.259
MISF3	*M. ischiofemoralis 3*	H	0.259
MITC1	*M. iliotrochantericus caudalis 1*	H	0.396
MITC2	*M. iliotrochantericus caudalis 2*	H	0.396
MITC3	*M. iliotrochantericus caudalis 2*	H	0.396
MITCR	*M. iliotrochantericus cranialis*	H	0.003
MITM	*M. iliotrochantericus medius*	H	0.057
MOL	*M. obturatorius lateralis*	H	0.112
MOM	*M. obturatorius medialis*	H	0.431
MPIFL	*M. puboischiofemoralis pars lateralis*	H	0.388
MPIFM	*M. puboischiofemoralis pars medialis*	H	0.448
MFCLP	*M. flexor cruris lateralis pars pelvica*	H, K	0.346
MFCM	*M. flexor cruris medialis*	H, K	0.238
MIC	*M. iliotibialis cranialis*	H, K	0.218
MIF	*M. iliofibularis*	H, K	0.458
MILcaudal1	*M. iliotibialis lateralis caudalis 1*	H, K	0.254
MILcaudal2	*M. iliotibialis lateralis caudalis 2*	H, K	0.254
MILcaudal3	*M. iliotibialis lateralis caudalis 3*	H, K	0.254
MILcranial1	*M. iliotibialis lateralis cranialis 1*	H, K	0.036
MILcranial2	*M. iliotibialis lateralis cranialis 2*	H, K	0.036
MILcranial3	*M. iliotibialis lateralis cranialis 3*	H, K	0.036
MFTI	*M. femorotibialis intermedius*	K	0.614
MFTL	*M. musculus femorotibialis lateralis*	K	0.013
MFTM	*M. femorotibialis medialis*	K	0.490
MFHL	*M. flexor hallucis longus*	K, A	0.843
MFPD2	*M. flexor perforates digiti 2*	K, A	0.357
MFPD3	*M. flexor perforates digiti 3*	K, A	0.362

MFPD4	*M. flexor perforates digiti 4*	K, A	0.483
MFPPD2	*M. flexor perforans et perforates digiti 2*	K, A	0.236
MGI	*M. gastrocnemius pars intermedia*	K, A	0.621
MGL	*M. gastroc-nemius pars lateralis*	K, A	1.824
MTCF	*M. tibialis cranialis caput femorale*	K, A	0.385
MEDL	*M. extensor digitorum longus*	A	0.031
MFB	*M. fibularis brevis*	A	0.366
MFDL	*M. flexor digitorum longus*	A	1.003
MFL	*M. fibularis longus*	A	0.861
MFPPD3	*M. flexor perforans et perforates digiti 3*	A	0.894
MGM	*M. gastrocnemius pars medialis*	A	1.153
MP	*M. plantaris*	A	0.079
MTCT	*M. tibialis cranialis caput tibiale*	A	0.516

5.4.5 Biomechanical analysis

5.4.5.1 Kinematics

Detailed 3D kinematics were derived from previously published X-ray reconstruction of moving morphology (XROMM) data of the left hindlimb throughout two autonomous take-off leaps of the zebra finch (Provini and Abourachid, 2018). For these analyses three tantalum bead markers with an approximate diameter of 0.5 mm were attached to the tarsometatarsus, while two markers were implanted to the tibia, one to the femur, and one at the pelvis. In order to reliably track 3D skeletal kinematics for the current study, the location of the pelvis was determined using the implanted pelvic marker and, while its orientation was determined using scientific rotoscoping, a reliable process in particular for bones with specific shapes such as the pelvis (Brainerd et al., 2010). Owing to the generally higher precision of the 3D marker positions compared to 3D position and orientation data derived from scientific rotoscoping (Brainerd et al., 2010; Provini and Abourachid, 2018), a method for reconstructing 3D skeletal motion that maximised usage of the marker data while minimising reliance on the manual process of scientific rotoscoping was developed. Here, 3D positions and orientations of the long bones of the hindlimb were obtained using the attached physical markers, supplemented by functionally defined virtual markers, and detailed 3D bone surface models. A full detailed description of the methodology used to define these virtual markers and track 3D skeletal motion using a combination of XROMM data, bone surfaces and virtual markers is provided in the supplementary materials section (Appendix B1).

An inverse kinematics analysis was then carried out in OpenSim (Seth et al., 2011; Pizzolato et al., 2017; Seth et al., 2018) to map the kinematics from the XROMM data to the constrained biomechanical model using physical and virtual markers placed at their known locations on the model bones. Across the two kinematics trials, the ranges of motion for the skeletal kinematics with respect to hip flexion/extension (FE), abduction/adduction (ABAD) and internal/external rotation (IER) recovered in that manner were 42° (-4° to 38°), 15° (-37° to -22°), and 20° (8° to 28°), respectively. Knee and ankle FE range of motion were 40° (123° to 163°) and 74° (61° to 135°), respectively (see supplementary Figure 34). Substantial internal/external rotation range of motion at the knee and ankle was also measured, with a range of motion of 16° (5° to 21°) and 30° (-15° to 15°), respectively.

The take-off velocity of the bird was defined by measuring the velocity of its centre of mass at the instant the feet left the ground (Earls, 2000; Tobalske, 2004; Provini et al., 2012). To that end, the centre of mass of the zebra finch was determined using the soft tissue envelope of the zebra finch and the RigidBodyParams (Semechko, 2021) function under the assumption of a homogenous body soft tissue density (Semechko, 2021). The velocity of the centre of mass of the zebra finch was then

measured by tracking its location throughout the take-off trials using the OpenSim 4.1 BodyKinematics Tool. Take-off velocity was determined as the velocity at the instant all toes on the hindlimb being tracked, left the perch. Take-off velocities for the two trials investigated were determined to be 1.39 and 1.08 m/s.

5.4.5.2 Kinetics

Previously reported ground reaction forces of the take-off leap of a zebra finch (Provini and Abourachid, 2018) were used as inputs to the current study in this study. Since full details for the collection of these data were previously reported, the experimental setup is only briefly summarized below. Vertical and horizontal ground reaction forces were recorded at 400 Hz from a force platform (Squirrel force plate, Kistler France, Les Ulis, France; resolution ±0.01N), to which a wooden perch, 1.5 cm in diameter, was attached. The ground reaction forces measured from nine trials of a zebra finch taking off from a perch (Provini et al., 2012) were used to drive the take-off simulations.

Each of the nine zebra finch kinetics trials were paired with the two sets of kinematics trials enabling analysis of 18 distinct take-off conditions. Here, the ground reaction forces were temporally aligned to the kinematic data such that at the instant at which the resultant ground force fell to zero was matched to the instant at which the toes left the ground. Ground reaction forces were assumed to act through the centre of the perch (Figure 26).

For use in the current study, the ground reaction force vectors were scaled in magnitude so that the impulse imparted by the legs resulted in 94% take-off velocity that was measured from the kinematics for the two trials considered here. This scaling was performed to reflect previously identified relationships for the take-off mechanics of the zebra finch, in which it was measured that the hindlimb produced 94% of take-off velocity (Provini et al., 2012). Here, the method for calculating the velocity as a result of the impulse (V_{GRF}) imparted by the hindlimb followed the approach by Provini and colleagues (2012) and is outlined below. Firstly, the acceleration resulting from the ground reaction forces, $\dot{V}_{GRF}$, were calculated as follows:

$$\dot{V}_{GRF} = \frac{\sqrt{F_x^2 + F_y^2 + (F_z^2 - mg)}}{m} \qquad \text{(equation 4)}$$

where F_x is forward force, F_y is lateral force, F_z is vertical force, m is the mass of the bird, and g is the acceleration due to gravity. The integral of the acceleration over the duration of the take-off then provides the take-off velocity as a result of the ground reaction forces, V_{GRF}:

$$V_{GRF} = \int_{t_0}^{lo} \frac{\sqrt{F_x^2 + F_y^2 + (F_z^2 - mg)}}{m} dt \qquad \text{(equation 5)}$$

where t_0 is the time when the jump starts and lo the time at lift off.

5.4.5.3 External joint moments

Ground reaction forces were applied to the tarsometatarsus, with the centre of pressure placed in the centre of the perch (Figure 26). Using kinematics and ground reaction forces as input to the inverse dynamics analysis, external joint moments were calculated about hip FE, ABAD, IER, knee FE and ankle FE. Joint moments were normalised by the product of bodyweight and leg length L (defined as the sum of the segment lengths of femur, tibiotarsus, tarsometatarsus, and digit III) (Parslew et al., 2018), and time normalised to the duration of the jump cycle. Mean and standard deviations of the external joint moments were calculated across all 18 take-off sequences to obtain a robust estimate of the envelope of zebra finch take-off biomechanics. Here, joint moments are identified by the direction of joint movement induced by the action of the muscle group activating the respective degree of freedom.

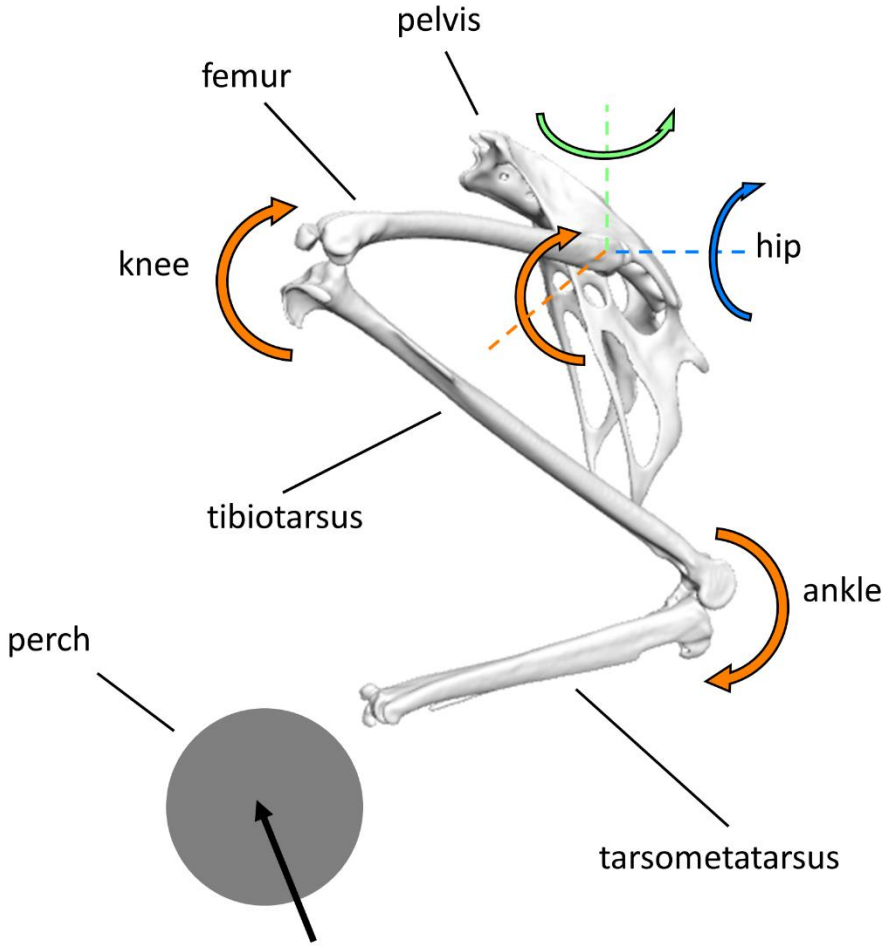

Figure 26 Force and moment diagram for the zebra finch hindlimb, including the pelvis, femur, tibiotarsus and tarsometatarsus in a lateral view. The musculoskeletal model described the hip, knee and ankle as three, two and two degree of freedom joints respectively. The straight black arrow on the perch represents the ground reaction force acting through the centre of the perch. Curved arrows reflect external moments acting at the joints and are colour coded such that the orange arrows identify the moment about the joint's flexion/extension axes, blue arrows identify moments about a joints' internal/external rotation axis, and green arrow identifies the moments about the joints' ab/adduction axis. At the hip, the ground reaction forces consistently result in flexion, abduction and an internal rotation moments throughout the leap cycles. At the knee and ankle joints, the ground reaction forces result in extension, and flexion moments, respectively.

5.4.5.4 Muscle moment generating capacity

The methodology for calculating muscle moment generating capacity followed the approach described by Meilak and colleagues (2021) and is outlined below. The moment generating capacity for each muscle about each joint degree of freedom (DoF) being considered was calculated by multiplying the muscle maximum isometric force (F_{max}) by the instantaneous moment arm ($MA_{t,i,j}$), evaluated at each time increment (*t*) throughout the kinematics trials. These moments were evaluated for each muscle *i (where i=1..43)* as the product of the maximum isometric muscle force (F_{max}) and the instantaneous moment arm ($MA_{t,i,j}$) determined throughout the take-off kinematics for each rotational DoF *j (where j=1..5* for hip FE, ABAD, IER, knee FE and ankle FE):

$$M_{t,i,j} = F_{max,i} \cdot MA_{t,i,j} \qquad \text{(equation 6)}$$

The moments of muscles acting in the same direction (i.e. their moments have the same sign) were summed for each degree of freedom to provide the total joint moment generating capacity in relation to that specific action ($M_{t,j}$):

$$M_{t,j} = \sum_{i=1}^{43} M_{t,i,j} \qquad \text{(equation 7)}$$

5.4.5.5 Comparing biomechanical conditions across the group of Passerine birds

To address the hypothesis that passerines share similar take-off behaviour, conditions across the Passerine clade were compared. The ground reaction force data available for the zebra finch was amended with similar data from further animals within the group of passerines. In a study approved by the local ethics committee of the University of Southampton (ERGO II ID 32207), a crow (*Corvus corone*) and raven (*Corvus corax*) took off 6 times each from a force platform (9260AA, Kistler) while 3D ground reaction forces (GRFs) were sampled at 10 kHz. For all species, vertical and horizontal forces were filtered using a zero-phase low-pass (40Hz) custom filter in Matlab. The peak ground reaction forces of the zebra finch, starling (Earls, 2000), crow and raven were all normalised by bodyweight and, together with key measures of hind limb geometry (Table 8) to compare take-off conditions within the group of passerines.

Table 8 Key morphometric parameters of zebra finch (Taeniopygia guttata), starling (Sturnis vulgaris), crow (Corvus corone), and raven (Corvus corax).

species	mass [g]	femur length (L_{fem}) [cm]	tibiotarsus length (L_{tib}) [cm]	tarsometatarsus length (L_{tars}) [cm]	digit III length [cm]	hindlimb length [cm]	hindlimb index ((L_{tars} + L_{tib})/ L_{fem})
zebra finch	15.4	1.40	2.24	1.46	1.10	6.2	2.64
starling (Earls, 2000)	77.3	2.53	4.37	2.82			2.84
crow	440	5.28	8.74	5.77			2.75
raven	1100	6.92	11.42	6.80			2.63

5.5 Results

The duration of the take-off leap ranged between 62-65ms (Figure 27). Mean resultant peak ground reaction forces per leg were 1.81±0.21 BW (range: 1.42 to 2.15 BW, c.f. supplementary Figure 34) and occurred at about 62 % leap cycle time. Across the two kinematics trials, the largest ranges of motions were 74°, 42° and 40° about the ankle, hip, and knee FE axes, respectively. The ranges of motion about the joints' secondary degrees of freedom were similar, with hip IER and ABAD RoMs of 20° and 15°, respectively and knee and ankle IER RoMs of 16° and 30°, respectively (see supplementary Figure 35).

The largest external moments observed were the moments around the flexion/extension axes. Here, the mean peak external joint flexion moments at the hip and ankle were of similar magnitude (0.66±0.04 and 0.68±0.05 BWL, respectively) while the mean knee extension moment was only about half that value (0.38±0.05 BWL, Figure 28, Table 9). The smallest peak moments were computed about hip IER and ABAD with mean peak moments of 0.27±0.07 and 0.20±0.07 BWL, respectively (Figure 28, Table 9). At the instances that these peak moments occurred, the muscles had the ability to generate 120%, 282% and 61% of the mean peak hip FE, IER and ABAD joint moments, respectively (Figure 28, Table 9). The hindlimb muscles were able to generate 177% and 176% of the mean peak joint moments about the FE axes of the ankle and knee, respectively (Figure 28 B and C, Table 9).

Comparing conditions across the group of passerines, the zebra finch as bird with the smallest mass by far (15.4 g) had the smallest normalised peak ground reaction forces per leg of 1.94±0.25 BW, while starling (77.3 g), crow (440 g), and raven (1.1 kg) exerted very similar peak GRFs with values of 2.15±0.14 BW (Earls, 2000), 2.20±0.29 BW, and 2.25±0.14 BW, respectively (see supplementary Figure 36).

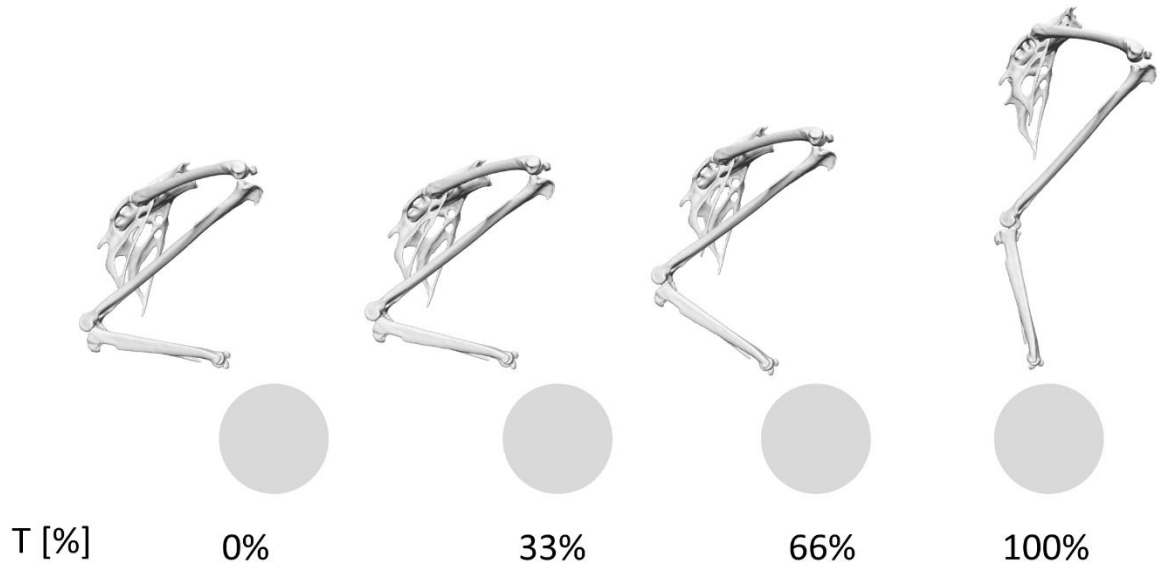

Figure 27 Lateral view of right zebra finch hindlimb throughout the normalised take-off leap cycle. The duration of the take-off jump duration ranged from 62 to 67 ms while all of the ankle, knee, and hip joint undergo substantial extension.

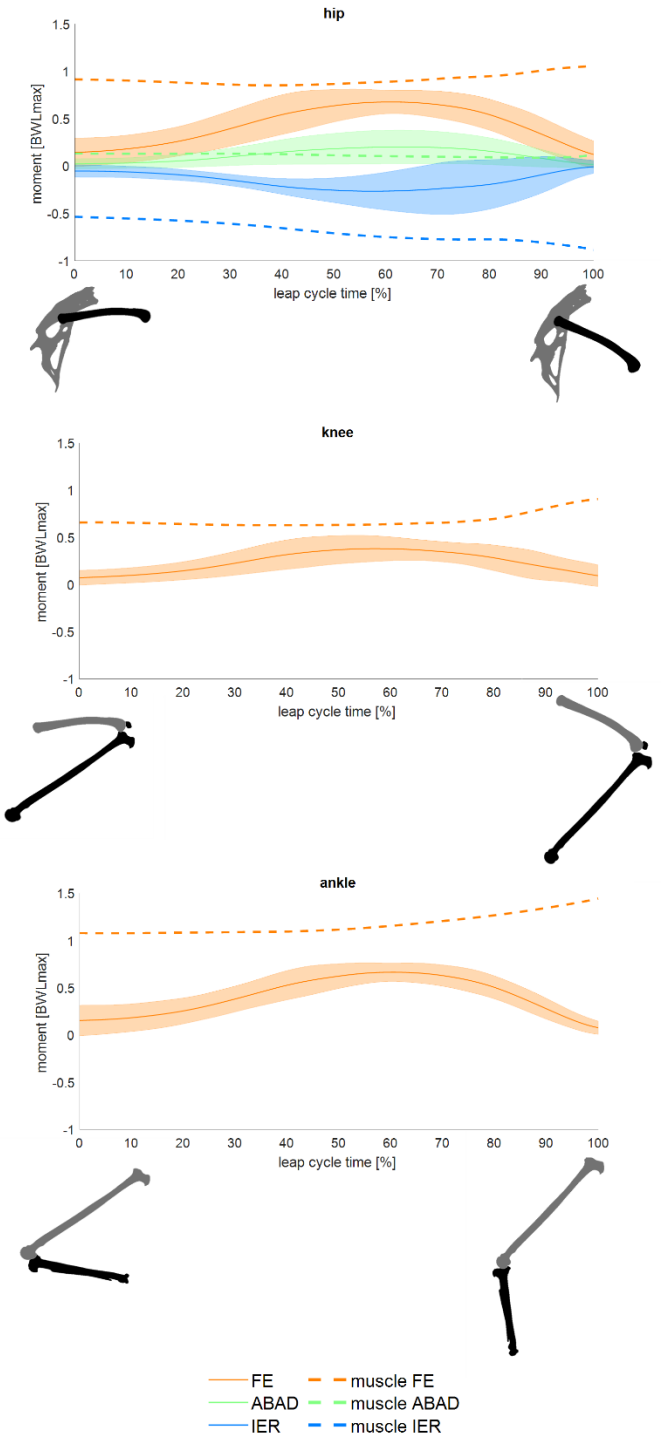

Figure 28 External joint moments at the hip, knee and ankle together with the total moment generating capacity of the muscles, plotted over normalised leap cycle time. Solid lines depict the mean external joint moments (requirements), bands depict ±2.5 standard deviations, while dashed lines depict the total moment generating capacity of the muscles (capacity). Colours are used to differentiate the axis around which the moments act, with orange representing flexion/extension, green ab/adduction, and blue internal/external rotation. Positive moments represent (internal/external) moments that act to extend, adduct, and internally rotate, respectively.

Table 9 External joint moments and total muscle moment generating capacities of the zebra finch at the instances at which the peak external joint moments occur. To actively power the take-off leap by muscle action, the combined(total) moment generating capacity of all muscles must at least reach if not exceed the level of the external joint moments . Positive moments act in extension, external rotation, and adduction, while negative moments act in flexion, internal rotation, and abduction.

joint DoF	joint moment [BWL] (requirement)	total muscle moment generating capacity [BWL] (capacity to meet requirement)
ankle extension	0.66±0.04	1.18
knee extension	-0.38±0.05	-0.67
hip extension	0.68±0.05	0.81
hip internal rotation	-0.27±0.07	-0.75
hip abduction	-0.20±0.07	-0.12

5.6 Discussion

This is the first detailed investigation into the hindlimb mechanics of a flying bird as it takes to the air with a take-off leap using modern biomechanical analyses. The model presented here simulated 18 distinct take-off trials of a zebra finch's take-off leap from a perch covering a range of take-off conditions in a passerine bird, the group that makes up approximately 60% of all extant bird species (Raikow, 1987; Ricklefs, 2012; Selvatti et al., 2015). In doing so our study revealed a consistent pattern of internal mechanics across the trials that was characterised by the largest peak external moments occurring around the FE axis of the hip and ankle (requirements, 0.68 and 0.66 BWL, respectively), while considerably smaller external moments were observed about the FE axis of the knee, amounting to only 56% of the respective peak moments at the hip. On the other hand, peak hip IER and ABAD moments were 40% and 29% of peak hip FE moments respectively. Together with previous findings regarding the substantial extent of joint range of motion in IER exercised by birds (Kambic et al., 2014; Provini and Abourachid, 2018) and the substantial moment generating capacity of the hip joint muscles around that axis (Meilak et al., 2021a), these novel data on the internal hind limb mechanics during the take-off leap strongly support the notion that the execution and control of hindlimb motion in birds is not limited to a single (sagittal) plane but is essentially 3D in nature (Allen et al., 2021).

Across the hip, knee and ankle FE degrees of freedom, the muscles had the ability to generate 120%, 176%, and 177% of the mean peak external joint moments, respectively. In relative terms therefore, muscles spanning the hip were closest to reaching the capacity limit whilst muscles spanning the knee and ankle joints had the largest reserves. Although for the most typical (mean) of the conditions studied here the capacity of the muscles to generate moments was always larger than the requirement (Figure 28), the closing gap between the upper limit of the 2.5 SD range of the external hip flexion moments and available hip muscle extension capability suggests that more powerful take-off leaps than those observed here would likely require further activation of the more distal, knee and ankle joint spanning muscles for which the requirements remained more comfortably within their capability (Bishop et al., 2021a). An explanation as to why capacity to balance the moments at the more distal joints retains a larger reserve may be found in the design of the avian hindlimb and specifically the biarticular muscles (Carr et al., 2011; Daley Monica and Biewener Andrew, 2011; Allen et al., 2017). Such biarticular muscles include in particular the m. caudofemoralis pars caudalis (MFCLP), m. flexor cruris medialis (MFCM) and m. iliofibularis (MIF) which span the caudal side of the hip and knee (Figure 24, Table 7). MFCLP and MFCM form a major part of the hip extensor moment generating capacity, together generating 35% of the total hip extensor moments whereas the MIF has a greater role as a hip abductor, generating 20% of the muscle abduction generating capacity (Meilak et al., 2021a). Whilst during the take take-off leap of

the zebra finch the hip, knee and ankle are all extending (Figure 34), the muscles need to generate a net knee flexion moment, suggesting that knee flexors may be activated. Biarticular muscles, which if activated generate an extension moment at the hip but a flexion moment at the knee such as the MFCLP and MFCM, would thus appear to be prime candidates for meeting the demands during the take-off leap. Moreover, co-activation of knee flexors and extensor muscles (muscle co-contraction) though energetically less optimal, may help to increase compressive forces across the knee joint and help to stabilise or at least minimise the extent of internal/external rotation (Kambic et al., 2014; Kambic et al., 2017; Trepczynski et al., 2018). Further analysis to examine muscle activation patterns, though beyond the scope of the current work, could corroborate whether activation of these biarticular muscles to extend the hip and generate the extension moment applied to the knee suggested by the analyses here does indeed occur and help to further elucidate how avian hindlimb muscles are orchestrated during the take-off leap.

Here, it is also informative to consider absolute moments where indeed the ankle extensors had the largest joint moment generating capacity, capable of generating peak total extension moments of up to 1.18 BWL at the ankle, followed by the hip extensors, with a peak total capacity of 0.81 BWL. The passerine bird ankle muscles' capacity to produce the largest moments indicates the importance of the ankle joint throughout the take-off, a finding in line with previous research on the ground dwelling elegant-crested tinamou *Eudromia elegans* (Bishop et al., 2021a) where the take-off heavily depended on the parameters and activation of the ankle extensors. Though to the authors knowledge no similar studies reporting internal mechanics during a take-off leap of a flying bird are available for comparison, similar analyses have been performed in ground-dwelling birds such as the emu and the ostrich. Here, data on the running of the ostrich obtained using similar analysis methods revealed that the peak normalised FE moments across all of the hip, knee, and ankle joint of the ostrich were considerably smaller than those reported during the take-off leap of the zebra finch reported here. The largest differences in normalised moment magnitudes were observed for the ankle and hip joints where the peak moments during running in the ostrich amounted to only 24% (0.16 BWL) and 25% (0.17 BWL) of the values for the zebra finch leap. The external moment at the knee during running in the ostrich was the largest of all 3 hindlimb joints with 0.20 BWL yet amounted to only about 53% of the value the current study calculated for the take-off leap of the zebra finch. In the comparison of the absolute moment magnitudes it is important to consider that speed at which the ostriches were running was rather slow (3.24 m/s) compared to the maximum speed ostriches can achieve (about 13.9 m/s) and higher speeds will be associated with higher external forces and moments. However, not only absolute magnitudes but also the ratios of their magnitudes at the hip, knee, and ankle differed between the zebra finch take-off leap and ostrich running. While the largest external moment during running of the ostrich

was computed at the knee, suggesting that that ostrich running is knee driven, the external knee moment during the take-off leap of the zebra finch was the smallest of all the hind limb joints. For the zebra finch leap, peak moments were observed at the hip and ankle suggesting that this motion is hip and ankle driven instead and signifying that an interesting avenue for future work would be to investigate whether the different motor behaviours are indeed associated with different muscle coordination patterns and that care must be taken when speculating about design principles and interpreting optimality of the musculoskeletal system based on a limited repertoire of motor behaviours.

Previous studies have demonstrated that avian pelvic muscles have a considerable capacity to produce IER moments at the hip (Hutchinson et al., 2015; Allen et al., 2021; Meilak et al., 2021a). The current study revealed not only that substantial external moments about the IER axis occur during the take-off leap of the zebra finch, approaching 40% of the hip extension moment, but also demonstrated that the hip muscles had the greatest relative capacity to actively balance these moments, with muscles capable of generating up to 280% of the mean peak external IER moments. Together these data provide further evidence that IER rotation is actively controlled during routine, straight line take-off leap of passerine birds. The ample capacity of the muscles to enable IER during such jumps further allows for take-off leaps to occur with substantially more axial turning/rotation while the bird remains on the ground, offering the bird a wider repertoire of take-off and escape behaviours. On the other hand, foraging behaviours have been shown to be linked with substantial extents of hindlimb IER (Kambic et al., 2014) and it may well be that substantial IER capability of the hip muscles are particularly crucial in supporting those behaviours (particularly for single limb support) in addition to allowing variation in the take-off leap.

In contrast to the well powered hip IER DoF during the take-off leap, the pelvic muscles of the zebra finch were only able to balance 61% of the peak mean external adduction moments. Analysis of the relationship of the relative moment generating capacity of the avian hip muscles do indeed demonstrate that the smallest capacity to generate a moment exists with respect to the ABAD axis. However, even though the avian hip has a relatively limited capacity to actively produce hip ABAD moments, birds can rely on a passive mechanism using the antitrochanter and associated ligamentous structures to balance external abduction moments (Hutchinson et al., 2015). The utilisation of the antitrochanter is also a feature in the hip mechanics of the ostrich: though substantial external abduction moments are generated during walking and running in these flightless birds, the design of the hip allows to stabilise the joint passively such that ostriches neither require nor possess muscles to do so actively (Hutchinson et al., 2007; Hutchinson et al., 2015). The antitrochanter is indeed a feature shared across all extant birds that was not present in some of the

very earliest birds such as *Archaeopteryx*, who likely relied on powerful hip adductors to generate the required adduction moments (Allen et al., 2021).

Maintaining substantial lever arms of the muscles throughout the functional range of motion of a joint is a prerequisite to maintain high levels of muscle capacity to generate moments. Passive structures can play a key role to help maintaining muscle lever arms include sesamoid bones such as the patella which is key to enable joint function in flexion at the knees in human and avian bipeds (Trepczynski et al., 2012; Allen et al., 2017) The hypotarsus is another anatomical feature of the avian hindlimb that helps to guide tendons around the ankle joint and to and maintain their lever arms (Mayr, 2016). The posterior side of the ankle further includes the cartilagio tibialis which constrains the muscle line of action to act further away from the joint axis of rotation thus helping to maintain its moment (Verstappen et al., 1998). The model presented here therefore modelled the patellofemoral joint in an approach informed by the birds' bone surface anatomy and kinematic model data from the literature (Cox et al., 2019) and in incorporated these passive structures of the ankle with wrapping objects and via points informed by CT scans.

The relative peak ground reaction forces during the take-off leap of all passerines considered here were rather similar in magnitude, despite the large range in body mass. During the take-off leap the zebra finch (15.4 g), starling (77.3 g), crow (440 g) and raven (1.1 kg) generated peak ground reaction forces per leg of 1.94±0.25 BW, 2.15±0.14 BW (Earls, 2000), 2.2±0.29 BW, and 2.25±0.14 BW, respectively. Similarities do not stop with the ground reaction forces but are also apparent in the morphology of their hindlimbs. The passerines considered here, the zebra finch, starling, crow, and raven, possess very similar hindlimb indices, a measure of relative segment lengths of the hindlimb ((tarsometatarsus length + tibiotarsus length) / femur length (Field et al., 2018)) with values of 2.64, 2.84, 2.75, and 2.63, respectively (Tomek and Bochenski, 2000) (Table 8). The similarities in normalised leg segment lengths and ground reaction forces spanning a range of passerines, which differ in mass by approximately two orders of magnitude, support the hypothesis that passerines share a similar take-off behaviour, as reported here. Forward dynamics simulations of the tinamou (0.55 kg) leaping predict similar but somewhat higher peak ground reaction forces of 2.62 BW per leg during the jump (Bishop et al., 2021a). On the other hand, predicted joint kinematics profiles for the take-off leap of the tinamou demonstrated ranges of motion at the hip knee and ankle of 65°, 91° and 109° respectively, consistently greater than the range of motion measured in the zebra finch (42°, 40° and 74° respectively), while the hindlimb index of the tinamou *Eudromia elegans* (belonging to the group Tinamiformes) was 2.21, substantially smaller than that of the passerines considered here. The relative difference in relative leg morphology between the passerines and tinamou could be one of the determining factors resulting in the variability in take-off mechanics between the clades of birds.

The kinematics used to drive the take-off simulation were informed by previously obtained XROMM data of the zebra finch take-off leaps (Provini and Abourachid, 2018). In this study, the use of the tantalum bead markers, detailed bone surface geometry from high resolution µCT, and anatomical-functional relationships (Ehrig et al., 2007; Ehrig and Heller, 2019) were all used to increase repeatability in tracking 3D skeletal kinematics and reduce the influence of the user during scientific rotoscoping (Brainerd et al., 2010). Across the two kinematics trials, the difference between the originally published orientation angles of the femur, tibiotarsus and tarsometatarsus was smallest about FE and ABAD axes of the bones, with mean differences ranging from 0.6±0.5° to 3.3±2.7°. The degree of freedom most difficult to determine during scientific rotoscoping was IER due to the cylindrical shape of the long bones. Predictably, the largest difference was observed when comparing the bone IER orientations, with mean differences in IER orientations across the three long bones ranging from 7.3±4.8° to 11.5±6.3°. Differences in bone locations between the two methods were minimal, mean differences across all three long bones ranged between 185 – 333 microns.

Due to the limited number of specimens in which sufficient bones had had a minimum of three tantalum markers attached, only two sets of kinematics trials were used in this study. However, by pairing each set of kinematic trials with nine sets of kinetics trials, we maximised the variability in take-off conditions studied here. Future studies, using XROMM to capture detailed kinematics of passerines should ensure that at least one of the long bones includes at least 3 markers to reduce the reliance on the user during scientific rotoscoping. The simulations here included IER motion of the knee and ankle joints, however the active muscle actuation of these degrees of freedom was not considered in line with previous studies and under the assumption that typically small moments are balanced by passive structures such as ligaments (Marieswaran et al., 2018; Seth et al., 2018). Previous studies reported the take-off velocity of the zebra finch to be around 1.7 m/s (Tobalske, 2004; Provini et al., 2012) which is faster than the take-off velocity, measured here from the XROMM data which ranged between 1.08-1.39 m/s. Previously published studies measuring the kinematics of animal subjects using implanted markers have reported the markers causing a limp (Taylor et al., 2006). The comparatively slower take-off velocities reported here could thus be attributed to a response to the implantation of the tantalum bead markers on the hindlimb bones. However, varying levels of motivation between experimental conditions may also explain the observed difference and the similar protocols using tantalum bead markers have been used to study a range of motor behaviours in birds (Kilbourne et al., 2016; Allen et al., 2017; Brown et al., 2018). This study did not include the mechanics of phalanges in the analysis, as the take-off trajectories of the hindlimb are defined primarily by the motion at the more proximal hindlimb joints where also more substantial joint moments are generated. Future studies which may

consider hind limb mechanics during landing, when the detailed mechanics of foot are likely to play a more important role, should aim to capture the detailed kinematics of the phalanges.

This study considered the maximal moment generating capacity of the muscles, taking into account the muscle maximum isometric force and instantaneous moment arm throughout the take-off leap and contrasted these to the external moments applied to the joints of the hind limb. In this way general patterns of mechanical requirement and hindlimb muscles capability to meet the requirements of a take-off leap were analysed. Although the sensitivity of muscle moment generating capacity with respect to uncertainty in the definition of muscle geometry was not directly investigated in this study, a thorough sensitivity analysis was performed for pelvic muscles in the magpie hindlimb model that was the basis for the current study (Meilak et al., 2021a), which, given the similarity in overall hindlimb design and specific hindlimb bone morphology, can reasonably be expected to remains valid for the musculature of the zebra finch model here. Though the determination of the detailed muscle activation patterns to balance the external moments was not within the scope of the current study, further analyses of the biomechanical model (such as static optimisation (Delp et al., 2007; Seth et al., 2011; Seth et al., 2018)) would help to further elucidate the detailed activation patterns of individual muscles as well as providing estimates for the likely bon-on-one joint contact forces being transferred at le large joints of the avian hind limb during a take-off leap.

This study is the first to establish the biomechanical requirements of the hindlimb of a flying bird as it takes to the air. We present biomechanical conditions that hindlimbs of passerines, a clade of birds that include over half of all avian species, experience during take-off. The zebra finch take-off leap is primarily hip and ankle driven, which is in direct contrast to ostrich running mechanics which indicates avian running is a primarily knee driven activity. The ability of the zebra finch muscles to produce over double the mechanical requirements at the ankle and knee axes and about 20% more than the requirements about the hip FE axis along with the suspected use of biarticular muscles and passive structures is consistent with the hypothesis that the take-off leap as reported here is an optimized way for the zebra finch to take to the air. Striking similarities in ground reaction forces and relative leg morphology of multiple passerines suggest that the take-off behaviour described here could be shared across all passerines, despite differences in mass by two orders of magnitude.

5.7 Acknowledgements

We would like to acknowledge the skill, hard work, and patience of the bird handlers Lloyd and Rose Buck who helped with the collection of the ground reaction force data of the crow and raven. This work was supported by the Natural Environmental Research Council [grant number

NE/L002531/1] and grants from the UMR 7179, l'Action Transversale du Muséum National d'Histoire Naturelle formes possibles, formes réalisées and from Ecole Doctorale Frontières du Vivant and Bettencourt-Schueller Foundation fellowships as well as the National Science Foundation [grant nos IOS-0923606 and IOS-0919799]. Travels were paid by the UMR 7179.

Chapter 6 Hop, hop and away: On the take-off leap of *Archaeopteryx*

Chapter 6 tests the leaping ability of *Archaeopteryx* to become airborne. By carefully adapting a published model of *Archaeopteryx* to reflect the novel understanding of avian hindlimb kinematics and kinetics developed here, the capability of *Archeopteryx* to leap is confirmed, obtaining robust estimates of the maximum take-off velocity powered by their hind limbs. Using a conservative approach to integrate contributions of hindlimbs and wings we demonstrated that *Archaeopteryx*, taking successive leaps like a living bird, could generate sufficient velocity with its hindlimbs to reach the minimum sustainable flight speed within two to three hops.

6.1 Citation

In this chapter the full manuscript, titled "Hop, hop and away: On the take-off leap of *Archaeopteryx*" prepared for submission to Nature Communications is presented. Supplementary information is provided in Appendix C.

6.2 Abstract

Archaeopteryx is at the centre of the debate on the evolution of avian flight. The jumping hypothesis proposes that *Archaeopteryx* used its wings to extend its trajectory from a bipedal leap. Here we present a novel biomechanical model informed by data of the take-off of living birds to test the leaping ability of *Archaeopteryx* to become airborne. By calculating the external joint moments being applied to the hip, knee and ankle and the muscle capability to balance these moments, we determine robust estimates of the maximum take-off velocity of *Archaeopteryx.* We show that *Archaeopteryx,* leaping like a living bird, could generate enough velocity with its hindlimbs that its wings extended its trajectory and that subsequent leaps would have propelled it to the minimum sustainable flight speed. Our state-of-the-art biomechanical analyses thus provide new evidence towards a ground-up leaping mechanism for the evolution of avian flight.

6.3 Introduction

How birds evolved the capability of powered flight remains a topic of great debate and how the first birds may have taken to the air is one of the biggest uncertainties of this debate (Burgers and Chiappe, 1999; Dyke et al., 2013; Heers, 2013; Voeten et al., 2018). Here we present a novel biomechanical model testing the leaping ability of *Archaeopteryx* to become airborne, informed by data of the take-off of living birds. Of the more than 10 distinct mechanisms (Heers, 2013) that have previously been proposed to address the evolution of avian flight, the mechanisms of wing assisted incline running (WAIR), gliding (trees down/arboreal hypothesis) and jumping (Chatterjee and Templin, 2003; Dial, 2003; Long et al., 2003; Zhou, 2004; Longrich, 2006) are all linked to behaviours that can be readily observed in extant birds. A unique feature shared by these hypotheses on the behaviour of extinct species is the ability to rigorously test them by detailed analysis in modern birds (Hutchinson et al., 2015; Rankin et al., 2016; Heers et al., 2018; Bishop et al., 2021a). Although there is abundant literature about gliding in modern birds (Thomas and Taylor, 2001; Alerstam et al., 2007; Lentink et al., 2007; Henningsson and Hedenström, 2011) and the ability of paravians (microraptor) (Dyke et al., 2013; Palmer, 2014) to glide has also been demonstrated, the analysis of WAIR and jumping have received less attention so far. Although WAIR has been found to support an animal in navigating steep terrains, in modern birds that demonstrate WAIR the behaviour does not result in flight even though the animals are capable of it (Dial, 2003; Baier et al., 2013). On the other hand, the direct ancestors of birds were small theropod dinosaurs which would have become prey items themselves unless they could evade capture. The jumping hypothesis, first proposed by Garner et al. (1999) and expanded upon by Earls (2000), suggests that the first birds were jumping with enough velocity that they could use their feathered forelimbs to extend their jump trajectory (Garner et al., 1999; Earls, 2000). The jumping model uses a behaviour still commonly used by birds today, whilst explaining the selective pressure for a more developed wing to evolve; the better the wing, the further the protobird could extend its trajectory, escaping predation, surviving to reproductive age, passing on the selected and better adapted flight apparatus down the line. Additionally, we have a mechanism that supports this idea and has been tested for the last 162 years, Natural Selection (Darwin, 1859). All organisms actively try to survive, and as such, a small, feathered animal, with powerful legs could jump out of the way of danger. Adding in a flap from its feathered forelimbs could extend the distance of the jump. As stated, this exact behaviour is seen in living birds as they take off from the ground. Is it a plausible mechanism for the evolution of flight in the earliest bird?

We know that the take-off of extant land birds from the ground most commonly relies on a powerful, leg-propelled take-off leap to produce the initial momentum needed to take to the air. In birds that have been studied so far, the wings do not start the downstroke until after the foot

has left the ground and through sweeping wing strokes, the wings accelerate the bird until a continuous flight speed is achieved (Heppner and Anderson, 1985; Bonser and Rayner, 1996; Earls, 2000; Tobalske and Dial, 2000; Tobalske, 2004; Henry et al., 2005; Berg and Biewener, 2010; Provini et al., 2012; Chin and Lentink, 2017; Provini and Abourachid, 2018). For example, during its take-off leap, the hindlimbs of the zebra finch generate 94% of the take-off velocity[8].

Archaeopteryx, the first bird, recognised as such since the 1860s, by Thomas Henry Huxley (Huxley, 1868), and confirmed in 2013 by Godefroit et al. (2013) (although it remains in a position that is affected by each discovery) had asymmetric feathers, unlike those of non-avian dinosaurs. *Archaeopteryx* could fly (Alonso et al., 2004), yet how proficient and powerful a flyer *Archaeopteryx* was, remains the topic of discussion (Burgers and Chiappe, 1999; Nudds and Dyke, 2010; Paul, 2010; Voeten et al., 2018). Beyond this specific debate about the rachis of feathers, *Archaeopteryx* lacks a keeled sternum; has a shoulder joint that would not allow dorsal elevation of the wings beyond the horizontal; has poor extensive pronation of the wing; and a relatively lower degree of feather asymmetry, when compared with extant birds (Olson and Feduccia, 1979; Poore et al., 1997; Senter, 2006; Zheng et al., 2014; Mayr, 2017; Voeten et al., 2018). But should we expect the first bird to be evolutionarily fully adapted? Probably not. However, the second aspect of uncertainty around *Archaeopteryx* flight, is how it got off the ground in the first place, and this is a crucial question. Relative to modern birds, *Archaeopteryx* did have long powerful hindlimbs: *Archaeopteryx lithographica* (400g) has been suggested to possess a hindlimb mass relative to its body mass of 13%. Modern birds that leap to take to the air such as the crow, *Corvus corone* (575 g) and zebra finch *Taeniopygia guttata* (15.4 g), possess a relative hindlimb mass of only 9% and 10%, respectively (Seebacher, 2001; Hutchinson, 2004b; Kilbourne, 2014; Provini and Abourachid, 2018; Allen et al., 2021). Given its larger relative hindlimb muscle mass, could *Archaeopteryx* have employed a similar behaviour to modern birds to get itself into the air?

The study aimed to use a biomechanical approach to investigate whether, and if so how, *Archaeopteryx*, leaping like a living bird, could have become airborne and model how its leaping ability compares with living birds.

With the development of novel technology to capture detailed 3D bone kinematics of extant avian take-off leaps, partnered with computational biomechanical analyses, the technology is finally available to accurately simulate the internal mechanics of the extant avian take-off (Rubenson et al., 2007; Rubenson et al., 2010; Kambic et al., 2014; Kambic et al., 2017; Provini and Abourachid, 2018; Allen et al., 2021; Meilak et al., 2021a). With the hypothesis that *Archaeopteryx* would have had strong leaping capability, the current study used scaled motion and ground reaction force take-

off data of a zebra finch to drive a computational musculoskeletal model of *Archaeopteryx* (Allen et al., 2021) and simulate its take-off leap.

With the understanding that passerine birds, who leap to take off, across a range of sizes share similar take-off mechanics (Meilak et al., 2021b), we used detailed 3D kinematic data obtained for the extant zebra finch, a representative of this group of birds, to inform the motion used by *Archaeopteryx lithographica*. Using OpenSim 4.1, we developed a computational biomechanical musculoskeletal model of the hindlimb of *Archaeopteryx lithographica based on a published model* (Allen et al., 2021), that followed the movement pattern experienced during the ground take-off leap of a zebra finch. External joint moments acting on the hindlimb joints of *Archaeopteryx* were calculated through inverse dynamics analyses, driven by scaled force and kinematic data of the zebra finch take-off. At any instance throughout the jump, moments acting on the hindlimb joints are balanced by muscles to keep the biomechanical system in equilibrium (Bergmann et al., 2001; Heller et al., 2001b; Heller et al., 2003; Taylor et al., 2006; Meilak et al., 2021a).

The key moments that were balanced throughout the take-off jump of the zebra finch are hip flexion/extension (FE), abduction/adduction (ABAD), internal/external rotation (IER), and knee and ankle flexion/extension (Meilak et al., 2021b). Accordingly, these are the moments that are analysed throughout the take-off of *Archaeopteryx*. Using the analysis tools in OpenSim 4.1 we calculated the muscle moment-generating capacity (the muscle's ability to provide sufficient leverage to actuate joints) for the jump trials. We compared the muscle moment-generating capacity to the external joint moments occurring throughout the take-off to evaluate *Archaeopteryx's* ability to balance these joint moments and in so doing, power the take-off.

The take-off velocity of a bird can be defined as the velocity of the centre of mass at the time the feet leave the ground (Earls, 2000; Tobalske, 2004; Provini et al., 2012). The legs create the take-off velocity by imparting a force against the ground, through the feet. By calculating the acceleration from the impulse resulting from this force and its duration, we calculate the resultant take-off velocity (Earls, 2000; Tobalske, 2004; Provini et al., 2012). The contribution of the wings was not included in the model as they do not play a major role in the propulsion phase of the take-off in extant birds and due to the uncertainty in the flapping ability of *Archaeopteryx.* The assumption that the wings do not contribute to the take-off velocity, our simulations represent conditions which pose the maximum mechanical requirement on the hindlimbs.

For modern birds, the transition period from take-off to the minimal sustainable flight speed, relies on powerful flapping strokes to keep airborne and accelerate (Klein Heerenbrink et al., 2015; Chin and Lentink, 2017). The minimum sustainable flight speed for *Archaeopteryx* has been estimated to be approximately 7 m/s (Rayner, 1988; Burgers and Chiappe, 1999; Longrich, 2006). Using our

biomechanical model of the hindlimb and maximising the data from modern extant birds we propose mechanisms by which *Archaeopteryx* could have used a combination of multiple jumps and flapping to meet the minimum sustainable flight speed of 7 m/s.

We report the maximum take-off velocity of *Archaeopteryx* that the hindlimbs could produce and assess the sensitivity of the result to the location of the centre of mass and location of the centre of pressure of the ground reaction forces. Results of our analyses point towards *Archaeopteryx* having a comparable jumping ability with extant birds. We report three scenarios resulting from the bipedal take-off leap of *Archaeopteryx. Archaeopteryx,* taking off like a living bird, would have generated enough initial velocity with its hindlimb that its wings could have extended its trajectory. Following the behaviour of extant birds further, two subsequent leaps, with no contribution of the wings would have propelled it to the minimum speed necessary to take to the air. Utilising aspects of both scenarios, if *Archaeopteryx* flapped its wings in between leaps, only one subsequent jump would be needed to reach the minimum sustainable flight speed.

6.4 Results

6.4.1 Biomechanical analysis

With the location of the centre of pressure of the ground reaction forces placed at the mid-length of the 3rd digit (Figure 29) and a body centre of mass (COM) situated in the location proposed by Allen et al. (2013), (supplementary Figure 39) *Archaeopteryx* could take off at a velocity of 2.98 m/s using only its hindlimbs. The duration of the jump varied between 66-74 ms and under these conditions, the peak ground reaction force was 3.64±0.40BW per leg. The largest mean peak joint moment, normalised by body weight leg length (BWL), was about the ankle FE axis, 0.91±0.06 BWL, followed by hip FE, 0.73±0.09 BWL, and then knee FE, 0.30±0.23 BWL (Figure 31, Table 10). The smallest moments were about hip IER and ABAD with peak mean moments of 0.15±0.04 and 0.07±0.03 BWL, respectively.

At the instances that these peak moments occurred, the muscles could produce 114%, 187% and 616% of the mean peak hip FE, IER and ABAD joint moments, respectively (Figure 31 A. Table 10). At the knee and ankle FE axes, the muscles were able to produce 130% and 100% of the mean peak joint moments, respectively (Figure 31 B and C, Table 10). The maximum take-off velocity was limited by the ankle muscles' ability to balance the ankle flexion moments, as this was the joint about which the muscle moment generating ability equalled the external joint moment.

6.4.2 Projectile trajectory analysis

Three leaping scenarios are presented in this study. Considering a single take-off jump where *Archaeopteryx* leaves the ground at 2.98 m/s and assuming subsequent flaps provided a thrust and lift of 0.3 BW and 0.17 BW respectively, *Archaeopteryx* reached a height of 0.39m at the peak of its trajectory, having travelled 1.67m (Figure 30 A). Living land birds have been documented taking multiple jumps to take to the air. Under the conditions described, if upon landing a second jump provided a further velocity increase of 2.98 m/s, *Archaeopteryx* would have had enough forward momentum to lift-off at 6.24 m/s. Assuming the flapping ability is unchanged, *Archaeopteryx* would have accelerated to the minimum flight speed of 7 m/s within 0.36s, having travelled a further 2.33m in the air (Figure 30, C). Alternatively, if we assume that between leaps *Archaeopteryx* did not flap its wings, as is often observed in birds today, *Archaeopteryx* could have a succession of three jumps, whereby forward velocity is conserved between jumps. By the end of the third jump, *Archaeopteryx* would have been travelling at a velocity of 6.66 m/s respectively and assuming *Archaeopteryx* would have then started to flap its wings, it could have accelerated for 0.23 s reaching a flight speed of 7 m/s having travelled 1.53 m through the air (Figure 30 C).

6.4.3 Sensitivity analysis

We explored the model's sensitivity to the location of the centre of mass and the location of the centre of pressure of the ground reaction forces. By varying the location of the centre of mass, spanning the upper and lower limits of likely centre of mass locations (supplementary Figure 39), informed by literature (Allen et al., 2013), we found that the maximum take-off velocity ranged from 2.87 m/s to 3.12 m/s (supplementary Figure 39). By varying the centre of pressure from the most caudal location on the digits to the most cranial (supplementary Figure 39), we found that the maximum take-off velocity varied from 2.58 to 3.12 m/s (supplementary Figure 39). When the centre of pressure was at its most caudal, the knee joint moments increased, and the capacity of the muscles to provide knee extension moments became the limiting factor rather than the moment generating capacity of the ankle extensors.

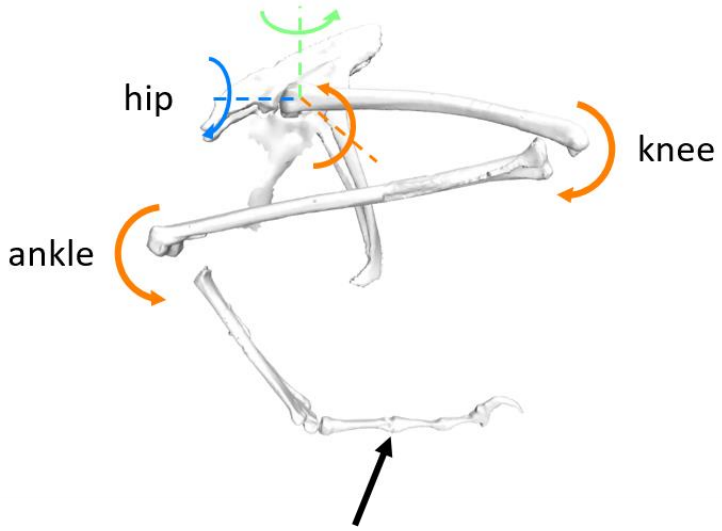

Figure 29 Force and moment diagram of the hindlimbs of Archaeopteryx in a lateral view. The black arrow represents the ground reaction force, while the orange arrows represent the external joint moments about the flexion/extension axes of the ankle, knee, and hip joints. The external joint moment about the hip internal/external rotation axis is represented by the green arrow while the blue arrow represents the external joint moment about the hip ab/adduction axis. The ground reaction force typically results in flexion, adduction, and external rotation moments at the hip while causing extension and flexion moments at the knee and ankle, respectively.

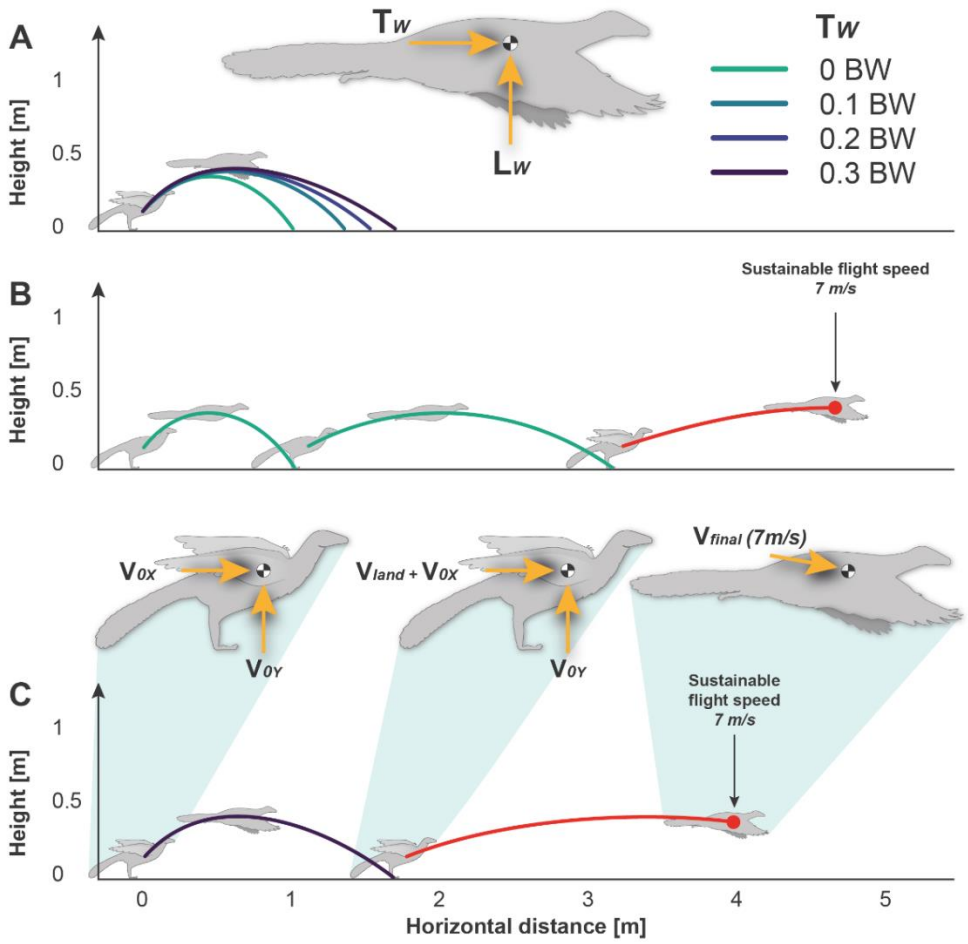

Figure 30 A) Trajectories of the centre of mass (CoM) of Archaeopteryx *for varying levels of wing thrust forces (T_w) for an initial take-off angle of 45 degrees and a take-off velocity of 2.98 m/s. The distance travelled varied as a function of the extent of forward thrust (0 bodyweight (BW) (ballistic trajectory), 0.1 BW, 0.2 BW, and 0.3 BW) the wings provide and ranged from 1.01, 1.35, 1.51, and 1.67m, respectively. While in the air and flapping its wings, it is assumed* Archaeopteryx *could produce a constant lift (L_w) of 0.17BW. B) Trajectory of the CoM of Archaeopteryx taking three consecutive jumps, with zero thrust from the wings. Assuming that upon landing the horizontal component of the velocity (V_{land}) is added to the horizontal velocity components of the subsequent jump ($V_{land} + V_{0x}$), the take-off velocities of the 2nd and 3rd jump are 4.71, and 6.66 m/s, respectively. After the third take-off,* Archaeopteryx *would have started to flap its wings and subsequently would have accelerated for 0.23 s reaching a sustainable flight speed of 7 m/s. C) Trajectories of the CoM of* Archaeopteryx *showing how it could, with multiple jumps while flapping its wings, reach a minimum sustainable flight speed of 7 m/s. With an initial take-off velocity of 2.98 m/s, distributed in to horizontal and vertical components V_{0x} and V_{0y} respectively,* Archaeopteryx *would land with a horizontal velocity (V_{land}) of 3.77 m/s, which is added to the horizontal component of the take-off velocity of the second jump (V_{0x}). The velocity of* Archaeopteryx *at the 2nd take-off is then 6.25 m/s, and it reaches its minimum sustainable flight speed (V_{final}) after travelling through the air for 0.36s.*

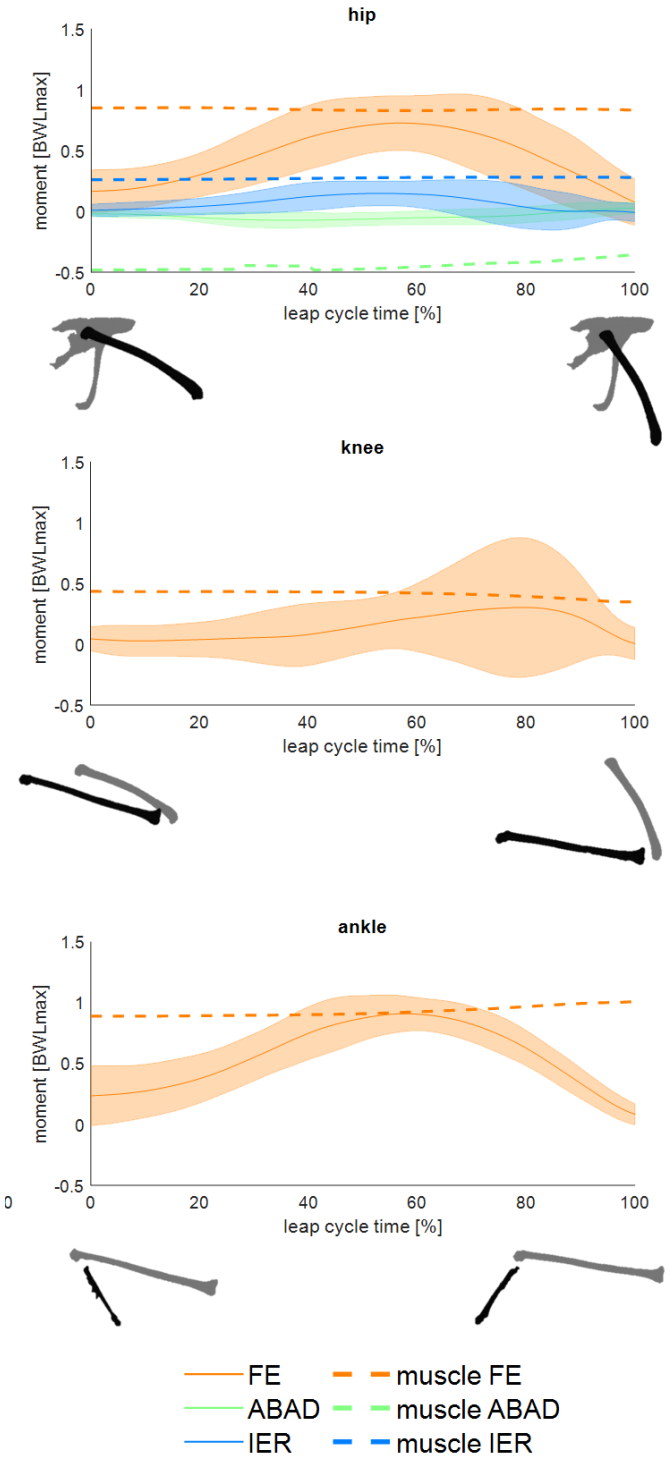

Figure 31 External joint moments at the hip, knee and ankle together with the total moment generating capacity of the muscles, plotted over normalised leap cycle time. Solid lines depict the mean external joint moments (requirements), bands depict ±2.5 standard deviations, while dashed lines depict the total moment generating capacity of the muscles (capacity). Colours are used to differentiate the axis around which the moments act, with orange representing flexion/extension, green ab/adduction, and blue internal/external rotation. Positive moments represent moments that act to extend, abduct, and internally rotate, respectively.

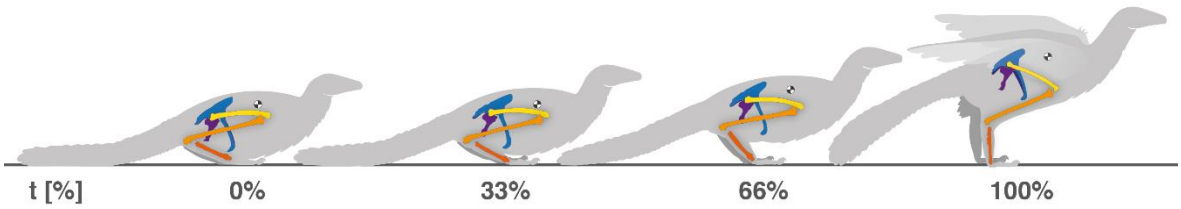

Figure 32 Lateral view of Archaeopteryx hindlimb depicting the most plausible location of the centre of mass throughout the time-normalised take-off leap cycle. The take-off jump duration ranged between 66-74 ms.

Table 10 Peak external joint moments and muscle moment generating capacities of Archaeopteryx *lithographica and zebra finch, informed by Meilak et al. (2021b). The muscle moment-generating capacity is required to actively balance the external joint moments (the requirement) occurring during the take-off leap. Moments in the zebra finch joints acting in opposite directions to* Archaeopteryx *are presented as negative values.*

joint DoF	external joint moment (BWL) (requirement)		muscle moment generating capacity (BWL) (capacity to meet requirement)	
	Archaeopteryx lithographica	Zebra finch	*Archaeopteryx lithographica*	Zebra finch
ankle extension	0.91±0.06	0.66±0.04	0.91	1.18
knee extension	0.30±0.23	-0.38±0.05	0.39	-0.67
hip extension	0.73±0.09	0.68±0.05	0.83	0.81
hip internal rotation	0.15±0.04	-0.27±0.07	0.28	-0.75
hip abduction	0.07±0.03	-0.20±0.07	0.45	-0.12

6.5 Discussion

We found that using a leaping motion adapted from the zebra finch, *Archaeopteryx,* a basal bird often compared in size to the magpie, *Pica pica* (Pilcher, 2004; Wellnhofer and Haase, 2009; Wellnhofer, 2010), could take off as many living land birds, such as corvids, do today - by taking a succession of bipedal leaps. The biomechanical ability of *Archaeopteryx* to generate the take-off speed reported here provides the first quantitative evidence supporting one possible mechanism for the evolution of avian powered flight. Importantly, our analyses support a take-off mechanism that generates a sustainable flight speed of 7 m/s from either two or three leaps depending on whether the wings are used in between jumps. The first leap would have propelled the 400g *Archaeopteryx lithographica* from the ground at a velocity of 2.98 m/s. Although there is disagreement as to the flapping ability of *Archaeopteryx*, it is generally agreed that it could have used its wings to generate some forward thrust. Burgers and Chiappe (Burgers and Chiappe, 1999) estimated that *Archaeopteryx* could produce a forward thrust ranging 0.16-0.34 BW, and Heerenbrink and co-workers (Klein Heerenbrink et al., 2015) found that at slow flying speeds (<5 m/s) the jackdaw can produce a thrust over 0.3 BW (Burgers and Chiappe, 1999; Klein Heerenbrink et al., 2015). Additionally, Burgers and Chiappe(Burgers and Chiappe, 1999) estimated that at an air velocity of 2.71 m/s, similar to our estimated take-off velocity of 2.98 m/s, *Archaeopteryx* could produce a lift of 0.17 BW. Therefore, assuming that *Archaeopteryx* could provide a constant forward thrust of 0.3BW and using a constant, conservatively low, estimate for the amount of lift available from the wings, it could have extended its flight trajectory by 65% from its otherwise ballistic path, accelerating forward up to 3.77 m/s by the end of the trajectory (Figure 30 A). With a second take-off leap *Archaeopteryx* could therefore have taken off with an air-speed of 6.25 m/s, and by flapping its wings could have reached the minimum sustainable flight speed within 0.36s of travelling through the air (Figure 30 C). Even if we consider that between leaps *Archaeopteryx* did not flap its wings, as observed in birds today, *Archaeopteryx* would have only needed 3 leaps before taking off at a velocity of 6.66 m/s and reaching a flight speed of 7 m/s within 0.36s of being airborne (Figure 30 B).

The kinematics, although altered to best match the limb proportions of *Archaeopteryx* (see methods), was based on the kinematics of the take-off leap of the extant zebra finch with take-off speeds ranging 1.08-1.39 m/s (Provini et al., 2012; Provini and Abourachid, 2018; Meilak et al., 2021b). In how far Archaeopteryx may have used the proposed take-off motion is uncertain however our analysis provides evidence to suggest that the morphology of the hindlimb makes this motion feasible. To allow the required hindlimb motion, the knee flexion axis was rotated to effectively allow abduction of the tibia during deep flexion. The rotated knee flexion axis is well established in modern birds based on morphological and functional axes (Stolpe; Kambic et al.,

2014; Meilak et al., 2021a). In general, the normalised peak external joint moments were lower for the zebra finch while the muscle moment-generating capacity was lower for *Archaeopteryx*. (Table 1). Both the zebra finch and *Archaeopteryx* take-offs required the muscles to produce an extension moment about the ankle and hip. However, the hindlimb muscles of *Archaeopteryx* needed to provide knee extension, hip internal rotation and abduction whereas the zebra finch needed to provide knee flexion, hip external rotation and adduction with its muscles. These differences in hip mechanics can be explained by morphological differences of the pelvis of *Archaeopteryx* and the extant zebra finch (Allen et al., 2021; Meilak et al., 2021a; Meilak et al., 2021b). *Archaeopteryx* has a comparatively slimmer pubis and ischium when compared to the zebra finch, causing its flexed knee to have a larger degree of abduction resulting in the ground reaction vector applying an external rotation moment and adduction moment which the muscles then need to balance. Previous investigations into the biomechanics of the extant avian leap have shown that the jumping ability of living birds is most sensitive to the strength of the ankle extensors (Bishop et al., 2021a; Meilak et al., 2021b). Indeed, for both the zebra finch and *Archaeopteryx*, the largest external joint moments were seen about the FE axis at the ankle joint (Table 1). The maximum take-off velocity of *Archaeopteryx* was limited by the ankle muscles' ability to produce ankle extension moments.

There have been many hypotheses on the evolution of avian flight (see Heers (2013) for review). WAIR has been proposed as one way for the 'ground up' model to lead to flight (Dial, 2003; Baier et al., 2013) and indeed adult partridges and their chicks can ascend a slope, more easily, by flapping their wings as they run. The WAIR model further assumes that with strong enough flapping and fast running, flight is eventually achieved. Another model for how powered flight came about is from the trees down, which is observed in flying squirrels and reptiles (Russell et al., 2001; Bishop, 2008; Heers, 2013). The model suggests that the protobird jumped from higher elevations to then glide to another, lower place. There was a loss of altitude with each glide, the animal eventually reaching the ground, forcing the protobird to climb to another high point, tree, hill, or, cliff, to be able to glide between points again (Chatterjee and Templin, 2003; Dial, 2003; Long et al., 2003; Zhou, 2004; Longrich, 2006).

A problem associated with both of these models is that there is a requirement for some element to teleology, an intention to fly, flapping harder to get up the slope causes flight, but it is more than required simply to get up the hill, which is the desired outcome. Similarly, with the trees down hypothesis, flight evolves to avoid the resultant need for a climb (Yalden, 1984; Chatterjee and Templin, 2003). The problem is neither model is evolutionarily testable. What is more, with the WAIR model, in the case of the adult modern birds observed displaying the behaviour, they can already fly but are choosing not to. WAIR does not equal and does not lead to flight in modern birds either, it is instead actively *not flying*.

If we want the earliest evidence for the evolution of flight we have to go to the fossil record, but most behaviours, including WAIR, are obviously absent and so we rely on the physical elements preserved. In the record, we see a range of different dinosaur morphologies, and feathers are found throughout the entire clade Ornithoscelida [Ornthischia + Theropoda], and where they are absent, they have been lost (Chen et al., 1998; Brusatte et al., 2015; Baron et al., 2017). The fossil record as currently understood thus provides ample evidence for small, bipedal, feathered, ground-dwelling, cursorial bird ancestors (Chiappe, 2009; Bell et al., 2017).

In this study, we used a quantitative approach to investigate a variation of the jumping hypothesis, which suggests that with the powerful jump available to a protobird, any downward motion from a feathered forelimb after the start of a leap could add distance to the otherwise ballistic path of their leaps (Garner et al., 1999; Earls, 2000). Along with wing assisted incline running, which postulates that birds evolved powered flight by using their wings to climb steep inclines, the jumping hypothesis is one of the few hypotheses which relies on behaviour that birds still use today (Dial, 2003; Dial et al., 2008; Heers, 2013; Heers et al., 2018). Whilst we propose a multiple leap mechanism for *Archaeopteryx* to reach the minimum flight speed needed, even a more conservative view in which *Archaeopteryx* would not achieve the forward speed required to take off, with a forward wing thrust ranging between 0.1-0.3 BW and uplift of 0.17 BW (Figure 30 A) it could increase its otherwise ballistic path by 34-65%, improving its ability to travel overland. The study presented here, building on the leaping hypothesis, adds quantitative evidence supporting a ground-up mechanism for the evolution of take-off and the transition to powered flight.

Although this is the first study calculating the leaping ability of *Archaeopteryx,* Voeten and co-workers (Voeten et al., 2018) placed the flight style of *Archaeopteryx* with volant birds with short bursting flight styles. The pheasant (*Phasianus colchicus*, 735 g), a bird known for taking flight in short bursts, takes off at 2.8 m/s (Tobalske and Dial, 2000; Tobalske, 2004). *Archaeopteryx* did not have the same flapping ability as a pheasant, however, the similarity in take-off velocity adds support for a short burst flight style.

The study had limitations. Muscle capacity to generate force is dependent on many parameters including fibre length, pennation angle, tendon slack length and moment arm (Hutchinson et al., 2015; Charles et al., 2016; Rankin et al., 2016; Bishop et al., 2021a). Our study focussed on a simplified model that solely considered maximal moment-generating capacity of the muscles, taking into account the muscle maximum isometric force and instantaneous moment arm throughout the leap cycle. To make the analysis as robust as possible we limited the number of parameters and in so doing number of assumptions needed were also limited (Allen et al., 2021; Meilak et al., 2021b).

On the basis that *Archaeopteryx,* which does not have the specialised morphology of modern birds for take-off or flight, to get airborne, *Archaeopteryx* would have needed to maximise the use of its hindlimb muscles, thereby approaching the maximum isometric force of the muscles. We do recognize that the zebra finch is over an order of magnitude smaller than Archaeopteryx in mass, however the detailed kinematics available for the smaller extant bird made this study possible. However, there is evidence in the literature to suggest that across the clade of passerine, similar behaviour and mechanics despite a variation in size by 2 orders of magnitude is observed (Meilak et al., 2021b). Future work could further validate this approach using data from larger avians, more comparable in size to *Archaeopteryx lithographica.*

To address the uncertainty in the location of the centre of mass and centre of pressure of the ground reaction forces, we explored the effect of varying both parameters. By varying both parameters, the maximum take-off velocity varied between 2.58-3.12 m/s, with take-off velocity being most sensitive to the location of the centre of pressure. Even taking the slowest take-off velocity (2.58 m/s), *Archaeopteryx* would have still been able to jump with enough velocity to make use of its wings, increasing its trajectory by 66%.

The multiple leap model presented here, necessary to meet the minimum flight speed of *Archaeopteryx*, relies on the second jump providing as much acceleration as the first and conserving the final velocity of the first. Although the investigation of the biomechanics of the landing and second jump is beyond the scope of this study, the ability of modern land birds to land with enough traction to power a second jump has been observed (see video xx included in supplementary materials). Further biomechanical investigations into the landing of modern birds along with biomechanical analyses into the flapping ability of *Archaeopteryx* are needed to better substantiate this hypothesis.

By using data on the take-off of an extant bird and simulating the take-off of *Archaeopteryx*, we have added evidence towards a ground-up leaping mechanism for the evolution of avian flight. *Archaeopteryx,* taking off like an extant bird, would have generated enough initial velocity with its hindlimb that its wings could have increased its trajectory. Following the behaviour of extant birds further, any subsequent leaps would have propelled it to the minimum speed necessary to take to the air.

6.6 Materials and methods

Following the rationale of using data obtained from extant birds to infer the ability of the extinct *Archaeopteryx,* we used force and motion data on the extant bird, the zebra finch (*Taeniopygia guttata*), to shed light on the jumping capabilities of *Archaeopteryx*. Previously published biplanar fluoroscopy data of the hindlimb bones throughout the take-off jump of the zebra finch were used to drive a biomechanical musculoskeletal model of the zebra finch hindlimb (Provini and Abourachid, 2018; Meilak et al., 2021b). Joint angles were applied to a musculoskeletal model of *Archaeopteryx lithographica* along with scaled ground reaction forces to conduct inverse dynamics analyses to estimate the external moments acting on the joints. Further analyses of the muscle moment-generating capacity were used to calculate the maximum take-off velocity of *Archaeopteryx*. We trialled a range of different take-off velocities, for each, calculating the internal joint moments that the muscles would need to balance. By comparing these joint moments to the muscle moment-generating capacity, which is independent of take-off velocity, we ascertained for which biomechanical conditions, and therefore take-off velocity, Archaeopteryx was able to jump.

6.6.1 Musculoskeletal model of Archaeopteryx lithographica

We adapted a biomechanical musculoskeletal model (OpenSim 4.1) of the right hindlimb of *Archaeopteryx lithographica* by Allen and co-workers (Allen et al., 2021) to make it suitable for the take-off range of motion used in this study and the subsequent muscle analysis. The joint ranges of motion were adapted from the original range, which encompassed the likely maximum range of motion during locomotion, to the range of motion experienced during the zebra finch take-off leap. Hip flexion/extension (FE), abduction/adduction (ABAD) and internal/external rotation (IER) ranges of motion were 41° (25° to 66°), 15° (-37° to -22°)-and 20° (-1° to 13°) respectively. The most significant changes were made at the knee and ankle where deep flexion (164° and 135° at the knee and ankle respectively) are seen in the take-off leap. Knee and ankle FE range of motion were 40° (-164° to -124°) and 73° (62 to 135) respectively. The zebra finch take-off shows substantial internal/external rotation range of motion at the knee and ankle, with a range of motion of 16° (5° to 21°) and 30° (-15° to 15°), respectively, accordingly these degrees of freedom were incorporated into the *Archaeopteryx* model also. To enable the fully crouched position while mapping the kinematics from the zebra finch to *Archaeopteryx,* the orientation of the knee flexion axis was rotated about the anterior/posterior axis (x-axis) by 17° to match the orientation of the zebra finch knee flexion axis (Meilak et al., 2021b). In the zebra finch the knee flexion axis was determined as the functional axis of the knee over the range of motion of the take-off jump (Ehrig and Heller, 2019). The musculoskeletal model was scaled to 400 grams and the leg segment lengths scaled to the lengths of the *Archaeopteryx Lithographica* London specimen (see supplementary table 1)

(Wellnhofer and Haase, 2009). Relative hindlimb body segment masses were informed by the *Archaeopteryx* model reported in the literature (Hutchinson, 2004b) and moments of inertia were scaled mass and leg segment length from the zebra finch model (Hutchinson, 2004b).

In this study, muscle parameters were added to the 32 muscle-tendon units included in the musculoskeletal model of Archaeopteryx. Muscle maximum isometric force of 28 muscles was scaled by body mass from the magpie (*Pica pica*) (Meilak et al., 2021a), 2 muscles from the guineafowl (*Numida meleagris*) (Cox et al., 2019) and 2 from the Nile crocodile (*Crocodylus niloticus*) (Allen et al., 2014) (Table 12). By evaluating the Archaeopteryx hindlimb muscle's instantaneous moment arms throughout the take-off and considering the muscles' maximum isometric force we estimated the maximum moment-generating capacity of the muscles.

6.6.2 Biomechanical analyses

The following sections describe the biomechanical analyses we conducted in this study. In order to estimate the maximum take-off velocity of *Archaeopteryx,* the velocity as measured from the kinematics (V_{kin}), and kinetics (V_{GRF}) were altered to incrementally (every 0.01 m/s) increase the take-off velocity being tested (V_{test}).

For each take-off velocity tested, external joint moments were calculated through inverse dynamics analysis and then compared to the moment generating capacity of the muscles. Unlike modern birds, whose hindlimbs contribute 80-94% of take-off velocity, we conservatively assumed that 100% of the initial take-off velocity came from the hindlimb through the ground reaction force. Therefore V_{kin} was temporally warped and V_{GRF} scaled so that the following condition was met:

$$V_{kin} = V_{GRF} = V_{test} \qquad \text{(equation 8)}$$

6.6.2.1 Kinematics

Hip (FE, ABAD and IER), knee (FE and IER) and ankle (FE and IER) joint angles of two zebra finch take-off trials[7] were used to inform the kinematics for the jumping simulations *Archaeopteryx Lithographica*. Zebra finch and *Archaeopteryx* have different relative hindlimb proportions with hindlimb indices ((tarsometatarsus length + tibiotarsus length) / femur length) of 2.64 and 2.05 respectively. Due to the morphological difference in relative leg segment lengths between the zebra finch and *Archaeopteryx*, the extension of the hindlimb throughout the take-off resulted in the lateral motion of the foot of 0.04 m, whereas in the zebra finch the foot does not move laterally. It is assumed that such lateral motion did not occur when *Archaeopteryx* was taking off, therefore to reduce the lateral motion, at each millisecond throughout the take-off, hip rotation was amended to keep the foot lateral motion below 0.0001 m from its initial starting position. Translation of the

pelvis was calculated by fixing the most distal point of the tarsometatarsus to the ground and allowing the pelvis to move as a function of the joint angles (Figure 32).

The take-off velocity of a bird can be defined by measuring the velocity of the centre of mass at the instant the feet leave the ground (Earls, 2000; Tobalske, 2004; Provini et al., 2012). The velocity of the centre of mass of *Archaeopteryx* was measured using the OpenSim 4.1 BodyKinematics Tool throughout the take-off trials (Figure 41). To alter the take-off velocity measured from the kinematics (V_{kin}), the kinematics were temporally warped so that the velocity at the point of take-off matched the take-off velocity being queried.

6.6.2.2 Kinetics

Ground reaction forces of nine zebra finch take-offs (Provini et al., 2012) were used to drive the take-off simulations of *Archaeopteryx*. Each of the nine kinetics trials was paired with the two sets of kinematics trials giving a set of 18 distinct take-off trials. The ground reaction forces were temporally synchronised so that the instant the force components fell to zero occurred at the instant the toes left the ground. Following synchronisation, the ground reaction forces were warped by the same factor as the kinematics. The ground reaction force vectors were scaled in magnitude so that the impulse imparted by the leg resulted in the take-off velocity being tested.

Methods for calculating the velocity as a result of the impulse (V_{GRF}) imparted by the hindlimb followed the approach by Provini and colleagues and are only outlined below (Provini et al., 2012).

Acceleration resulting from the ground reaction forces, $\dot{V}_{GRF}$, were calculated with equation 9.

$$\dot{V}_{GRF} = \frac{\sqrt{F_x^2+F_y^2+(F_z^2-mg)}}{m} \qquad \text{(equation 9)}$$

Where, where F_x is the forward force, F_y is the lateral force, F_z is the vertical force, m is the mass (0.4 kg) and g is the acceleration due to gravity.

Integrating acceleration over the duration of the take-off results in the take-off velocity as a result of the ground reaction forces, V_{GRF}.

$$V_{GRF} = \int_{t0}^{lO} \frac{\sqrt{F_x^2+F_y^2+(F_z^2-mg)}}{m} dt \qquad \text{(equation 10)}$$

Where $t0$ is the time when the jump starts and lO is the time at liftoff.

6.6.2.3 Inverse dynamics analyses

Eight sets of kinetics records were paired with each of the two sets of kinematics records and temporally synchronised, resulting in 18 distinct take-off sequences. For each test velocity, the kinematics were temporally warped and the kinetics scaled so that the impulse applied to the ground resulted in V_{test}. Ground reaction forces were applied to the tarsometatarsus, with the centre pressure placed midway along the foot (Hutchinson, 2004b) (Figure 29). Using kinematics and kinetics as input to the inverse dynamics analysis, external joint moments were calculated about hip FE, ABAD, IER, knee FE and ankle FE. Joint moments were normalised by the bodyweight times leg length (Parslew et al., 2018), and time normalised over the duration of the jump cycle. Mean and standard deviations of the external joint moments were calculated across 18 take-off sequences.

6.6.2.4 Muscle moment generating analyses

Methods for calculating muscle moment-generating capacity followed the approach described by Meilak and colleagues (Meilak et al., 2021a; Meilak et al., 2021b) and are only outlined below.

The moment-generating capacity for each muscle about each joint degree of freedom (DoF) being considered was calculated by multiplying the muscle maximum isometric force (F_{max}) by the instantaneous moment arm ($MA_{t,i,j}$), evaluated at each time increment (t) throughout the kinematics trials. These moments were evaluated for each muscle *i (where i=1..32)* with the muscle maximum isometric force (F_{max}) at the instantons moment arm ($MA_{t,i,j}$) determined throughout the take-off kinematics for each rotational DoF (*j (where j=1..5* for hip FE, ABAD, IER, knee FE and ankle FE)).

$$M_{t,i,j} = F_{max,i} \cdot MA_{t,i,j} \qquad \text{(equation 11)}$$

Muscles acting in the same direction per degree of freedom were summed to obtain the instantaneous joint moment generating capacity ($M_{t,j}$).

$$M_{t,j} = \sum_{i=1}^{32} M_{t,i,j} \qquad \text{(equation 12)}$$

As a muscle's maximum isometric force does not change as a result of the kinematics, the muscle moment-generating capacity was a function of the moment arm, which in turn changes with joint angles. Instantaneous muscle moment-generating capacity for each degree of freedom was determined by evaluating the mean external joint moment and summing all muscle moments acting in that direction. Muscle moment-generating capacity was compared to the peak mean external joint moments. Starting at 0.1 m/s, test velocities were increased until the muscle moment-generating capacity was less than the mean external joint moments of any of the degrees of

freedom. The take-off velocity where the muscles no longer could balance one of the external joint moments formed the upper limit for the maximum take-off velocity of *Archaeopteryx* (V_{0max}).

6.6.3 Projectile trajectory analysis

Using the estimated take-off velocity and assuming at low flying speeds there is negligible drag acting on *Archaeopteryx* we estimated the trajectory of its centre of mass following its take-off leap. The equations of motion were used for all conditions (see supplementary material) and assumed an initial take-off trajectory of 45 degrees while varying either the initial take-off velocity or the contribution of the wings. Trajectories were calculated for three distinct cases:

We calculated trajectories using a range of forward thrust coefficients (T_w, 0.1-0.3 BW) based on thrust estimations of *Archaeopteryx* (Burgers and Chiappe, 1999) wing and the low-velocity flight ability of the jack daw (Klein Heerenbrink et al., 2015). We used a conservative value for the lift of the wings (L_w), 0.17 BW, based on the estimated lift of *Archaeopteryx* wings by Burgers and Chiappe (1999) while moving at the modelled take-off velocity. Using the equations of motion, we calculated the horizontal velocity of *Archaeopteryx* at the landing and calculated the trajectory of a subsequent jump, assuming that no vertical component of the landing velocity was contributing to the next jump (Figure 30 B).

6.6.4 Sensitivity analysis

We explored the model's sensitivity to the location of the centre of mass and the location of the centre of pressure. The take-off velocity of *Archaeopteryx* was defined by measuring the velocity of the centre of mass at the time the feet leave the ground (Earls, 2000; Tobalske, 2004; Provini et al., 2012). Due to the inherent uncertainty in the location of the centre of mass of *Archaeopteryx*, we tested the estimated range of locations of the centre of mass, informed from literature, and the effect these changes had on the maximum take-off velocity (Allen et al., 2013). The study by Allen and co-workers (Allen et al., 2013) used 3D computational reconstructions of Archaeopteryx body shape to posit the most plausible location for the centre of mass with upper and lower bounds. Maximum take-off velocities were calculated for 3 possible centre of mass locations; the most plausible location, the location most caudal and ventral from the hip centre and the location most caudal and dorsal to the hip centre (Figure 30). The centre of mass locations tested spanned 0.03m caudal-cranially and 0.007m ventral-dorsally.

Evidence in the literature suggests that the ground reaction force exerted through the foot throughout the avian take-off leap are exerted cranially relative to the subtalar joint (Earls, 2000; Parslew et al., 2018). However there, there is uncertainty about where along the toes of

Archaeopteryx the centre of pressure of the ground reaction forces was acting. Therefore, the centre of pressure was varied, spanning the most caudal position (underneath the subtalar joint) to the most cranial position (underneath the third phalange of the third digit), ranging between 0 to 33 mm away from the subtalar joint (Figure 39). The change in joint moments as a result of varying the centre of pressure was calculated and therefore the effect this had on the maximum take-off velocity was also quantified.

6.7 Acknowledgments

We to acknowledge the skill of the science graphic designer, Dr. Nuria Melisa Morales García who helped in creating the figures in this manuscript. This work was supported by the Natural Environmental Research Council [grant number NE/L002531/1].

Chapter 7 Conclusions and Future Work

Chapter 7 A concise summary of the essential contributions of the thesis, its limitations, and recommendations for future research.

7.1 Overview of thesis and conclusions

This thesis developed detailed computational biomechanical models of extant taxa, the magpie (*Pica pica),* and the zebra finch (*Taeniopygia guttata*), to establish the biomechanical conditions associated with successful take-off leaps in modern birds. Following the established approach of using detailed understanding derived from the analyses of extant taxa to inform analyses on extinct taxa (*Archaeopteryx lithographica*), we used detailed biomechanical analyses to obtain quantitative evidence supporting a ground-up hypothesis on the evolution of avian flight.

Chapter 4 reports on the first study to apply a rigorous approach to quantify the moment generating capacity of the hip muscles of the magpie, a species of bird using a jump to take to the air. Considering both muscle attachments and the 3D paths between origin and insertion sites, our study reveals that across the joint range of motion of a take-off jump 11 of 14 muscles can act as either extensor or flexor, but all muscles have substantial capability to act as internal or external rotators. The study adds to the growing body of knowledge on the critical importance of the 3D nature of the musculoskeletal structures for function not only in cursorial but also in aerial birds that take to the air utilising the forces generated by their hindlimbs. The methods developed here reveal the level of detail required to comprehensively capture the moment-generating capacity of the muscles at the hip and our approach can serve as a blueprint for similar studies in other animals. Moreover, the data and computational model established here provided the essential basis for further analysis into the role of muscles and their orchestration during the take-off in aerial birds.

The manuscript presented in **Chapter 5** deals with the question of how flying birds negotiate the interface between terrestrial and aerial locomotion and specifically investigates how they take to the air. Though many modern birds use a jump or a leap to take to the air and despite suggestions that such leaping behaviour was used already by the earliest birds, how exactly birds use their hindlimbs to propel them to the air remains largely unknown. Our study is the first to combine experimental data on the external forces and robustly identified skeletal kinematics together with state-of-the-art in silico modelling techniques to simulate the leap of a flying bird to gain an understanding of the internal biomechanics necessary for take-off. We show that the take-off leap is characterised by substantial external moments at the hip and ankle joints, reaching magnitudes of about two times the values previously reported during the running of a flightless bird. These magnitudes of the external moments speak to the mechanical demands associated with the leap. Building upon the comprehensive biomechanical analysis of muscle function developed in chapter 4 we determined that the muscles of the hind limbs are well equipped to balance the external moments during a take-off leap. Whilst the hip muscles appear to be rather close to their maximum capacity, muscles acting at the ankle joint could generate moments of over two times the peak

requirements recorded during the leap. A somewhat unexpected finding was that although all joints of the hindlimb undergo substantial extension during the leap, the knee joint experienced a net external flexion moment. Those findings point towards a key role for bi-articular muscles which extend the hip and flex the knee which might be preferentially activated to satisfy these mechanical requirements of the take-off leap at both joints. Together with the activation of the knee extensors, such use of bi-articular muscles (co-contraction) would result in increased compressive forces across the joint and could therefore provide a mechanism to actively stabilise the relatively unconstrained avian knee joint against excessive long-axis rotation. The work presented here therefore not only sheds new light on the mechanics of the take-off leap in flying birds but also helps to put the associated biomechanical demands in perspective to previously considered demanding conditions such as running in flightless birds. Our analysis of the role of the hindlimb muscles identifies fruitful avenues for further research to unravel how the detailed orchestration of specific muscles helps birds to efficiently take to the air by using their hind limbs. Such work appears to be even more promising as comparisons of external forces and hind limb geometry of the zebra finch studied here with further passerine birds, animals within the most numerous order of birds, suggests that the effective take-off strategy employed by the zebra finch may even be shared across half of all birds.

The manuscript presented in **Chapter 6** reports on the first biomechanical analysis of the jumping ability of *Archaeopteryx*, the first bird. For as long as people have watched birds flying, how birds first took to the skies has been the subject of immense interest, and speculation. Several potential mechanisms have been described for the evolution of avian flight, but most remain speculative, and sadly untestable. Our study is the first to combine experimental kinematics data and external forces of a living bird (the zebra finch) with state-of-the-art computational modelling techniques to simulate the leaping ability of an extinct avian (*Archaeopteryx*), to investigate a leaping mechanism for the evolution of avian flight. We show that *Archaeopteryx,* taking off like an extant bird, would have generated enough initial velocity with its hindlimbs that its wings could have increased its trajectory. Following the behaviour of extant birds further, any subsequent leaps would have propelled it to the minimum speed necessary to take to the air. By following a sound approach using unique data from extant taxa to inform comprehensive computational analyses of extinct taxa, we have added key quantitative evidence in support of a jumping hypothesis for the evolution of avian flight.

This study not only supports the compelling jumping hypothesis for the evolution of avian flight but speaks to the effectiveness of using biomechanical analyses to investigate how extinct taxa may have moved.

7.2 Limitations and future work

The studies conducted in this thesis had limitations. The model of the magpie developed in chapter 4 was based on data from one specimen only. However, the length of the femur of the scanned specimen and the mass of the specimen place it within 1 standard deviation of the morphometrics reported in the literature (Verstappen et al., 1998; Tomek and Bochenski, 2000). Furthermore, muscle attachment sites were not obtained from the specimen itself but were instead informed by the literature (Verstappen et al., 1998) following a careful approach to map attachments on the surfaces of the 3D CT scanned specimen. Although the crow, the species informing the locations of the via points, is a different species to the magpie, they are closely related and belong both to the family of Corvidae within which hindlimb morphology is very conserved (Verstappen et al., 1998) and differences in the skeletal structures are found to be minimal. Future studies, supported by dedicated contrast-enhanced CT imaging (Descamps et al., 2014; Sullivan et al., 2019), should investigate multiple birds to firmly establish intra- and interspecies variations in the functional morphology of the muscles in Corvidae. Considering the substantial size difference between magpies and crows (crows possessing approximately double the mass of magpies) a direct comparison could help to not only ascertain how far hindlimb morphology across corvids is conserved but would also offer further insight into the role of scaling for the functional morphology of the muscles of the avian hindlimb.

In chapter 5, the kinematics used to drive the take-off simulation of the zebra finch were informed by previously obtained XROMM data of the zebra finch take-off leaps (Provini and Abourachid, 2018). In this thesis, the use of the tantalum bead markers, detailed bone surface geometry from high-resolution µCT, and anatomical-functional relationships (Ehrig et al., 2007; Ehrig and Heller, 2019) were all used to increase repeatability in tracking 3D skeletal kinematics and reduce the influence of the user during scientific rotoscoping (Brainerd et al., 2010). Due to the limited number of specimens in which bones had had a minimum of three tantalum markers attached, only two sets of kinematics trials could be amended in that way and were available for further analysis. However, by combining each set of kinematic trials with nine sets of kinetics trials, we maximised the variability in take-off conditions studied here. Future studies using XROMM to capture detailed kinematics should ensure that at least one of the long bones includes at least 3 markers to reduce the reliance on the user during scientific rotoscoping. This thesis did not include the mechanics of phalanges, as the take-off trajectories of the hindlimb are defined primarily by the motion at the more proximal hindlimb joints where also more substantial joint moments are generated. Future studies considering the hind limb mechanics during landing, when the detailed mechanics of the foot are likely to play a more important role, should aim to capture the detailed kinematics of the phalanges. Finally, this study considered the maximal moment-generating capacity of the muscles,

taking into account the muscle maximum isometric force and instantaneous moment arms throughout the take-off leap and contrasted these to the external moments applied to the joints of the hind limb. In this way, general patterns of mechanical requirement and hindlimb muscle capability to meet the requirements of a take-off leap were analysed. Though the determination of the detailed muscle activation patterns to balance the external moments was not within the scope of the current study, further analyses of the biomechanical model (such as static optimisation (Heller et al., 2001b; Taylor et al., 2006; Delp et al., 2007; Seth et al., 2011; Trepczynski et al., 2012; Seth et al., 2018; Trepczynski et al., 2018)) would help to further elucidate the detailed activation patterns of individual muscles as well as providing estimates for the likely bone-on-bone joint contact forces being transferred at the joints of the avian hind limb during a take-off leap. Future studies could use the muscle optimisation methods described, with the models presented in this thesis, to get a better understanding of organ and tissue tissue level mechanics in the hindlimb throughout the avian take-off leap. For the latter, tissue level conditions, a comparison against experimentally confirmed failure loads could serve to establish the validity of such predictions at least against the upper bound represented by the failure loads.

In chapter 6 kinematics and kinetics of the zebra finch feed into analyses of the take-off mechanics of *Archaeopteryx* though the zebra finch is over an order of magnitude smaller (in mass) than Archaeopteryx. However, the accurate 3D kinematics available for the smaller extant bird were instrumental to drive the model of the extinct bird. Moreover, our analysis of similarities of hind limb morphology and external forces during the take-off leap suggests that similar behaviour and mechanics may be present despite a variation in size (mass) by 2 orders of magnitude across Passerines (Meilak et al., 2021b). Future work should corroborate this hypothesis through developing models and using data from larger avians that are more comparable in size to *Archaeopteryx lithographica.* The thesis focussed on the maximal moment-generating capacity of the muscles as a key parameter to assess the ability to leap, taking into account the muscle maximum isometric force and instantaneous moment arm throughout the leap cycle. Muscle capacity to generate force is, however, dependent on further architectural parameters including fibre length, pennation angle, and tendon slack length (Hutchinson et al., 2015; Charles et al., 2016; Rankin et al., 2016; Bishop et al., 2021a). Although we sought to minimise both the assumptions required for analysis and the risk of overfitting by limiting the number of parameters and assumptions in our model (Allen et al., 2021; Meilak et al., 2021b), future studies could explore the use of the aforementioned muscle optimisation methods to estimate muscle activation profiles, muscle, and joint contact forces. Following thorough validation against experimentally measured muscle activation patterns and after ensuring that muscle and joint forces remain well within force ranges tolerated by the bones, the more detailed information about the orchestration of muscles

to accommodate a range of locomotor behaviors across a range of basal to more derived birds could shed more light on the role of biomechanics for avian evolution. Although an investigation of the biomechanics of landing was beyond the scope of the thesis, a more detailed analyses of the multiple leap model presented here to estimate the conditions required for *Archaeopteryx* to achieve minimum flight speed would benefit from a more detailed understanding of the biomechanics of the landing itself. The biomechanical models and analysis framework developed here will provide the essential basis to enable studies to develop such an understanding. Finally, although the current thesis focussed on the role of the hindlimbs in the evolution of avian flight, the work presented here lays the foundation for the development of biomechanical models that capture the contribution of both hind- and forelimbs to the ability of *Archaeopteryx* and further basal birds with contested ability to negotiate the aerial environment, an exciting area for future work that applies rigorous biomechanical analyses to test hypotheses regarding the evolution of avian flight.

Appendix A Supplementary Material accompanying the manuscript presented in chapter 4

A.1 Description of bone anatomical and joint coordinate systems

Bone local coordinate systems were defined using least squares shape-fitting techniques (Least Squares Geometric Elements library (Forbes, 1989)) applied to select regions of the bone surfaces. Here, derived features such as the femoral head centre, and the axes of the distal femoral, tibiotarsal, tarsometatarsal condyles informed the definition of segment coordinate systems as explained in detail below. Anatomical and joint coordinate systems (ACS and JCS, respectively (Kambic et al., 2014)) were defined for the long bones where ACSs were defined at the proximal end of long bones whilst the JCSs were defined at the distal portion of the bone. Orientation of the coordinate systems followed conventions described in the literature (Kambic et al. (2014), Provini and Abourachid (2018), Figure 33).

Surfaces defining the spherical regions of the left and right acetabula were isolated (Paraview 5.6.0, Ahrens et al. (2005); Ayachit (2015)). Using Matlab (2018a, The Mathworks, Nantucket, USA) the origin of the pelvic ACS was then defined at the midpoint between the two spheres fitted to isolated regions of the acetabular joint surfaces (lssphere.m v1.0). A midsagittal plane was defined using an iterative approach where the mirrored pelvis surface was registered to its original shape (Chen et al., 2018). The Z axis of the pelvis ACS was the normal of the midsagittal plane pointing from left to right. The Y axis was derived from a Principal Component Analysis (Jolliffe, 2011) of the surface nodes as projection of the 1st principal axis on the midsagittal plane. The pelvic ACS X axis was determined from the cross product of the Y and Z axes. The positive direction of the X axis pointed cranially and the Y axis positive dorsally. The axes of the JCS of the left and right hips were aligned with the axes of the pelvic ACS while their origins were located at the respective femoral centres of rotation.

To define the centre of rotation of the hip, the spherical region of the femoral head was identified (Paraview 5.6.0 Ahrens et al. (2005); Ayachit (2015)) and fitted by a sphere. The X axis direction of the femoral ACS (positive proximally) was defined by determining the centroid line of the femoral shaft to which a straight line was fitted (lls3dline.m v1.0). Its Z axis (positive medially) was defined between the femoral head centre and its projection on to fitted shaft axis. The Y axis of the femoral ACS (positive anteriorly) was determined from the cross product of the X and Z axes. To define the femoral JCS, CT scans of the magpie hindlimb in three different orientations were used to identify

the primary axis of rotation using a functional approach (Ehrig et al., 2007; Ehrig and Heller, 2019). The knee centre of rotation was then determined as the midpoint of the medial and lateral intersections of the functional axis of rotation with the bone surface. The functional knee axis of rotation defined the Z axis of the JCS (positive medially). The Y axis of the femoral JCS (positive anteriorly) was determined from the cross-product of the Z axis of the JCS with the X axis of the ACS. The X axis of the femoral JCS (positive proximally) was determined from the cross-product of its Y and Z axes.

The processes for defining the local coordinate systems of the tibiotarsus and tarsometatarsus were the same: the ACS X axis direction (positive proximally) was defined by fitting a line to a centroid axis of the bone shaft. The Z axis of the JCS (positive medially) was defined between the points of intersection of cylinders fitted to the distal medial and lateral condyles with the bone surface (lscylinder.m v1.0). The Y axes (positive anteriorly) of both the ACS and JCS were defined by calculating the cross product between the JCS Z and ACS X axes. JCS X axes (positive proximally) were defined by calculating the cross product between the JCS Y and Z axes. ACS Z axis (positive medially) was defined by calculating the cross product between the ACS X and Y axes. Tibiotarsal and tarsometatarsal ACS origins were defined at the intersection of the shaft axes with the proximal surface of the respective bone. The origin of the JCS defined as the midpoint of intersections of the Z axis with the bone surface.

A.2 Supplementary Figures

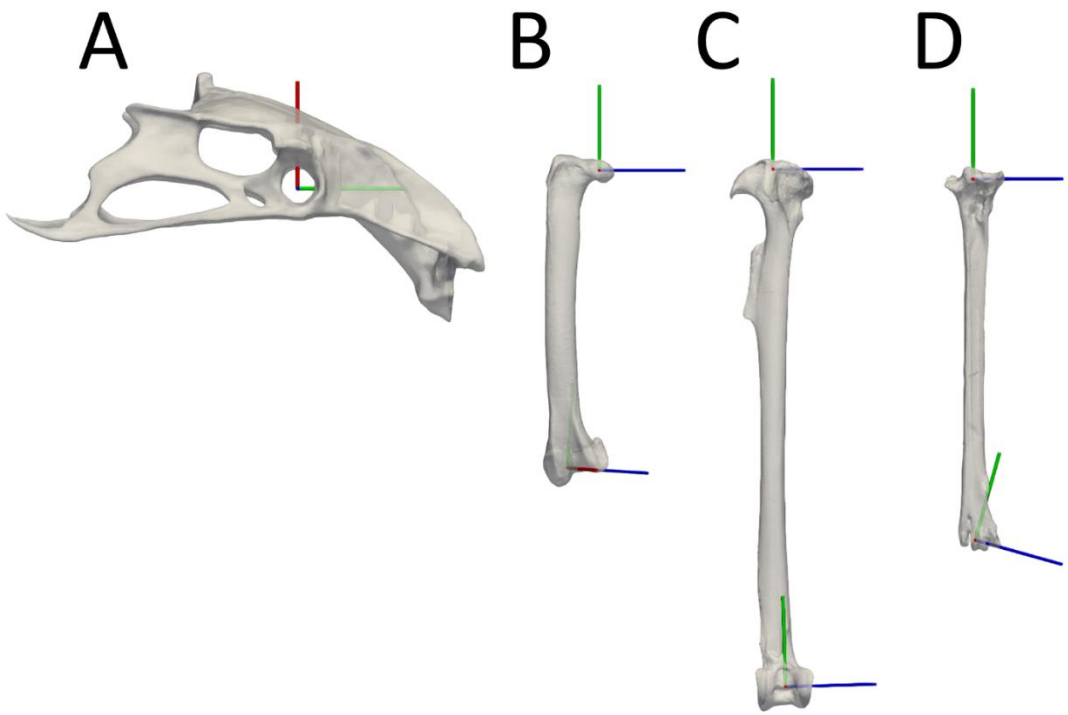

Figure 33 Anatomical and joint coordinate systems of the right hindlimb bones of the magpie. For the pelvis (A), the x axis direction (green) points from caudal to cranial, the y axis direction (red) points from ventral to dorsal, and the z axis direction (blue) points from left to right. For the long bones (B to D), the x axis direction points from distal to proximal, the y axis direction points from posterior to anterior, and the z axis direction points from lateral to medial.

Appendix B Supplementary Material accompanying the manuscript presented in chapter 5

B.1 Optimised tracking of skeletal kinematics

In order to reliably track the 3D skeletal kinematics for use in the musculoskeletal analyses, bone surfaces were mapped from the CT space to the XROMM space using a combination of physical and virtual markers while additionally minimising penetration of the hindlimb bone surfaces as detailed below.

B.1.1 Functional – anatomical definition of virtual markers

The 3D positions of the physical markers which were tracked throughout the leaping motion using XrayProject 2.2.4 in MATLAB (Brainerd et al., 2010; Provini and Abourachid, 2018) formed the basis for mapping the bone surfaces from the CT system to the XROMM space using Ordinary Procrustes Analyses (OPA). To enable mapping of the surfaces using OPA, knowledge of the location of at least 3 markers was required for each tracked bone. Since the tarsometatarsus was the only bone to be tracked on which 3 physical markers were placed in the experiment, additional virtual markers were defined at the hip, knee and ankle joint centres. The definition of these virtual markers commenced by calculating functional axes of rotation (Taylor et al., 2006; Ehrig et al., 2007; Ehrig and Heller, 2019; Richards et al., 2021) of the ankle, knee and hip using the µCT data and the bone surfaces derived from that data. After confirming minimal morphological difference between bone surfaces of the left and right hindlimbs, the surface of the pelvis was mirrored at its mid-sagittal plane (Chen et al., 2018) and registered to its original shape using rigid ICP registration (Manu, 2021b). The right femur was then mirrored similarly and mapped with the registration matrix previously established for the pelvis. The left femur was then registered to the mirrored and mapped right femur, eventually providing two different poses for a left femur with respect to the left acetabulum. Using these two joint poses, the functional axis of rotation of the left hip was calculated from the vertex positions of the respective bone surfaces (Figure 37 A) (Ehrig and Heller, 2019). Spheres were fitted

to the articulating surfaces of the femoral heads (in two poses) and acetabulum (Mesh2Surface for Rhino v6.1.5 in Rhino v7) (McNeel, 2020). The centres of these spheres were projected on to the functional axis of rotation of the hip and their mean position was taken as the functional-anatomical hip centre of rotation (Figure 37 A). This hip centre could be expressed with respect to both the pelvis and the femur, providing a virtual marker for both bones and an objective means to link them via a ball and socket joint. A similar approach was used for functionally defining the knee and ankle joint centres. The right femur was mirrored and registered to the left, again using rigid ICP registration (Manu, 2021b). Using the transformation matrix resulting from the aforementioned registration, the right tibiotarsus was mapped to the left hind limb before the left tibiotarsus was ICP-registered to that pose, resulting in two poses of the left tibiotarsus with respect to the left femur (Figure 37 B). Using these two joint poses, the functional axis of rotation of the knee was calculated (Ehrig and Heller, 2019). The midpoint of the intersection of this functional axis with the surface of the femur defined the functional-anatomical knee joint centre (Figure 37 B). In a similar manner, the mirrored right tibiotarsus was registered to the left, and that registration was used to map the mirrored right tarsometatarsus to the left before ICP-registering the left tarsometatarsus to that pose (Figure 37 C). Using the two resulting joint poses, the functional axis of rotation of the ankle was found (Ehrig and Heller, 2019). The midpoint of the intersection of the resulting axis of rotation with the tibiotarsus provide a further virtual marker at the functional-anatomical ankle centre.

B.1.2 Collision detection supported reconstruction of skeletal kinematics

After augmenting the physical markers with the virtual markers located at the hip, knee and ankle joint centres, reconstruction of skeletal kinematics proceeded with mapping bone surfaces from the space of the CT system to the XROMM system by OPA between markers associated to each bone. Given that 3 physical markers were attached to the tarsometatarsus only, the surface mapping process started from that bone. OPA computed between the 3 physical markers attached to the bone in the CT and XROMM systems was used to map the tarsometatarsus surface and also

the ankle joint centre (virtual marker) from the CT to the XROOM. Further OPA calculated from the virtual ankle joint centre and the two physical markers of the tibiotarsus and their respective µCT location was then used to map the tibiotarsus surface and the knee joint centre (virtual marker) from the CT to the XROMM system.

As only a single physical marker was attached to the femur, at this stage of the process the position of only two femoral markers (1 virtual, 1 physical) were known in the XROMM space. To determine the position of a third marker that maximised the use of the XROMM marker data in a manner consistent with the kinematic model of a ball and socket joint for the hip, a virtual hip joint centre marker was derived as follows. Using the previously determined functional anatomical hip centre it was possible to construct two spheres, centred at the location of the respective physical markers of the femur and pelvis, respectively, with radii corresponding to the previously determined distance between these physical markers and the functional-anatomical hip centre. By determining the intersection between these spheres, a circle could be determined on which the hip centre was known to lie. The exact location of hip centre on the circumference of the circle was determined by preventing any collision between the surfaces of the tibiotarsus and the distal femur while also minimising the extent of collision between the surfaces of the femur and the pelvis (acetabulum and anti-trochanter). The implementation of this process in Matlab (2019b, The Mathworks, Nantucket, USA) sampled the circumference of the circle on which the hip centre was known to lie in 1 degree intervals to find the pose of the femur for which there was no intersection with the surface of the tibiotarsus and minimal intersection with the surface of the acetabulum. At the final stage of the process, the maximum intersection volume remained at very small values at below 0.37% of the volume of the femur.

B.2 Definition of anatomical bone and joint coordinate systems

Anatomical coordinate systems for the bones and joint coordinate systems (ACS and JCS, respectively (Kambic et al., 2014)) were defined for the long bones where ACSs were defined at the proximal end of long bones whilst the JCSs were defined at the distal portion of the bone. Orientation of the coordinate systems followed conventions described in the literature (Kambic et al., 2014; Provini and Abourachid, 2018; Meilak et al., 2021a) (Figure 38). The origin of the pelvic ACS was defined at the midpoint between the two spheres fitted to isolated regions of the acetabular joint surfaces using the methods of least squares (lssphere.m v1.0, Matlab (2018a, The Mathworks, Nantucket, USA)). A midsagittal plane was defined using an approach where the mirrored pelvis surface was registered to its original shape (Chen et al., 2018). The Z axis of the pelvis ACS was the normal of the midsagittal plane pointing from right to left and the Y axis (positive axis direction pointing dorsally) was derived from a projection of the 1^{st} principal axis of the pelvis (Jolliffe, 2011) on the midsagittal plane. The pelvic ACS X axis was determined from the cross product of the Y and Z axes, with the positive axis pointing cranially. The axes of the JCS of the left hip were aligned with the axes of the pelvic ACS while its origin was located at the respective functional-anatomic hip centre of rotation determined previously.

The X axis direction of the femoral ACS (positive direction pointing proximally) was defined by determining the centroid line of the femoral shaft to which a straight line was fitted using the method of least squares (lls3dline.m v1.0). Its Z axis (positive direction pointing laterally) was defined between the femoral head centre and its projection on to the fitted shaft axis. The Y axis of the femoral ACS (positive direction pointing anteriorly) was determined from the cross product of the X and Z axes. The functional-anatomical knee centre of rotation, determined previously, was defined as the origin of the femoral JCS. The functional knee axis of rotation defined the Z axis of the JCS (positive axis direction pointing medially). The Y axis of the femoral JCS (positive axis direction pointing anteriorly) was determined from the cross-product of the Z axis of the JCS with

the X axis of the ACS. The X axis of the femoral JCS (positive axis pointing proximally) was determined from the cross-product of its Z and Y axes.

The processes for defining the local coordinate systems of the tibiotarsus and tarsometatarsus were similar: the ACS X axis direction (positive axis pointing proximally) was defined by least squares fitting a line to a centroid axis of the bone shaft. The Z axis of the JCS (positive axis pointing laterally) of the tibiotarsus was defined using the ankle axis of rotation whereas for the tarsometatarsus the Z axis was defined between the points of intersection of cylinders fitted to the distal medial and lateral condyles with the bone surface (lscylinder.m v1.0). The Y axes (positive axis pointing anteriorly) of both the ACS and JCS were defined by calculating the cross product between the JCS Z and ACS X axes. JCS X axes (positive axis pointing proximally) were defined by calculating the cross product between the JCS Y and Z axes. ACS Z axis (positive axis pointing laterally) was defined by calculating the cross product between the ACS X and Y axes. Tibiotarsal and tarsometatarsal ACS origins were defined at the intersection of the shaft axes with the proximal surface of the respective bone. The functional-anatomical ankle joint centre of rotation was taken as the origin of the JCS of the tibiotarsus.

B.3 Supplementary Figures

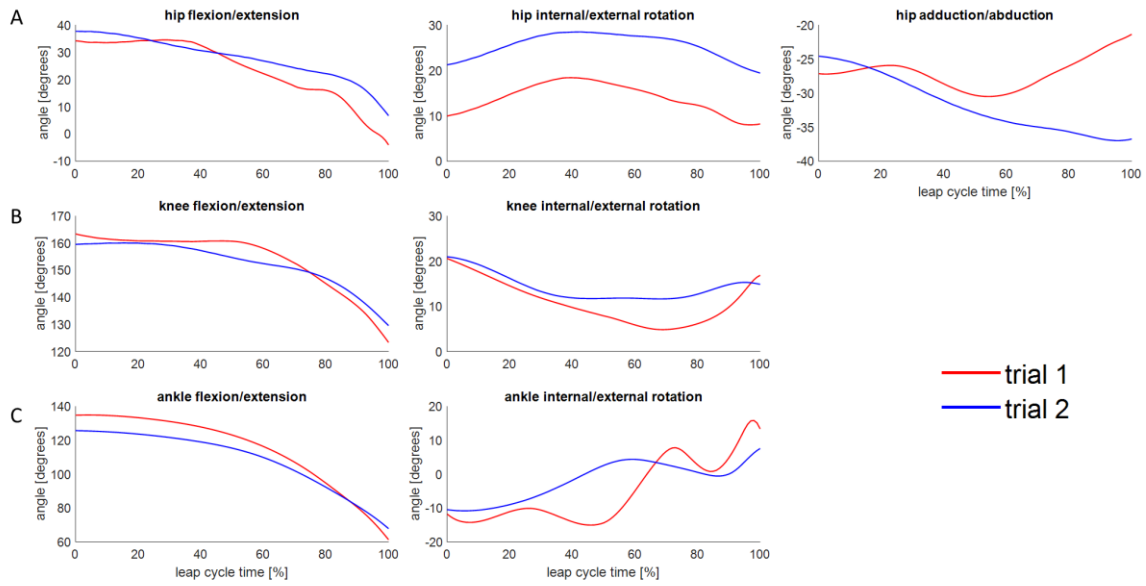

Figure 34 Joint angles at the A) hip, B) knee and C) ankle for 2 take-off trials derived from XRoMM data. Hip joint flexion/extension (FE), internal/external rotation (IER), abduction/adduction (ABAD), knee, and ankle FE and IER are shown here where positive values for FE, ABAD and IER are flexion, adduction, and internal rotation, respectively. Line colours represent the specific trial from which the data was derived (red: trial 1; blue trial 2).

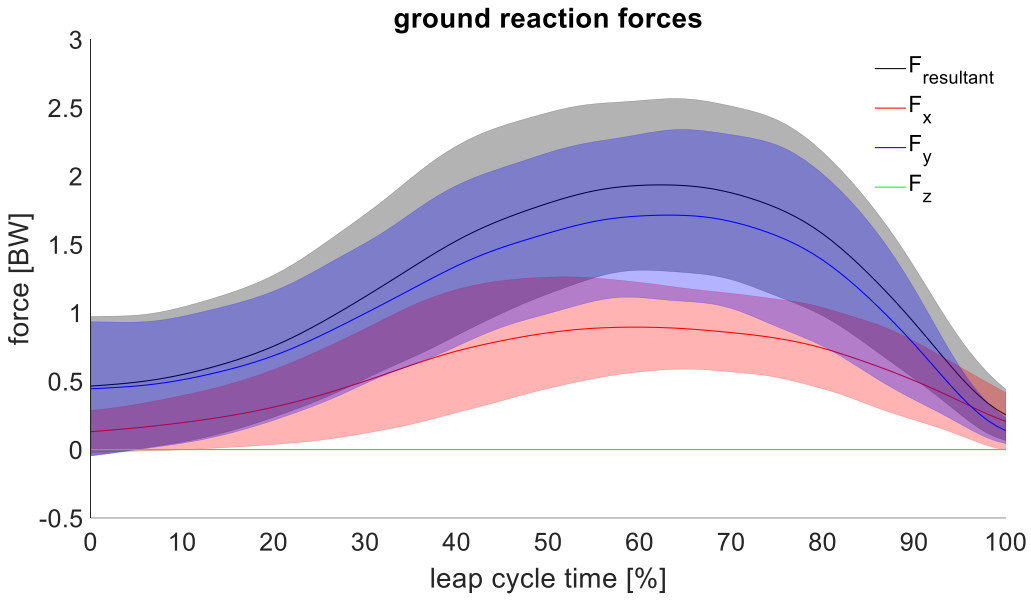

Figure 35 Resultant and individual x, y, z components of the ground reaction force during a full take-off cycle. Solid lines represents mean values while shaded bands surrounding the mean represent ±2.5 standard deviations (SDs). Force components Fx, Fy, and Fz are horizontal (caudal-cranial), vertical (ventral-dorsal), and sideways (medial-lateral) directions, respectively.

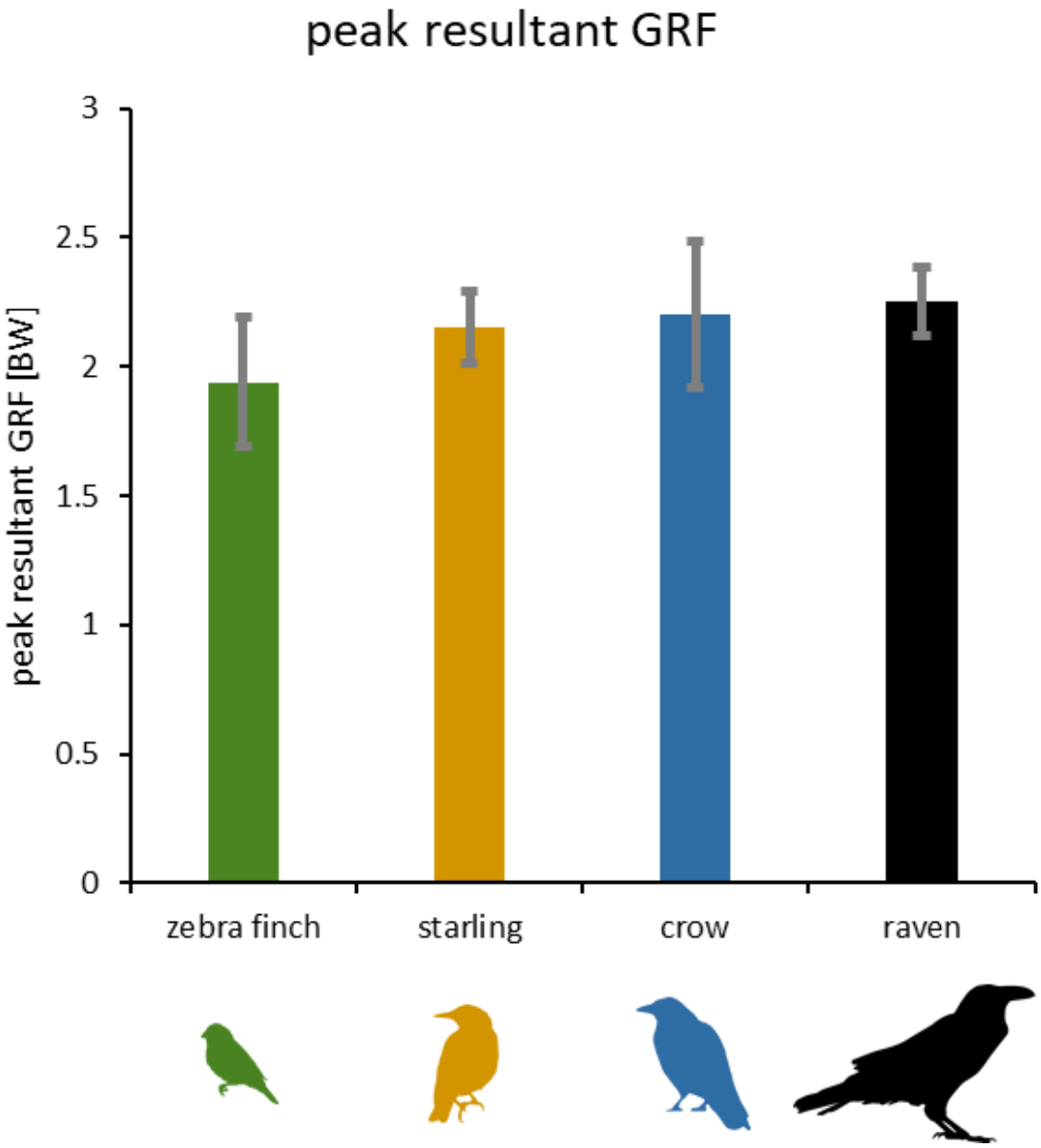

Figure 36 Mean ± standard deviation of the peak resultant ground reaction forces (GRFs) acting on one leg of the zebra finch, starling (Earls, 2000), crow, and raven during their respective take-off leaps. Silhouettes from phlyopic.org.

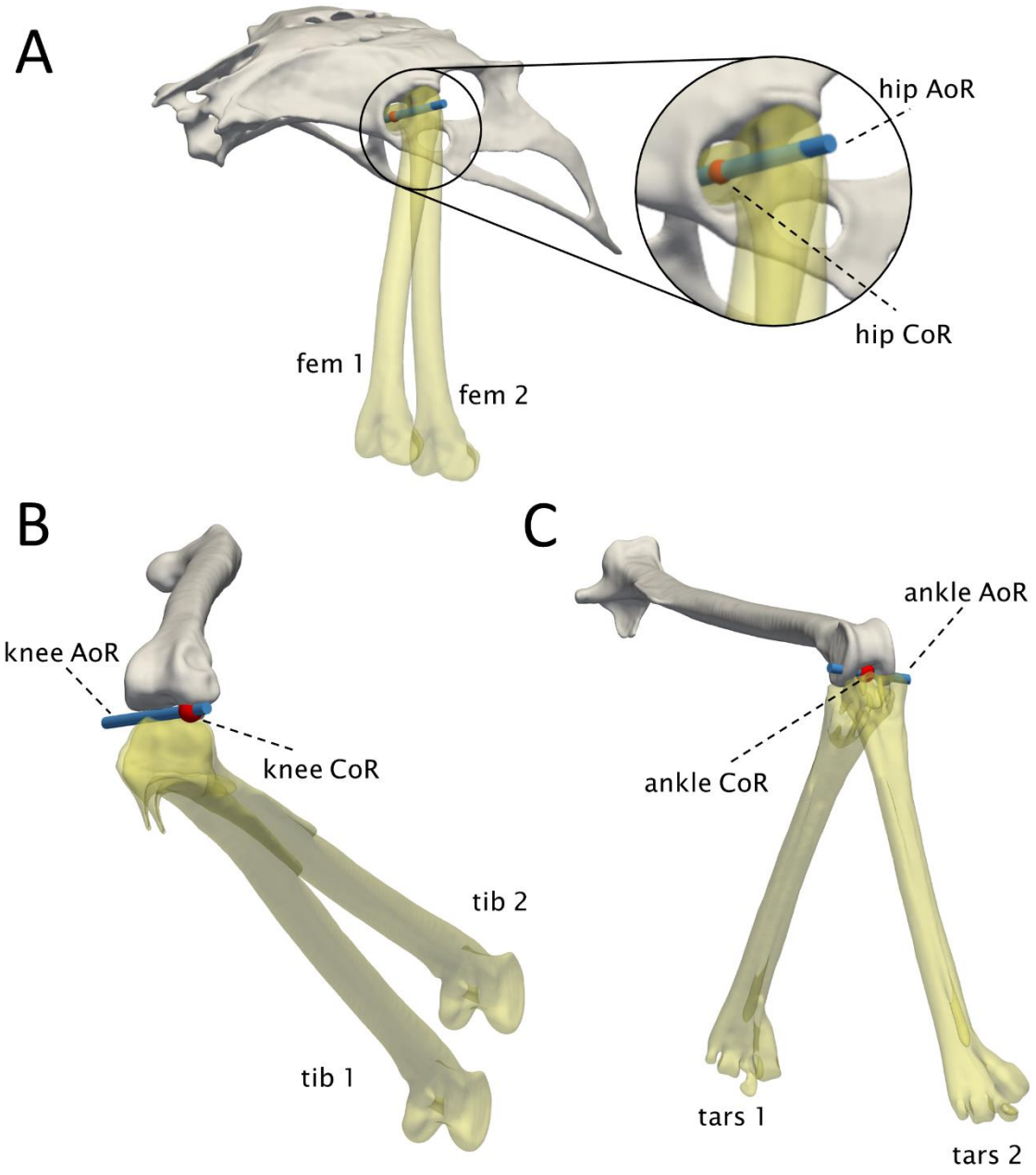

Figure 37 Functional anatomical joint centres for the hip, knee and ankle joint were derived from a CT scan of the zebra finch hindlimbs. For each joint, the difference in pose between the left and right hindlimbs was used to estimate a functional joint axis of rotation (AoR) while joint centres were derived from the intersection of the AoR with the surface of the proximal bone. Blue cylinders represent the functionally determined joint axes of rotation (AoR) and red spheres represent the functional-anatomical joint centres of rotation (CoR). A pose of the mirrored right femur (fem 2) registered to the left side, together with the original pose of the left femur (fem 1). B mirrored right tibiotarsus (tib 2) registered to the left, together with the original pose of the left tibiotarsus (tib 1). C pose of the right tarsometatarsus (tar 2) registered to the left, together with original pose of the left tarsometatarsus (tar 1).

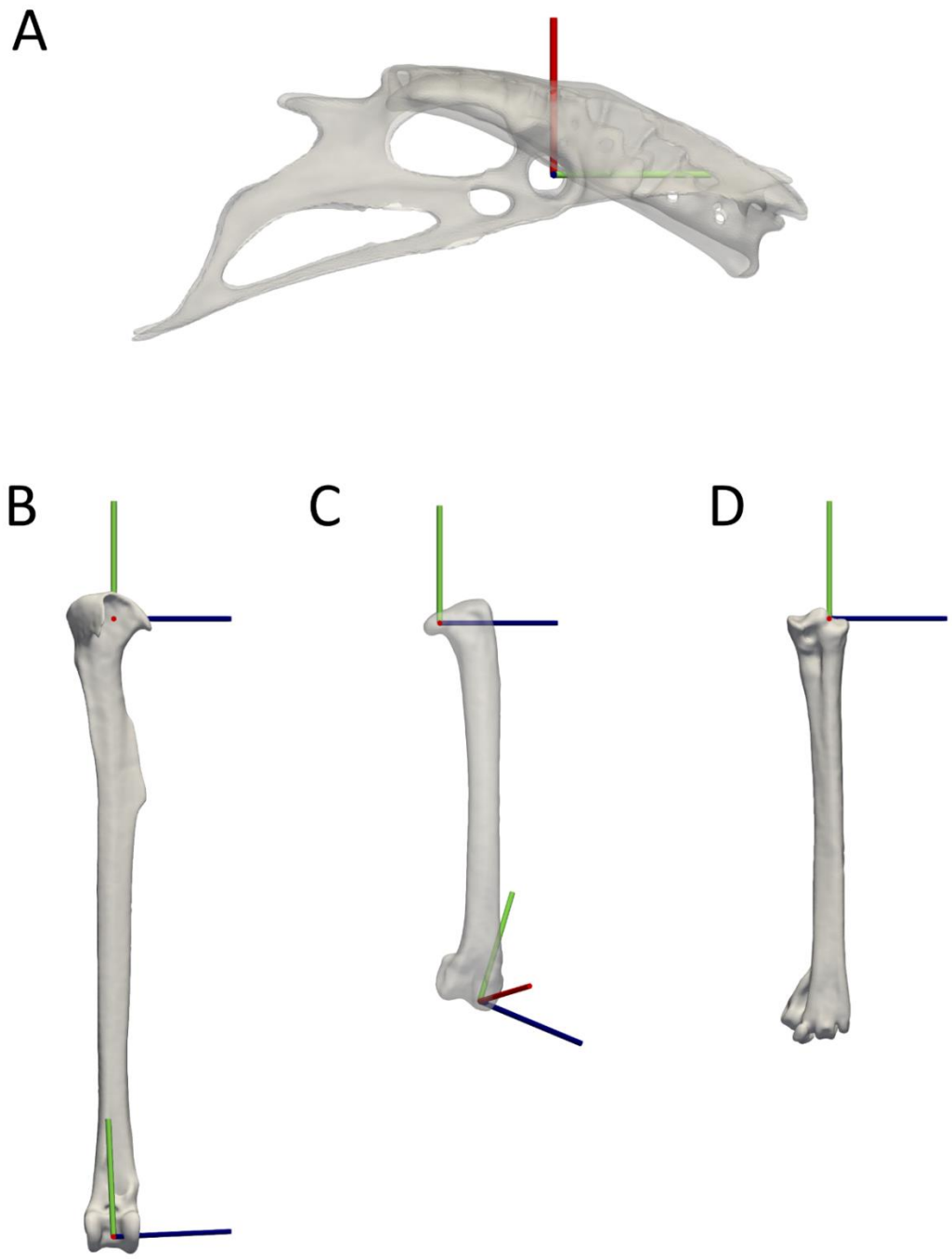

Figure 38 Anatomical and joint coordinate systems of the left hindlimb bones of the zebra finch. For the pelvis (A), the positive x axis direction (green) points from caudal to cranial, the positive y axis direction (red) points from ventral to dorsal, and the positive z axis direction (blue) points from right to left. For the long bones (B, C and D), the proximal and distal coordinate systems are the anatomical and joint coordinate systems respectively where the positive x axis direction points from distal to proximal, the positive y axis direction points from posterior to anterior, and the z axis direction points from medial to lateral.

Appendix C Supplementary Material accompanying the manuscript presented in chapter 6

C.1 Projectile trajectory analysis and equations of motion

The analyses to calculate the trajectory of the centre of mass (CoM) of *Archaeopteryx* following the take-off leap are based on the constant acceleration equations of motion(Calvert and Farrar, 2008) and the assumption that there is negligible drag acting on *Archaeopteryx* at low flying speeds. The equations of motion were used for all conditions and assumed an initial take-off trajectory of 45 degrees while varying either the initial take-off velocity or the contribution of the wings.

The horizontal position of the CoM as a function of time $x(t)$ was calculated as follows:

$$x(t) = x_0 + V_{0x} \times t + \frac{1}{2} a_{wt} \times t^2 \qquad \text{(equation 13)}$$

where x_0 is the mean initial starting position of the CoM in the horizontal direction (0 m), V_{0x} is the initial horizontal velocity, t is the amount of time spent in the air, and $a_{wt}$is the horizontal acceleration due to the thrust provided by the wings.

The vertical position of the CoM as a function of time $y(t)$ was calculated as follows:

$$y(t) = y_0 + V_{0y} \times t - \frac{1}{2} a_v \times t^2 \qquad \text{(equation 14)}$$

where y_0 is the mean initial starting position of the CoM in the vertical direction, V_{0y} is the initial vertical velocity, t is the amount of time spent in the air, and a_v is the acceleration in the vertical direction. The acceleration a_v is obtained by subtracting the acceleration due to the lift provided by the wings from the acceleration due to gravity:

$$a_v = g - a_{wl} \qquad \text{(equation 15)}$$

where g is the acceleration due to gravity, and a_{wl} is the vertical acceleration resulting from the vertical lift provided by the wings.

Assuming that the take-off angle was 45 degrees, the initial horizontal and vertical velocities of the CoM were calculated from the overall take-off velocity V_{0max}:

$$V_{0y} = V_{0x} = sin\ (45)\ V_{0max} \qquad \text{(equation 16)}$$

where V_{0max} is the maximum take-off velocity calculated from the biomechanical analysis of the hindlimb mechanics during a leap.

The peak vertical height of the CoM was calculated by differentiating equation 16:

$$\frac{dy}{dt} = V_{0y} - a_v \times t \qquad \text{(equation 17)}$$

The time at which the maximum vertical height (t_{ymax}) is then obtained, under the assumption that the vertical velocity of the CoM reduced to zero at the peak of the trajectory, as follows:

$$t_{ymax} = \frac{V_{0y}}{a_v} \qquad \text{(equation 18)}$$

Substituting t_{ymax} (18) into equation (14) provides the peak vertical height:

$$y_{max} = y_0 + V_{0y} \times t_{ymax} - \frac{1}{2} a_v \times {t_{ymax}}^2 \qquad \text{(equation 19)}$$

The time *Archaeopteryx* travelled through the air (t_{final}) was calculated by setting the vertical position of the CoM trajectory (equation (14)) to a value of zero and solving the resulting quadratic equation for the non-negative value:

$$-\frac{1}{2} a_v {t_{final}}^2 + V_{0y}\ t_{final} + y_0 = 0 \qquad \text{(equation 20)}$$

Rearrange the equation and solve for t_{final}:

$$t_{final} = \frac{-V_{0y} \pm \sqrt{{V_{0y}}^2 + 2 a_v y_0}}{-a_v} \qquad \text{(equation 21)}$$

Substituting t_{final} (21) into equation (13) and solving for $x(t_{final})$ then provided the horizontal distance travelled at the time of landing:

$$x(t_{final}) = x_0 + V_{0x} \times t_{final} + \frac{1}{2} a_{wt} \times {t_{final}}^2 \qquad \text{(equation 22)}$$

The time required for *Archaeopteryx* to reach the minimum sustainable flight speed (v_{final} = 7 m/s) after its final leap was calculated as detailed below. First, the resulting velocity v_{final} was calculated by adding the horizontal (v_{xfinal}) and vertical (v_{yfinal}) components as follows:

$$v_{final} = \sqrt{v_{xfinal}^2 + v_{yfinal}^2} \qquad \text{(equation 23)}$$

where v_{xfinal} can be expressed as:

$$v_{xfinal} = v_{0x} + a_{wt} \times t_{final} \qquad \text{(equation 24)}$$

and v_{yfinal} can be expressed as:

$$v_{yfinal} = v_{0y} + a_v \times t_{final} \qquad \text{(equation 25)}$$

Substituting equations (23) and (24) into equation (22) while setting v_{final} to a value of 7 m/s results in the following quadratic equation:

$$(a_{wt}^2 + a_v^2)t_{final}^2 + \left(2a_{wt}v_{0x} + 2a_v v_{0y}\right)t_{final} + \left(v_{0x}^2 + v_{0y}^2 - v_{final}^2\right) = 0 \qquad \text{(equation 26)}$$

Solving the quadratic equation (19) then provides t_{final}:

$$t_{final} = \frac{-\left(2a_{wt}v_{0x}+2a_v v_{0y}\right) \pm \sqrt{\left(2a_{wt}v_{0x}+2a_v v_{0y}\right)^2 - 4\left(a_{wt}^2+a_v^2\right)\left(v_{0x}^2+v_{0y}^2-v_{final}^2\right)}}{2\left(a_{wt}^2+a_v^2\right)} \qquad \text{(equation 27)}$$

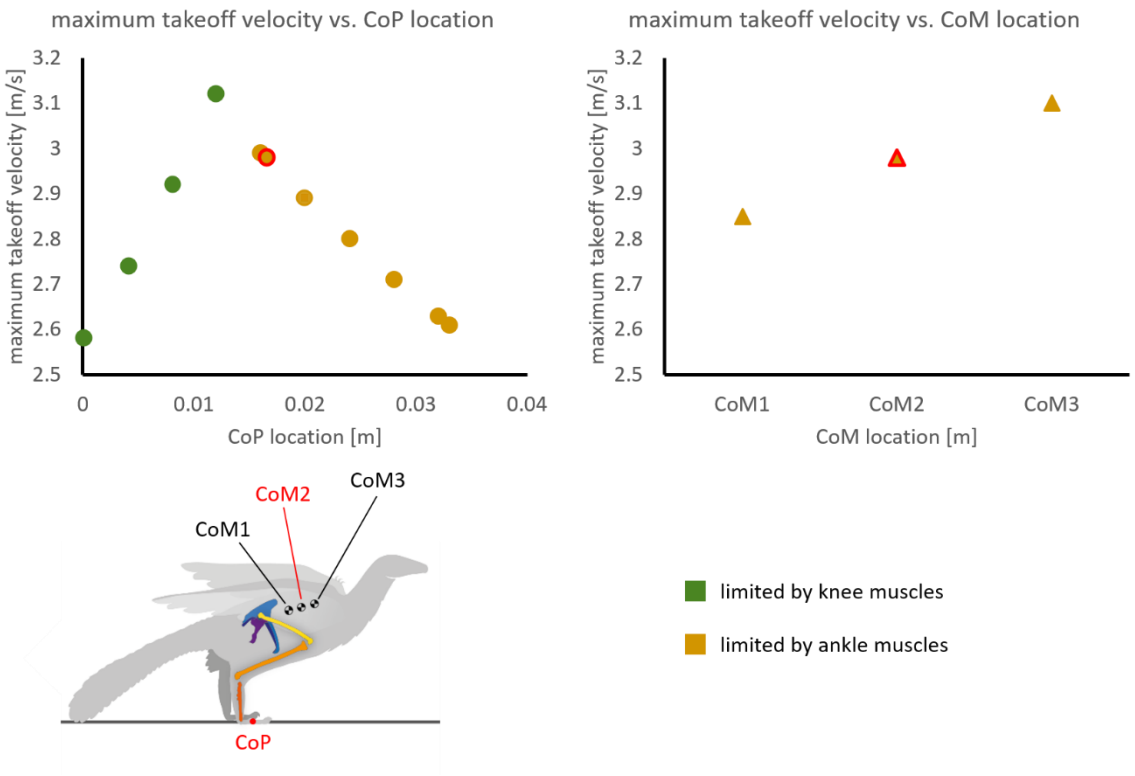

Figure 39 Sensitivity of the maximum take-off velocity to the location of the centre of mass (CoM) and location of the centre of pressure (CoP) at which the ground reaction forces act. The position of the CoM was varied between reasonable lower and upper limits of likely centre of mass locations, informed by literature (Allen et al., 2013). The CoP was varied from the most caudal location on the digits to the most cranial. Most likely conditions which were used in the trajectory analysis are highlighted in red (CoP location 0.0166 m away from the tip of the tarsometatarsus and CoM location (0.051 m cranially and 0.014 m ventrally from the hip centre). Green and orange markers denote conditions in which the take-off velocity was limited by the moment-generating capacity of the knee muscles and the ankle muscles, respectively.

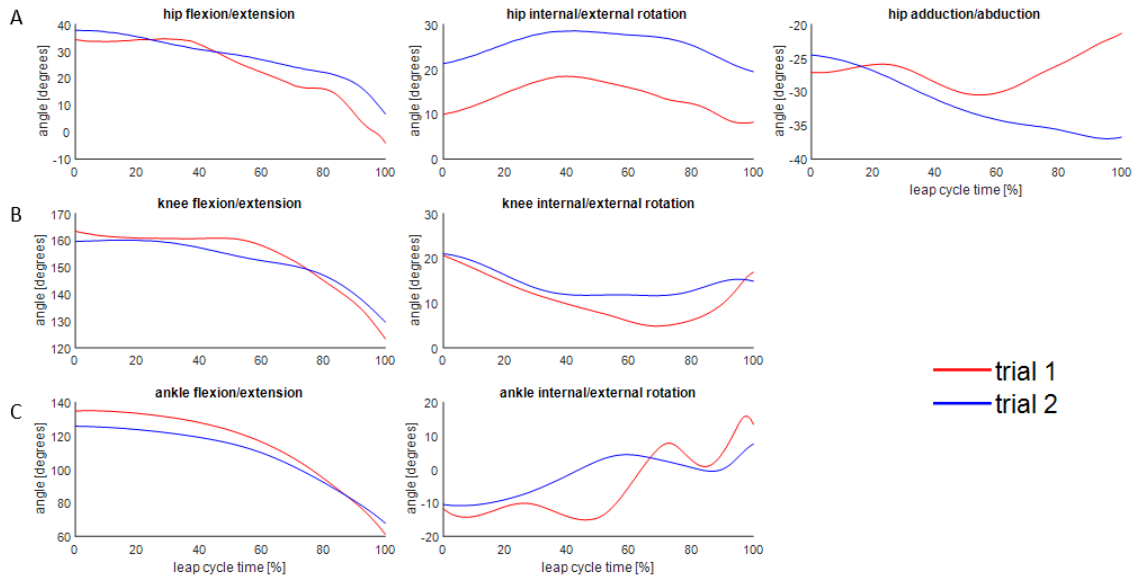

Figure 40 Joint angles at the A) hip, B) knee and C) ankle for 2 take-off trials. Joint angles plotted include flexion/extension (FE), internal/external rotation (IER), abduction/adduction (ABAD), at the hip, as well as FE and IER at the knee and ankle joints. Positive values for FE, ABAD and IER angles are generally extension, adduction, and internal rotation, respectively, except for the knee joint for which positive IER angles denote external rotation. Line colours represent the trial from which the data was derived (red: trial 1; blue: trial 2).

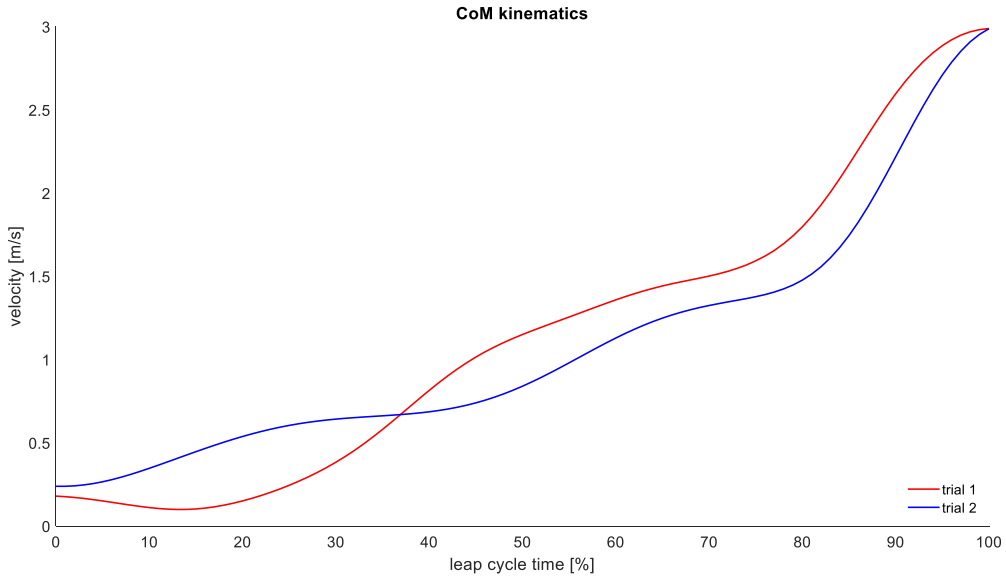

Figure 41 The velocity of the Centre of Mass (CoM) of Archaeopteryx during a take-off leap for two kinematics trials under the most likely conditions for the locations of the CoM and the Centre of Pressure (CoP, the location at which the ground reaction forces act) (see Figure 39). The velocity profiles of both jumps converge to a maximum take-off velocity of 2.98 m/s.

Table 11 Hindlimb segment lengths of Archaeopteryx lithographica and the zebra finch

species	mass [g]	femur length (L_{fem}) [cm]	tibiotarsus length (L_{tib}) [cm]	tarso-metatarsus length (L_{tars}) [cm]	digit III length [cm]	hindlimb length [cm]	hindlimb index ((L_{tars} + L_{tib})/ L_{fem})
Archaeopteryx lithographica	400	6.10	8.07	4.41	4.93	23.51	2.05
zebra finch	15.4	1.40	2.24	1.46	1.10	6.2	2.64

Table 12 M*usculotendon units included in the musculoskeletal model of* Archaeopteryx lithographica, *grouped by the joints they cross. The letters H, K and A denote the hip, knee, and ankle joints, respectively. Muscles which are categorised by two joints are biarticular. The maximum isometric forces were calculated by scaling the maximum isometric force of the corresponding muscles of the magpie (Meilak et al., 2021a; Meilak et al., 2021b) by the relation of* Archaeopteryx *to magpie body mass unless indicated otherwise.*

abbreviation	muscle name	muscle acts at joints	maximum isometric force [N]
ADD1	*M. puboischiofemoralis medialis*	H	11.637
ADD2	*M. puboischiofemoralis lateralis*	H	10.074
AMB**	*M. ambiens*	H, K	2.663
CFB**	*M. caudofemoralis pars pelvica*	H	4.244
CFL	*M. caudofemoralis pars caudalis*	H	4.002
EDL	*M. tibialis cranialis caput femorale and caput tibiale*	K, A	23.384
FB	*M. fibularis brevis*	A	9.503
FDL	*M. flexor digitorum longus*	K, A	26.063
FHL	*M. flexor hallucis longus*	K, A	21.898
FL	*M. fibularis longus*	K, A	22.359
FMTE	*M. femorotibialis lateralis*	K	35.614
FMTI	*M. femorotibialis intermedius*	K	20.708
FTE	*M. flexor cruris lateralis pars pelvica*	H, K	8.984
FTI1*	*M. flexor tibialis internus 1*	H, K	1.793
FTI3	*M. flexor cruris medialis*	H, K	6.188
GL	*M. gastrocnemius (pars) lateralis*	K, A	47.384
GM	*M. gastrocnemius (pars) medialis*	A	29.935
IFE	*M. iliofemoralis externus*	H	5.539
ILFB	*M. iliofibularis*	H, K	11.883
ISTR	*M. ischiofemoralis*	H	20.205
IT1	*M. iliotibialis cranialis 3*	H, K	0.941
IT2A	*M. iliotibialis cranialis 2*	H, K	0.941
IT2P	*M. iliotibialis cranialis 1*	H, K	0.941
IT3	*M. iliotibialis caudalis*	H, K	11.079
ITCA	*M. iliotrochantericus caudalis anterior*	H	15.418
ITCP	*M. iliotrochantericus caudalis posterior*	H	15.418
PIFE1	*M. obturatorius lateralis*	H	2.899
PIFE2	*M. obturatorius medialis*	H	11.189
PIFE3*	*M. puboischiofemoralis externus 3*	H	6.46
PIFI1	*M. iliofemoralis internus*	H	1.109
PIFI2	*M. iliotrochantericus cranialis*	H	3.84

* The maximum isometric forces were scaled by body mass from data for the Nile crocodile (*Crocodylus niloticus*)(Allen et al., 2014)

** The maximum isometric forces of muscles were scaled by body mass from data for the guineafowl (*Numida meleagris*)(Cox et al., 2019)

List of References

Afschrift, M., Van Deursen, R., De Groote, F., and Jonkers, I. (2019). Increased use of stepping strategy in response to medio-lateral perturbations in the elderly relates to altered reactive tibialis anterior activity. *Gait & Posture* 68**,** 575-582.

Ahrens, J., Geveci, B., and Law, C. (2005). Paraview: An end-user tool for large data visualization. *The visualization handbook* 717.

Ait-Haddou, R., Binding, P., and Herzog, W. (2000). Theoretical considerations on cocontraction of sets of agonistic and antagonistic muscles. *J Biomech* 33**,** 1105-1111.

Alerstam, T., Rosén, M., Bäckman, J., Ericson, P.G.P., and Hellgren, O. (2007). Flight Speeds among Bird Species: Allometric and Phylogenetic Effects. *PLOS Biology* 5**,** e197.

Alexander, E.J., and Andriacchi, T.P. (2001). Correcting for deformation in skin-based marker systems. *Journal of Biomechanics* 34**,** 355-361.

Alexander, R.M. (1995). Leg design and jumping technique for humans, other vertebrates and insects. *Philosophical Transactions of the Royal Society of London Series B-Biological Sciences* 347**,** 235-248.

Allen, V., Bates, K.T., Li, Z., and Hutchinson, J.R. (2013). Linking the evolution of body shape and locomotor biomechanics in bird-line archosaurs. *Nature* 497**,** 104-107.

Allen, V., Molnar, J., Parker, W., Pollard, A., Nolan, G., and Hutchinson, J.R. (2014). Comparative architectural properties of limb muscles in Crocodylidae and Alligatoridae and their relevance to divergent use of asymmetrical gaits in extant Crocodylia. *Journal of Anatomy* 225**,** 569-582.

Allen, V.R., Kambic, R.E., Gatesy, S.M., and Hutchinson, J.R. (2017). Gearing effects of the patella (knee extensor muscle sesamoid) of the helmeted guineafowl during terrestrial locomotion. *Journal of Zoology* 303**,** 178-187.

Allen, V.R., Kilbourne, B.M., and Hutchinson, J.R. (2021). The evolution of pelvic limb muscle moment arms in bird-line archosaurs. *Science Advances* 7**,** eabe2778.

Alonso, P.D., Milner, A.C., Ketcham, R.A., Cookson, M.J., and Rowe, T.B. (2004). The avian nature of the brain and inner ear of Archaeopteryx. *Nature* 430**,** 666-669.

Anderson, F.C., and Pandy, M.G. (2001). Dynamic optimization of human walking. *J Biomech Eng* 123**,** 381-390.

Aristidou, A., and Lasenby, J. (2009). Inverse kinematics: a review of existing techniques and introduction of a new fast iterative solver.

Arnold, E., Ward, S., Lieber, R., and Delp, S. (2009). *A Model of the Lower Limb for Analysis of Human Movement.*

Ayachit, U. (2015). *The paraview guide: a parallel visualization application.* Kitware, Inc.

Baier, D.B., Gatesy, S.M., and Dial, K.P. (2013). Three-dimensional, high-resolution skeletal kinematics of the avian wing and shoulder during ascending flapping flight and uphill flap-running. *PLoS One* 8**,** e63982.

Baron, M.G., Norman, D.B., and Barrett, P.M. (2017). A new hypothesis of dinosaur relationships and early dinosaur evolution. *Nature* 543**,** 501.

Bell, P.R., Campione, N.E., Persons, W.S., Currie, P.J., Larson, P.L., Tanke, D.H., and Bakker, R.T. (2017). Tyrannosauroid integument reveals conflicting patterns of gigantism and feather evolution. *Biology Letters* 13**,** 20170092.

Bennett, M.B. (1996). Allometry of the leg muscles of birds. *Journal of Zoology* 238**,** 435-443.

Berg, A.M., and Biewener, A.A. (2010). Wing and body kinematics of takeoff and landing flight in the pigeon (Columba livia). *J Exp Biol* 213**,** 1651-1658.

Bergmann, G., Deuretzbacher, G., Heller, M., Graichen, F., Rohlmann, A., Strauss, J., and Duda, G.N. (2001). Hip contact forces and gait patterns from routine activities. *Journal of Biomechanics* 34**,** 859-871.

Besier, T.F., Sturnieks, D.L., Alderson, J.A., and Lloyd, D.G. (2003). Repeatability of gait data using a functional hip joint centre and a mean helical knee axis. *Journal of Biomechanics* 36**,** 1159-1168.

Bishop, K.L. (2008). The evolution of flight in bats: narrowing the field of plausible hypotheses. *Q Rev Biol* 83**,** 153-169.

Bishop, P.J., Falisse, A., De Groote, F., and Hutchinson, J.R. (2021a). Predictive simulations of musculoskeletal function and jumping performance in a generalized bird. *Integrative Organismal Biology*.

Bishop, P.J., Hocknull, S.A., Clemente, C.J., Hutchinson, J.R., Barrett, R.S., and Lloyd, D.G. (2018a). Cancellous bone and theropod dinosaur locomotion. Part II—a new approach to inferring posture and locomotor biomechanics in extinct tetrapod vertebrates. *PeerJ* 6**,** e5779.

Bishop, P.J., Hocknull, S.A., Clemente, C.J., Hutchinson, J.R., Farke, A.A., Barrett, R.S., and Lloyd, D.G. (2018b). Cancellous bone and theropod dinosaur locomotion. Part III—Inferring posture and locomotor biomechanics in extinct theropods, and its evolution on the line to birds. *PeerJ* 6**,** e5777.

Bishop, P.J., Michel, K.B., Falisse, A., Cuff, A.R., Allen, V.R., De Groote, F., and Hutchinson, J.R. (2021b). Computational modelling of muscle fibre operating ranges in the hindlimb of a small ground bird (Eudromia elegans), with implications for modelling locomotion in extinct species. *PLOS Computational Biology* 17**,** e1008843.

Blemker, S.S., and Delp, S.L. (2005). Three-Dimensional Representation of Complex Muscle Architectures and Geometries. *Annals of Biomedical Engineering* 33**,** 661-673.

Bonser, R., and Rayner, J. (1996). Measuring leg thrust forces in the common starling. *The Journal of Experimental Biology* 199**,** 435-439.

Brainerd, E.L., Baier, D.B., Gatesy, S.M., Hedrick, T.L., Metzger, K.A., Gilbert, S.L., and Crisco, J.J. (2010). X-ray reconstruction of moving morphology (XROMM): precision, accuracy and applications in comparative biomechanics research. *Journal of Experimental Zoology Part A: Ecological Genetics and Physiology* 313A**,** 262-279.

Brand, R.A., Pedersen, D.R., Davy, D.T., Kotzar, G.M., Heiple, K.G., and Goldberg, V.M. (1994). Comparison of hip force calculations and measurements in the same patient. *The Journal of Arthroplasty* 9**,** 45-51.

Brand, R.A., Pedersen, D.R., and Friederich, J.A. (1986). The sensitivity of muscle force predictions to changes in physiologic cross-sectional area. *Journal of Biomechanics* 19**,** 589-596.

Brown, N.P., Bertocci, G.E., Cheffer, K.A., and Howland, D.R. (2018). A three dimensional multiplane kinematic model for bilateral hind limb gait analysis in cats. *PLOS ONE* 13**,** e0197837.

Brusatte, S.L. (2017). Evolution: Uprooting the Dinosaur Family Tree. *Current Biology* 27**,** R390-R392.

Brusatte, Stephen l., Lloyd, Graeme t., Wang, Steve c., and Norell, Mark a. (2014). Gradual Assembly of Avian Body Plan Culminated in Rapid Rates of Evolution across the Dinosaur-Bird Transition. *Current Biology* 24**,** 2386-2392.

Brusatte, S.L., O'connor, J.K., and Jarvis, E.D. (2015). The Origin and Diversification of Birds. *Current Biology* 25**,** R888-R898.

Burgers, P., and Chiappe, L.M. (1999). The wing of Archaeopteryx as a primary thrust generator. *Nature* 399**,** 60.

Byström, A., Hardeman, A.M., Serra Bragança, F.M., Roepstorff, L., Swagemakers, J.H., Van Weeren, P.R., and Egenvall, A. (2021). Differences in equine spinal kinematics between straight line and circle in trot. *Sci Rep* 11**,** 12832.

Cahouët, V., Luc, M., and David, A. (2002). Static optimal estimation of joint accelerations for inverse dynamics problem solution. *Journal of Biomechanics* 35**,** 1507-1513.

Calvert, J.R., and Farrar, R. (2008). *An engineering data book.* Macmillan International Higher Education.

Caple, G., Balda, R.P., and Willis, W.R. (1983). The physics of leaping animals and the evolution of preflight. *The American Naturalist* 121**,** 455-476.

Cappozzo, A., Catani, F., Leardini, A., Benedetti, M.G., and Della Croce, U. (1996). Position and orientation in space of bones during movement: experimental artefacts. *Clinical Biomechanics* 11**,** 90-100.

Carr, J.A., Ellerby, D.J., and Marsh, R.L. (2011). Function of a large biarticular hip and knee extensor during walking and running in guinea fowl (Numida meleagris). *The Journal of Experimental Biology* 214**,** 3405.

Carrano, M.T. (1998). Locomotion in Non-Avian Dinosaurs: Integrating Data from Hindlimb Kinematics, in Vivo Strains, and Bone Morphology. *Paleobiology* 24**,** 450-469.

Carrano, M.T., and Hutchinson, J.R. (2002). Pelvic and hindlimb musculature of Tyrannosaurus rex (Dinosauria: Theropoda). *Journal of Morphology* 253**,** 207-228.

Carril, J., Mosto, M.C., Picasso, M.B.J., and Tambussi, C.P. (2014). Hindlimb myology of the monk parakeet (Aves, Psittaciformes). *Journal of Morphology* 275**,** 732-744.

Challis, J.H. (1997). Producing physiologically realistic individual muscle force estimations by imposing constraints when using optimization techniques. *Med Eng Phys* 19**,** 253-261.

Chao, E.Y.-S., and Rim, K. (1973). Application of optimization principles in determining the applied moments in human leg joints during gait. *Journal of Biomechanics* 6**,** 497-510.

Charles, J.P., Cappellari, O., and Hutchinson, J.R. (2018). A Dynamic Simulation of Musculoskeletal Function in the Mouse Hindlimb During Trotting Locomotion. *Frontiers in Bioengineering and Biotechnology* 6.

Charles, J.P., Cappellari, O., Spence, A.J., Wells, D.J., and Hutchinson, J.R. (2016). Muscle moment arms and sensitivity analysis of a mouse hindlimb musculoskeletal model. *Journal of Anatomy* 229**,** 514-535.

Chatterjee, S., and Templin, R.J. (2003). The flight of Archaeopteryx. *Naturwissenschaften* 90**,** 27-32.

Chen, P.-J., Dong, Z.-M., and Zhen, S.-N. (1998). An exceptionally well-preserved theropod dinosaur from the Yixian Formation of China. *Nature* 391**,** 147-152.

Chen, X., Jia, P., Wang, Y., Zhang, H., Wang, L., Frangi, A.F., and Taylor, Z.A. (2018). A surface-based approach to determine key spatial parameters of the acetabulum in a standardized pelvic coordinate system. *Medical Engineering & Physics* 52**,** 22-30.

Chiappe, L.M. (2009). Downsized Dinosaurs: The Evolutionary Transition to Modern Birds. *Evolution: Education and Outreach* 2**,** 248-256.

Chin, D.D., and Lentink, D. (2017). How birds direct impulse to minimize the energetic cost of foraging flight. *Science Advances* 3.

Correa, T.A., Crossley, K.M., Kim, H.J., and Pandy, M.G. (2010). Contributions of individual muscles to hip joint contact force in normal walking. *Journal of Biomechanics* 43**,** 1618-1622.

Courty, N., and Arnaud, E. (Year). "Inverse Kinematics Using Sequential Monte Carlo Methods", in: *Articulated Motion and Deformable Objects*, eds. F.J. Perales & R.B. Fisher: Springer Berlin Heidelberg), 1-10.

Cowen, R., and Lipps, J.H. (Year). "An adaptive scenario for the origin of birds and of flight in birds", in: *Proceedings of the Third North American Paleontological Convention*), 109-112.

Cox, S.M., Easton, K.L., Lear, M.C., Marsh, R.L., Delp, S.L., and Rubenson, J. (2019). The Interaction of Compliance and Activation on the Force-Length Operating Range and Force Generating Capacity of Skeletal Muscle: A Computational Study using a Guinea Fowl Musculoskeletal Model. *Integrative Organismal Biology* 1.

Crowninshield, R.D. (1978). Use of Optimization Techniques to Predict Muscle Forces. *Journal of Biomechanical Engineering* 100**,** 88-92.

Currey, J.D. (2012). The structure and mechanics of bone. *Journal of Materials Science* 47**,** 41-54.

Daley, M.A., and Biewener, A.A. (2003). Muscle force-length dynamics during level versus incline locomotion: a comparison of in vivo performance of two guinea fowl ankle extensors. *Journal of Experimental Biology* 206**,** 2941-2958.

Daley Monica, A., and Biewener Andrew, A. (2011). Leg muscles that mediate stability: mechanics and control of two distal extensor muscles during obstacle negotiation in the guinea fowl. *Philosophical Transactions of the Royal Society B: Biological Sciences* 366**,** 1580-1591.

Darwin, C. (1859). On the origin of the species by natural selection.

Delp, S.L., Anderson, F.C., Arnold, A.S., Loan, P., Habib, A., John, C.T., Guendelman, E., and Thelen, D.G. (2007). OpenSim: open-source software to create and analyze dynamic simulations of movement. *IEEE Trans Biomed Eng* 54**,** 1940-1950.

Delp, S.L., and Loan, J.P. (2000). A computational framework for simulating and analyzing human and animal movement. *Computing in Science & Engineering* 2**,** 46-55.

Delp, S.L., Loan, J.P., Hoy, M.G., Zajac, F.E., Topp, E.L., Rosen, J.M., Thelen, D.G., Anderson, F.C., and Seth, A. "Gait 2354, 3D, 23 DOF gait model". 30000 ed.).

Descamps, E., Sochacka, A., De Kegel, B., Van Loo, D., Van Hoorebeke, L., and Adriaens, D. (2014). Soft tissue discrimination with contrast agents using micro-CT scanning. *BELGIAN JOURNAL OF ZOOLOGY* 144**,** 20-40.

Dial, K.P. (2003). Wing-Assisted Incline Running and the Evolution of Flight. *Science* 299**,** 402-404.

Dial, K.P., Jackson, B.E., and Segre, P. (2008). A fundamental avian wing-stroke provides a new perspective on the evolution of flight. *Nature* 451**,** 985-989.

Doube, M., Yen, S.C., Klosowski, M.M., Farke, A.A., Hutchinson, J.R., and Shefelbine, S.J. (2012). Whole-bone scaling of the avian pelvic limb. *J Anat* 221**,** 21-29.

Duda, G.N., Brand, D., Freitag, S., Lierse, W., and Schneider, E. (1996). Variability of femoral muscle attachments. *Journal of Biomechanics* 29**,** 1185-1190.

Duda, G.N., Eckert-Hübner, K., Sokiranski, R., Kreutner, A., Miller, R., and Claes, L. (1997a). Analysis of inter-fragmentary movement as a function of musculoskeletal loading conditions in sheep. *Journal of Biomechanics* 31**,** 201-210.

Duda, G.N., Heller, M., Albinger, J., Schulz, O., Schneider, E., and Claes, L. (1998). Influence of muscle forces on femoral strain distribution. *J Biomech* 31**,** 841-846.

Duda, G.N., Schneider, E., and Chao, E.Y.S. (1997b). Internal forces and moments in the femur during walking. *Journal of Biomechanics* 30**,** 933-941.

Dul, J., Johnson, G.E., Shiavi, R., and Townsend, M.A. (1984). Muscular synergism--II. A minimum-fatigue criterion for load sharing between synergistic muscles. *J Biomech* 17**,** 675-684.

Dyke, G., De Kat, R., Palmer, C., Van Der Kindere, J., Naish, D., and Ganapathisubramani, B. (2013). Aerodynamic performance of the feathered dinosaur Microraptor and the evolution of feathered flight. *Nature Communications* 4**,** 9pp.

Earls, K.D. (2000). Kinematics and mechanics of ground take-off in the starling Sturnis vulgaris and the quail Coturnix coturnix. *Journal of Experimental Biology* 203**,** 725-739.

Ehrig, R.M., and Heller, M.O. (2019). On intrinsic equivalences of the finite helical axis, the instantaneous helical axis, and the SARA approach. A mathematical perspective. *Journal of Biomechanics* 84**,** 4-10.

Ehrig, R.M., Taylor, W.R., Duda, G.N., and Heller, M.O. (2006). A survey of formal methods for determining the centre of rotation of ball joints. *Journal of Biomechanics* 39**,** 2798-2809.

Ehrig, R.M., Taylor, W.R., Duda, G.N., and Heller, M.O. (2007). A survey of formal methods for determining functional joint axes. *Journal of Biomechanics* 40**,** 2150-2157.

Erdemir, A., Mclean, S., Herzog, W., and Van Den Bogert, A.J. (2007). Model-based estimation of muscle forces exerted during movements. *Clinical Biomechanics* 22**,** 131-154.

Fedorov, A., Beichel, R., Kalpathy-Cramer, J., Finet, J., Fillion-Robin, J.-C., Pujol, S., Bauer, C., Jennings, D., Fennessy, F., Sonka, M., Buatti, J., Aylward, S., Miller, J.V., Pieper, S., and Kikinis, R. (2012). 3D Slicer as an image computing platform for the Quantitative Imaging Network. *Magnetic resonance imaging* 30**,** 1323-1341.

Field, D.J., Bercovici, A., Berv, J.S., Dunn, R., Fastovsky, D.E., Lyson, T.R., Vajda, V., and Gauthier, J.A. (2018). Early Evolution of Modern Birds Structured by Global Forest Collapse at the End-Cretaceous Mass Extinction. *Current Biology*.

Fletcher, R. (2013). *Practical methods of optimization.* John Wiley & Sons.

Forbes, A.B. (1989). Least-squares best-fit geometric elements. NPL Report DITC 140/89. *DOI: https://doi. org/10.1007/978-1-4899-3422_028*.

Foth, C., Tischlinger, H., and Rauhut, O.W.M. (2014). New specimen of Archaeopteryx provides insights into the evolution of pennaceous feathers. *Nature* 511**,** 79.

Frankel, V.H., and Nordin, M. (2001). *Basic biomechanics of the musculoskeletal system.* Philadelphia : Lippincott Williams & Wilkins.

Gangl, D., Weissengruber, G.E., Egerbacher, M., and Forstenpointner, G. (2004). Anatomical Description of the Muscles of the Pelvic Limb in the Ostrich (Struthio camelus). *Anatomia, Histologia, Embryologia* 33**,** 100-114.

Garner, J.P., Taylor, G.K., and Thomas, A.L.R. (1999). On the origins of birds: the sequence of character acquisition in the evolution of avian flight. *Proceedings of the Royal Society B-Biological Sciences* 266**,** 1259-1266.

Gatesy, S., and Biewener, A. (1991). Bipedal locomotion: effects of speed, size and limb posture in birds and humans. *Journal of Zoology* 224**,** 127-147.

Gatesy, S.M., Baier, D.B., Jenkins, F.A., and Dial, K.P. (2010). Scientific rotoscoping: a morphology-based method of 3-D motion analysis and visualization. *Journal of Experimental Zoology Part A: Ecological Genetics and Physiology* 313A**,** 244-261.

Gatesy, S.M., and Middleton, K.M. (1997). Bipedalism, flight, and the evolution of theropod locomotor diversity. *Journal of Vertebrate Paleontology* 17**,** 308-329.

Gignac, P.M., and Kley, N.J. (2014). Iodine-enhanced micro-CT imaging: Methodological refinements for the study of the soft-tissue anatomy of post-embryonic vertebrates. *Journal of Experimental Zoology Part B: Molecular and Developmental Evolution* 322**,** 166-176.

Glitsch, U., and Baumann, W. (1997). The three-dimensional determination of internal loads in the lower extremity. *J Biomech* 30**,** 1123-1131.

Godefroit, P., Cau, A., Dong-Yu, H., Escuillié, F., Wenhao, W., and Dyke, G. (2013). A Jurassic avialan dinosaur from China resolves the early phylogenetic history of birds. *Nature* 498**,** 359-362.

Goetz, J.E., Derrick, T.R., Pedersen, D.R., Robinson, D.A., Conzemius, M.G., Baer, T.E., and Brown, T.D. (2008). Hip joint contact force in the emu (Dromaius novaehollandiae) during normal level walking. *J Biomech* 41**,** 770-778.

Gregory, S. (1998). Limb design function and running performance in ostrich-mimics and tyrannosaurus.

Grochow, K., Martin, S.L., Hertzmann, A., Popovi, Z., and #263 (2004). Style-based inverse kinematics. *ACM Trans. Graph.* 23**,** 522-531.

Hall, S.J. (2007). Basic biomechanics.

Hayes, G., and Alexander, R.M. (1983). The hopping gaits of crows (Corvidae) and other bipeds. *Journal of Zoology* 200**,** 205-213.

Heers, A.M. (2013). "Evolution of Avian Flight," in *eLS*.).

Heers, A.M., Rankin, J.W., and Hutchinson, J.R. (2018). Building a Bird: Musculoskeletal Modeling and Simulation of Wing-Assisted Incline Running During Avian Ontogeny. *Frontiers in bioengineering and biotechnology* 6.

Hege, H.-C., Seebass, M., Stalling, D., and Zöckler, M. (1997). "A Generalized Marching Cubes Algorithm Based on Non-Binary Classifications".).

Heintz, S., and Gutierrez-Farewik, E.M. (2007). Static optimization of muscle forces during gait in comparison to EMG-to-force processing approach. *Gait Posture* 26**,** 279-288.

Helgason, B., Taddei, F., Pálsson, H., Schileo, E., Cristofolini, L., Viceconti, M., and Brynjólfsson, S. (2008). A modified method for assigning material properties to FE models of bones. *Medical Engineering & Physics* 30**,** 444-453.

Heller, M.O., Bergmann, G., Deuretzbacher, G., Claes, L., Haas, N.P., and Duda, G.N. (2001a). Influence of femoral anteversion on proximal femoral loading: measurement and simulation in four patients. *Clinical Biomechanics* 16**,** 644-649.

Heller, M.O., Bergmann, G., Deuretzbacher, G., Dürselen, L., Pohl, M., Claes, L., Haas, N.P., and Duda, G.N. (2001b). Musculo-skeletal loading conditions at the hip during walking and stair climbing. *Journal of Biomechanics* 34**,** 883-893.

Heller, M.O., Bergmann, G., Kassi, J.P., Claes, L., Haas, N.P., and Duda, G.N. (2005). Determination of muscle loading at the hip joint for use in pre-clinical testing. *Journal of Biomechanics* 38**,** 1155-1163.

Heller, M.O., Taylor, W.R., Perka, C., and Duda, G.N. (2003). The influence of alignment on the musculo-skeletal loading conditions at the knee. *Langenbeck's Archives of Surgery* 388**,** 291-297.

Henningsson, P., and Hedenström, A. (2011). Aerodynamics of gliding flight in common swifts. *Journal of Experimental Biology* 214**,** 382-393.

Henry, H.T., Ellerby, D.J., and Marsh, R.L. (2005). Performance of guinea fowl Numida meleagris during jumping requires storage and release of elastic energy. *J Exp Biol* 208**,** 3293-3302.

Heppner, F.H., and Anderson, J.G.T. (1985). Leg Thrust Important in Flight Take-Off in the Pigeon. *Journal of Experimental Biology* 114**,** 285-288.

Herzog, W., and Binding, P. (1993). Cocontraction of pairs of antagonistic muscles: analytical solution for planar static nonlinear optimization approaches. *Math Biosci* 118**,** 83-95.

Higham, T.E., and Biewener, A.A. (2011). Functional and architectural complexity within and between muscles: regional variation and intermuscular force transmission. *Philos Trans R Soc Lond B Biol Sci* 366**,** 1477-1487.

Higham, T.E., Biewener, A.A., and Wakeling, J.M. (2008). Functional diversification within and between muscle synergists during locomotion. *Biology Letters* 4**,** 41-44.

Holtz, T.R. (1996). Phylogenetic taxonomy of the Coelurosauria (Dinosauria: Theropoda). *Journal of Paleontology* 70**,** 536-538.

Hudson, G.E. (1937). Studies on the Muscles of the Pelvic Appendage in Birds. *The American Midland Naturalist* 18**,** 1-108.

Hutchinson, J.R. (2001). The evolution of pelvic osteology and soft tissues on the line to extant birds (Neornithes). *Zoological Journal of the Linnean Society* 131**,** 123-168.

Hutchinson, J.R. (2004a). Biomechanical modeling and sensitivity analysis of bipedal running ability. I. Extant taxa. *Journal of Morphology* 262**,** 421-440.

Hutchinson, J.R. (2004b). Biomechanical modeling and sensitivity analysis of bipedal running ability. II. Extinct taxa. *J Morphol* 262**,** 441-461.

Hutchinson, J.R., and Allen, V. (2009). The evolutionary continuum of limb function from early theropods to birds. *Naturwissenschaften* 96**,** 423-448.

Hutchinson, J.R., Anderson, F.C., Blemker, S.S., and Delp, S.L. (2005). Analysis of hindlimb muscle moment arms in Tyrannosaurus rex using a three-dimensional musculoskeletal computer model: implications for stance, gait, and speed. *Paleobiology* 31**,** 676-701.

Hutchinson, J.R., Ng-Thow-Hing, V., and Anderson, F.C. (2007). A 3D interactive method for estimating body segmental parameters in animals: Application to the turning and running performance of Tyrannosaurus rex. *Journal of Theoretical Biology* 246**,** 660-680.

Hutchinson, J.R., Rankin, J., Rubenson, J., Rosenbluth, K.H., Siston, R.A., and Delp, S.L. (2015). Musculoskeletal modelling of an ostrich (Struthio camelus) pelvic limb: influence of limb orientation on muscular capacity during locomotion. *Peerj* 3**,** 52.

Huxley, T.H. (1868). I. Remarks upon *Archaeopteryx lithographica*. *Proceedings of the Royal Society of London* 16**,** 243-248.

Jarvis, E.D., Mirarab, S., Aberer, A.J., Li, B., Houde, P., Li, C., Ho, S.Y.W., Faircloth, B.C., Nabholz, B., Howard, J.T., Suh, A., Weber, C.C., Da Fonseca, R.R., Li, J., Zhang, F., Li, H., Zhou, L., Narula, N., Liu, L., Ganapathy, G., Boussau, B., Bayzid, M.S., Zavidovych, V., Subramanian, S., Gabaldón, T., Capella-Gutiérrez, S., Huerta-Cepas, J., Rekepalli, B., Munch, K., Schierup, M., Lindow, B., Warren, W.C., Ray, D., Green, R.E., Bruford, M.W., Zhan, X., Dixon, A., Li, S., Li, N., Huang, Y., Derryberry, E.P., Bertelsen, M.F., Sheldon, F.H., Brumfield, R.T., Mello, C.V., Lovell, P.V., Wirthlin, M., Schneider, M.P.C., Prosdocimi, F., Samaniego, J.A., Velazquez, A.M.V., Alfaro-Núñez, A., Campos, P.F., Petersen, B., Sicheritz-Ponten, T., Pas, A., Bailey, T., Scofield, P., Bunce, M., Lambert, D.M., Zhou, Q., Perelman, P., Driskell, A.C., Shapiro, B., Xiong, Z., Zeng, Y., Liu, S., Li, Z., Liu, B., Wu, K., Xiao, J., Yinqi, X., Zheng, Q., Zhang, Y., Yang, H., Wang, J., Smeds, L., Rheindt, F.E., Braun, M., Fjeldsa, J., Orlando, L., Barker, F.K., Jønsson, K.A., Johnson, W., Koepfli, K.-P., O'brien, S., Haussler, D., Ryder, O.A., Rahbek, C., Willerslev, E., Graves, G.R., Glenn, T.C., Mccormack, J., Burt, D., Ellegren, H., Alström, P., Edwards, S.V., Stamatakis, A., Mindell, D.P., Cracraft, J., et al. (2014). Whole-genome analyses resolve early branches in the tree of life of modern birds. *Science* 346**,** 1320-1331.

Jensen, R.H., and Davy, D.T. (1975). An investigation of muscle lines of action about the hip: A centroid line approach vs the straight line approach. *Journal of Biomechanics* 8**,** 103-110.

Jinha, A., Ait-Haddou, R., Binding, P., and Herzog, W. (2006a). Antagonistic activity of one-joint muscles in three-dimensions using non-linear optimisation. *Math Biosci* 202**,** 57-70.

Jinha, A., Ait-Haddou, R., and Herzog, W. (2006b). Predictions of co-contraction depend critically on degrees-of-freedom in the musculoskeletal model. *J Biomech* 39**,** 1145-1152.

Jolliffe, I. (2011). "Principal Component Analysis," in *International Encyclopedia of Statistical Science,* ed. M. Lovric. (Berlin, Heidelberg: Springer Berlin Heidelberg), 1094-1096.

Kambic, R.E., Roberts, T.J., and Gatesy, S.M. (2014). Long-axis rotation: a missing degree of freedom in avian bipedal locomotion. *J Exp Biol* 217**,** 2770-2782.

Kambic, R.E., Roberts, T.J., and Gatesy, S.M. (2017). 3-D range of motion envelopes reveal interacting degrees of freedom in avian hind limb joints. *Journal of Anatomy* 231**,** 906-920.

Kaufman, K.R., An, K.N., Litchy, W.J., and Chao, E.Y. (1991). Physiological prediction of muscle forces--II. Application to isokinetic exercise. *Neuroscience* 40**,** 793-804.

Kilbourne, B.M. (2014). Scale effects and morphological diversification in hindlimb segment mass proportions in neognath birds. *Frontiers in zoology* 11**,** 37-37.

Kilbourne, B.M., Andrada, E., Fischer, M.S., and Nyakatura, J.A. (2016). Morphology and motion: hindlimb proportions and swing phase kinematics in terrestrially locomoting charadriiform birds. *J Exp Biol* 219**,** 1405-1416.

Klein Heerenbrink, M., Johansson, L.C., and Hedenström, A. (2015). Power of the wingbeat: modelling the effects of flapping wings in vertebrate flight. *Proceedings of the Royal Society A: Mathematical, Physical and Engineering Sciences* 471**,** 20140952.

Koschowitz, M.-C., Fischer, C., and Sander, M. (2014). Beyond the rainbow. *Science* 346**,** 416-418.

Kutzner, I., Küther, S., Heinlein, B., Dymke, J., Bender, A., Halder, A.M., and Bergmann, G. (2011). The effect of valgus braces on medial compartment load of the knee joint – in vivo load measurements in three subjects. *Journal of Biomechanics* 44**,** 1354-1360.

Kwan Wu, C., Konsky, B.R.V., and Marriott, A. (Year). "Closed-form and generalized inverse kinematics solutions for the analysis of human motion", in: *Proceedings of the 19th Annual International Conference of the IEEE Engineering in Medicine and Biology Society. 'Magnificent Milestones and Emerging Opportunities in Medical Engineering' (Cat. No.97CH36136)*), 1911-1914 vol.1915.

Kwon, Y.H. (2018). *Kwon3D* [Online]. Available: http://www.kwon3d.com/ [Accessed 2018].

Landis, E.N., and Keane, D.T. (2010). X-ray microtomography. *Materials Characterization* 61**,** 1305-1316.

Lebrun, R. (Year). "MorphoDig, an open-source 3D freeware dedicated to biology").

Lee, S.J., Witter, M.S., Cuthill, I.C., and Goldsmith, A.R. (1996). Reduction in Escape Performance as a Cost of Reproduction in Gravid Starlings, Sturnus vulgaris. *Proceedings of the Royal Society B: Biological Sciences* 263**,** 619-623.

Lentink, D., Müller, U.K., Stamhuis, E.J., De Kat, R., Van Gestel, W., Veldhuis, L.L.M., Henningsson, P., Hedenström, A., Videler, J.J., and Van Leeuwen, J.L. (2007). How swifts control their glide performance with morphing wings. *Nature* 446**,** 1082-1085.

Long, C.A., Zhang, G.P., George, T.F., and Long, C.F. (2003). Physical theory, origin of flight, and a synthesis proposed for birds. *Journal of Theoretical Biology* 224**,** 9-26.

Longrich, N. (2006). Structure and function of hindlimb feathers in Archaeopteryx lithographica. *Paleobiology* 32**,** 417-431.

Lu, M., Lin, C.C., Lu, T.W., Wang, S.N., and Wu, C.H. (2020). Effects of soft tissue artefacts on computed segmental and stifle kinematics in canine motion analysis. *Vet Rec* 186**,** 66.

Lund, K., and Hicks, J. (2012a). *Getting Started with Inverse Dynamics* [Online]. Available: http://simtk-confluence.stanford.edu:8080/display/OpenSim/Getting+Started+with+Inverse+Dynamics [Accessed 14/10/2015 2015].

Lund, K., and Hicks, J. (2012b). *Getting Started with Inverse Kinematics* [Online]. Available: https://simtk-confluence.stanford.edu/display/OpenSim/Getting+Started+with+Inverse+Kinematics [Accessed 17/05/2018 2018].

Lund, K., and Hicks, J. (2015). *Getting Started with Static Optimization* [Online]. Available: http://simtk-confluence.stanford.edu:8080/display/OpenSim/Getting+Started+with+Static+Optimization [Accessed 14/10/2015 2015].

Manafzadeh, A.R., and Padian, K. (2018). ROM mapping of ligamentous constraints on avian hip mobility: implications for extinct ornithodirans. *Proceedings of the Royal Society B: Biological Sciences* 285.

Manal, K., and Buchanan, T.S. (2004). Subject-specific estimates of tendon slack length: a numerical method. *Journal of Applied Biomechanics* 20**,** 195-203.

Manu (2021a). nonrigidICP. *MATLAB Central File Exchange*.

Manu (2021b). Rigid ICP registration. *MATLAB Central File Exchange*.

Marieswaran, M., Sikidar, A., Goel, A., Joshi, D., and Kalyanasundaram, D. (2018). An extended OpenSim knee model for analysis of strains of connective tissues. *BioMedical Engineering OnLine* 17**,** 42.

Martyniuk, M.P. (2012). *A field guide to Mesozoic birds and other winged dinosaurs.* Pan Aves.

Mayr, G. (2016). Variations in the hypotarsus morphology of birds and their evolutionary significance. *Acta Zoologica* 97**,** 196-210.

Mayr, G. (2017). Pectoral girdle morphology of Mesozoic birds and the evolution of the avian supracoracoideus muscle. *Journal of Ornithology* 158**,** 859-867.

Mayr, G., Pohl, B., and Peters, D.S. (2005). A Well-Preserved Archaeopteryx Specimen with Theropod Features. *Science* 310**,** 1483-1486.

Mckitrick, M.C. (1991). Phylogenetic analysis of avian hindlimb musculature.

Mcneel, R. (2020). Rhinoceros 3D, Version 4.0. *Robert McNeel & Associates, Seattle, WA*.

Meilak, E.A., Gostling, N.J., Palmer, C., and Heller, M.O. (2021a). On the 3D Nature of the Magpie (Aves: Pica pica) Functional Hindlimb Anatomy During the Take-Off Jump. *Frontiers in Bioengineering and Biotechnology* 9.

Meilak, E.A., Provini, P., Palmer, C., Gostling, N.J., and Heller, M.O. (2021b). On the hindlimb biomechanics of the avian take-off leap. *bioRxiv***,** 2021.2011.2019.469279.

Möbius, J., and Kobbelt, L. (Year). "OpenFlipper: An Open Source Geometry Processing and Rendering Framework", in: *Curves and Surfaces*, eds. J.-D. Boissonnat, P. Chenin, A.

Cohen, C. Gout, T. Lyche, M.-L. Mazure & L. Schumaker: Springer Berlin Heidelberg), 488-500.

Modenese, L., Ceseracciu, E., Reggiani, M., and Lloyd, D.G. (2016). Estimation of musculotendon parameters for scaled and subject specific musculoskeletal models using an optimization technique. *Journal of Biomechanics* 49**,** 141-148.

Modenese, L., and Kohout, J. (2020). Automated Generation of Three-Dimensional Complex Muscle Geometries for Use in Personalised Musculoskeletal Models. *Annals of Biomedical Engineering* 48**,** 1793-1804.

Monti, R.J., Roy, R.R., and Edgerton, V.R. (2001). Role of motor unit structure in defining function. *Muscle & Nerve* 24**,** 848-866.

Mow, V.C., and Huiskes, R. (2005). *Basic orthopaedic biomechanics & mechano-biology.* Lippincott Williams & Wilkins.

Murray, W.M., Delp, S.L., and Buchanan, T.S. (1995). Variation of muscle moment arms with elbow and forearm position. *Journal of Biomechanics* 28**,** 513-525.

Nelson, F.E., Gabaldón, A.M., and Roberts, T.J. (2004). Force–velocity properties of two avian hindlimb muscles. *Comparative Biochemistry and Physiology Part A: Molecular & Integrative Physiology* 137**,** 711-721.

Nigg, B.M., Macintosh, B.R., and Mester, J. (2000). *Biomechanics and biology of movement.* Human Kinetics.

Norberg, U.M. (1985). Evolution of flight in birds: Aerodynamic, mechanical and ecological aspects. *Major Patterns in Vertebrate Evolution***,** 293-302.

Nudds, R.L., and Dyke, G.J. (2010). Narrow Primary Feather Rachises in Confuciusornis and Archaeopteryx Suggest Poor Flight Ability. *Science* 328**,** 887-889.

O'neill, M.C., Lee, L.-F., Larson, S.G., Demes, B., Stern, J.T., and Umberger, B.R. (2013). A three-dimensional musculoskeletal model of the chimpanzee (Pan troglodytes) pelvis and hind limb. *The Journal of Experimental Biology* 216**,** 3709-3723.

Olson, S.L., and Feduccia, A. (1979). Flight capability and the pectoral girdle of Archaeopteryx. *Nature* 278**,** 247-248.

Ostrom, J.H. (1976). Archaeopteryx and the origin of birds. *Biological Journal of the Linnean Society* 8**,** 91-182.

Otero, A., Allen, V., Pol, D., and Hutchinson, J.R. (2017). Forelimb muscle and joint actions in Archosauria: insights from Crocodylus johnstoni (Pseudosuchia) and Mussaurus patagonicus (Sauropodomorpha). *PeerJ* 5**,** e3976.

Padian, K. (1982). Running, Leaping, Lifting Off. *The Sciences* 22**,** 10-15.

Padian, K. (1985). The origins and aerodynamics of flight in extinct vertebrates. *Palaeontology* 28**,** 413-433.

Padian, K. (2001). Stages in the origin of bird flight: beyond the arboreal-cursorial dichotomy. *New perspectives on the origin and early evolution of birds***,** 255-272.

Padian, K., and Chiappe, L.M. (1998). The origin and early evolution of birds. *Biological Reviews* 73**,** 1-42.

Palmer, C. (2014). The aerodynamics of gliding flight and its application to the arboreal flight of the Chinese feathered dinosaur Microraptor. *Biological Journal of the Linnean Society* 113**,** 828-835.

Parslew, B., Sivalingam, G., and Crowther, W. (2018). A dynamics and stability framework for avian jumping take-off. *Royal Society Open Science* 5**,** 181544.

Paul, G.S. (2010). Comment on “Narrow Primary Feather Rachises in Confuciusornis and Archaeopteryx Suggest Poor Flight Ability”. *Science* 330**,** 320-320.

Perillo-Marcone, A., and Taylor, M. (2006). Effect of Varus/Valgus Malalignment on Bone Strains in the Proximal Tibia After TKR: An Explicit Finite Element Study. *Journal of Biomechanical Engineering* 129**,** 1-11.

Peters, D.S. (2002). Anagenesis of early birds reconsidered. *Senckenbergiana lethaea* 82**,** 347-354.

Pfister, A., West, A.M., Bronner, S., and Noah, J.A. (2014). Comparative abilities of Microsoft Kinect and Vicon 3D motion capture for gait analysis. *Journal of Medical Engineering & Technology* 38**,** 274-280.

Pilcher, H. (2004). Flying dinosaur had 'bird brain'. *Nature*.

Pizzolato, C., Reggiani, M., Modenese, L., and Lloyd, D.G. (2017). Real-time inverse kinematics and inverse dynamics for lower limb applications using OpenSim. *Computer methods in biomechanics and biomedical engineering* 20**,** 436-445.

Poore, S.O., Sánchez-Haiman, A., and Goslow, G.E. (1997). Wing upstroke and the evolution of flapping flight. *Nature* 387**,** 799-802.

Prilutsky, B.I., Herzog, W., and Allinger, T.L. (1997). Forces of individual cat ankle extensor muscles during locomotion predicted using static optimization. *J Biomech* 30**,** 1025-1033.

Provini, P. (2021) Personal Communication.

Provini, P., and Abourachid, A. (2018). Whole-body 3D kinematics of bird take-off: key role of the legs to propel the trunk. *The Science of Nature* 105**,** 12.

Provini, P., Tobalske, B.W., Crandell, K.E., and Abourachid, A. (2012). Transition from leg to wing forces during take-off in birds. *J Exp Biol* 215**,** 4115-4124.

Prum, R.O., Berv, J.S., Dornburg, A., Field, D.J., Townsend, J.P., Lemmon, E.M., and Lemmon, A.R. (2015). A comprehensive phylogeny of birds (Aves) using targeted next-generation DNA sequencing. *Nature* 526**,** 569.

Raikow, R.J. (1987). Hindlimb Myology and Evolution of the Old World Suboscine Passerine Birds (Acanthisittidae, Pittidae, Philepittidae, Eurylaimidae). *Ornithological Monographs***,** iii-81.

Rankin, J.W., Rubenson, J., and Hutchinson, J.R. (2016). Inferring muscle functional roles of the ostrich pelvic limb during walking and running using computer optimization. *Journal of The Royal Society Interface* 13.

Rauhut, O.W.M., Foth, C., and Tischlinger, H. (2018). The oldest Archaeopteryx (Theropoda: Avialiae): a new specimen from the Kimmeridgian/Tithonian boundary of Schamhaupten, Bavaria. *PeerJ* 6**,** e4191.

Rayner, J.M.V. (1988). The evolution of vertebrate flight. *Biological Journal of the Linnean Society* 34**,** 269-287.

Richards, H.L., Bishop, P.J., Hocking, D.P., Adams, J.W., and Evans, A.R. (2021). Low elbow mobility indicates unique forelimb posture and function in a giant extinct marsupial. *Journal of Anatomy* 238**,** 1425-1441.

Ricklefs, R.E. (2012). Species richness and morphological diversity of passerine birds. *Proceedings of the National Academy of Sciences* 109**,** 14482.

Rode, C., Sutedja, Y., Kilbourne, B.M., Blickhan, R., and Andrada, E. (2016). Minimizing the cost of locomotion with inclined trunk predicts crouched leg kinematics of small birds at realistic levels of elastic recoil. *Journal of Experimental Biology* 219**,** 485-490.

Rohlmann, A., Bergmann, G., and Koelbel, R. (1980). The relevance of stress computation in the femur with and without endoprostheses. *Finite elements in biomechanics***,** 361-377.

Rohlmann, A., Mössner, U., Bergmann, G., and Kölbel, R. (1982). Finite-element-analysis and experimental investigation of stresses in a femur. *Journal of Biomedical Engineering* 4**,** 241-246.

Romer, A.S. (1923). The pelvic musculature of saurischian dinosaurs. Bulletin of the AMNH; v. 48, article 19.

Rubenson, J., Lloyd, D.G., Besier, T.F., Heliams, D.B., and Fournier, P.A. (2007). Running in ostriches (Struthio camelus): three-dimensional joint axes alignment and joint kinematics. *Journal of Experimental Biology* 210**,** 2548-2562.

Rubenson, J., Lloyd, D.G., Heliams, D.B., Besier, T.F., and Fournier, P.A. (2010). Adaptations for economical bipedal running: the effect of limb structure on three-dimensional joint mechanics. *Journal of The Royal Society Interface*.

Russell, A.P., Dijkstra, L.D., and Powell, G.L. (2001). Structural characteristics of the patagium of Ptychozoon kuhli (Reptilia: Gekkonidae) in relation to parachuting locomotion. *Journal of Morphology* 247**,** 252-263.

Schlager, S. (2015). *mesheR: Meshing operations on triangular meshes.*

Seebacher, F. (2001). A new method to calculate allometric length-mass relationships of dinosaurs. *Journal of Vertebrate Paleontology* 21**,** 51-60.

Sellers, W.I., Pond, S.B., Brassey, C.A., Manning, P.L., and Bates, K.T. (2017). Investigating the running abilities of Tyrannosaurus rex using stress-constrained multibody dynamic analysis. *PeerJ* 5**,** e3420.

Selvatti, A.P., Gonzaga, L.P., and Russo, C.a.D.M. (2015). A Paleogene origin for crown passerines and the diversification of the Oscines in the New World. *Molecular Phylogenetics and Evolution* 88**,** 1-15.

Semechko, A. (2021). Rigid body parameters of closed surface meshes.

Senter, P. (2006). Scapular orientation in theropods and basal birds, and the origin of flapping flight. *Acta Palaeontologica Polonica* 51.

Sereno, P.C., and Chenggang, R. (1992). Early Evolution of Avian Flight and Perching: New Evidence from the Lower Cretaceous of China. *Science* 255**,** 845-848.

Serrancolí, G., Kinney, A.L., Fregly, B.J., and Font-Llagunes, J.M. (2016). Neuromusculoskeletal Model Calibration Significantly Affects Predicted Knee Contact Forces for Walking. *Journal of Biomechanical Engineering* 138.

Seth, A., Hicks, J.L., Uchida, T.K., Habib, A., Dembia, C.L., Dunne, J.J., Ong, C.F., Demers, M.S., Rajagopal, A., Millard, M., Hamner, S.R., Arnold, E.M., Yong, J.R., Lakshmikanth, S.K., Sherman, M.A., Ku, J.P., and Delp, S.L. (2018). OpenSim: Simulating musculoskeletal dynamics and neuromuscular control to study human and animal movement. *PLOS Computational Biology* 14**,** e1006223.

Seth, A., Sherman, M., Reinbolt, J.A., and Delp, S.L. (2011). OpenSim: a musculoskeletal modeling and simulation framework for in silico investigations and exchange. *Procedia IUTAM* 2**,** 212-232.

Sharir, A., Barak, M.M., and Shahar, R. (2008). Whole bone mechanics and mechanical testing. *The Veterinary Journal* 177**,** 8-17.

Sherman, M., Seth, A., and Delp, S. (2010). How to compute muscle moment arm using generalized coordinates. *Report, Stanford University, Stanford, CA*.

Sherman, M.A., Seth, A., and Delp, S.L. (2013). WHAT IS A MOMENT ARM? CALCULATING MUSCLE EFFECTIVENESS IN BIOMECHANICAL MODELS USING GENERALIZED COORDINATES. *Proceedings of the ... ASME Design Engineering Technical Conferences. ASME Design Engineering Technical Conferences* 2013**,** V07BT10A052.

Smith, N.C., Wilson, A.M., Jespers, K.J., and Payne, R.C. (2006). Muscle architecture and functional anatomy of the pelvic limb of the ostrich (Struthio camelus). *Journal of Anatomy* 209**,** 765-779.

Sohn, M.H., and Ting, L.H. (2016). Suboptimal Muscle Synergy Activation Patterns Generalize their Motor Function across Postures. *Frontiers in Computational Neuroscience* 10.

Söhnel, K., Andrada, E., De Lussanet, M.H.E., Wagner, H., Fischer, M.S., and Rode, C. (2021). Single limb dynamics of jumping turns in dogs. *Res Vet Sci* 140**,** 69-78.

Speirs, A.D., Heller, M.O., Duda, G.N., and Taylor, W.R. (2007). Physiologically based boundary conditions in finite element modelling. *Journal of Biomechanics* 40**,** 2318-2323.

Stolpe, M. Physiologisch-anatomische Untersuchungen über die hintere Extremität der Vögel. *Journal für Ornithologie* 80**,** 161-247.

Sullivan, S.P., Mcgechie, F.R., Middleton, K.M., and Holliday, C.M. (2019). 3D Muscle Architecture of the Pectoral Muscles of European Starling (Sturnus vulgaris). *Integrative Organismal Biology* 1**,** oby010.

Tarsitano, S. (1983). Stance and gait in theropod dinosaurs. *Acta Palaeontologica Polonica* 28.

Taylor, C. (1973). Energy cost of animal locomotion. *Comparative physiology***,** 23-41.

Taylor, W.R., Ehrig, R.M., Duda, G.N., Schell, H., Seebeck, P., and Heller, M.O. (2005). On the influence of soft tissue coverage in the determination of bone kinematics using skin markers. *J Orthop Res* 23**,** 726-734.

Taylor, W.R., Ehrig, R.M., Heller, M.O., Schell, H., Seebeck, P., and Duda, G.N. (2006). Tibio-femoral joint contact forces in sheep. *Journal of Biomechanics* 39**,** 791-798.

Thomas, A.L., and Taylor, G.K. (2001). Animal flight dynamics I. Stability in gliding flight. *J Theor Biol* 212**,** 399-424.

Tobalske, B.W. (2004). Take-off mechanics in hummingbirds (Trochilidae). *Journal of Experimental Biology* 207**,** 1345-1352.

Tobalske, B.W., and Dial, K.P. (2000). Effects of body size on take-off flight performance in the Phasianidae (Aves). *Journal of Experimental Biology* 203**,** 3319-3332.

Tomek, T., and Bochenski, Z.M. (2000). *The comparative osteology of European corvids (Aves: Corvidae), with a key to the identification of their skeletal elements.* Instytutu Systematyki i Ewolucji Zwierząt PAN.

Trabelsi, N., Yosibash, Z., Wutte, C., Augat, P., and Eberle, S. (2011). Patient-specific finite element analysis of the human femur—A double-blinded biomechanical validation. *Journal of Biomechanics* 44**,** 1666-1672.

Trepczynski, A., Kutzner, I., Kornaropoulos, E., Taylor, W.R., Duda, G.N., Bergmann, G., and Heller, M.O. (2012). Patellofemoral joint contact forces during activities with high knee flexion. *Journal of Orthopaedic Research* 30**,** 408-415.

Trepczynski, A., Kutzner, I., Schwachmeyer, V., Heller, M.O., Pfitzner, T., and Duda, G.N. (2018). Impact of antagonistic muscle co-contraction on in vivo knee contact forces. *Journal of NeuroEngineering and Rehabilitation* 15**,** 101.

Veldpaus, F.E., Woltring, H.J., and Dortmans, L.J.M.G. (1988). A least-squares algorithm for the equiform transformation from spatial marker co-ordinates. *Journal of Biomechanics* 21**,** 45-54.

Verstappen, M., Aerts, P., and De Vree, F. (1998). Functional morphology of the hindlimb musculature of the black-billed magpie, Pica pica (Aves, Corvidae). *Zoomorphology* 118**,** 207-223.

Verstappen, M., Aerts, P., and Van Damme, R. (2000). Terrestrial locomotion in the black-billed magpie: Kinematic analysis of walking, running and out-of-phase hopping. *Journal of Experimental Biology* 203**,** 2159-2170.

Vickerton, P., Jarvis, J.C., Gallagher, J.A., Akhtar, R., Sutherland, H., and Jeffery, N. (2014). Morphological and histological adaptation of muscle and bone to loading induced by repetitive activation of muscle. *Proceedings of the Royal Society B: Biological Sciences* 281.

Videler, J.J. (2000). Archaeopteryx: a dinosaur running over water. *Archaeopteryx* 18**,** 27-34.

Videler, J.J. (2006). *Avian flight.* Oxford University Press.

Voeten, D.F.a.E., Cubo, J., De Margerie, E., Röper, M., Beyrand, V., Bureš, S., Tafforeau, P., and Sanchez, S. (2018). Wing bone geometry reveals active flight in Archaeopteryx. *Nature Communications* 9**,** 923.

Wellnhofer, P. (2010). A short history of research on Archaeopteryx and its relationship with dinosaurs. *Geological Society, London, Special Publications* 343**,** 237-250.

Wellnhofer, P., and Haase, F. (2009). *Archaeopteryx: The Icon of Evolution.* F. Pfeil.

Wilcox, H.H. (1952). The Pelvic Musculature of the Loon, Gavia Immer. *The American Midland Naturalist* 48**,** 513-573.

Witmer, L.M. (1995). The extant phylogenetic bracket and the importance of reconstructing soft tissues in fossils. *Functional morphology in vertebrate paleontology* 1**,** 19-33.

Xu, X., and Wang, X. (2003). A new maniraptoran dinosaur from the Early Cretaceous Yixian formation of western Liaoning. *Vertebrata Pal Asiatica* 41**,** 195-202.

Yalden, D.W. (1984). What size was Archaeopteryx? *Zoological Journal of the Linnean Society* 82**,** 177-188.

Yushkevich, P.A., Piven, J., Hazlett, H.C., Smith, R.G., Ho, S., Gee, J.C., and Gerig, G. (2006). User-guided 3D active contour segmentation of anatomical structures: Significantly improved efficiency and reliability. *NeuroImage* 31**,** 1116-1128.

Zajac, F.E. (1989). Muscle and tendon Properties models scaling and application to biomechanics and motor. *Critical reviews in biomedical engineering* 17**,** 359-411.

Zeffer, A. (2003). Leg morphology and locomotion in birds: requirements for force and speed during ankle flexion. *Journal of Experimental Biology* 206**,** 1085-1097.

Zhang, F., and Zhou, Z. (2004). Leg feathers in an Early Cretaceous bird. *Nature* 431**,** 925.

Zheng, X., O'connor, J., Wang, X., Wang, M., Zhang, X., and Zhou, Z. (2014). On the absence of sternal elements in Anchiornis (Paraves) and Sapeornis (Aves) and the complex early evolution of the avian sternum. *Proceedings of the National Academy of Sciences* 111**,** 13900.

Zhou, Z. (2004). The origin and early evolution of birds: discoveries, disputes, and perspectives from fossil evidence. *Naturwissenschaften* 91**,** 455-471.